Stony Brook University

Thermal and Mechanical properties of Graphene/Polymer Nanocomposites

A Dissertation Presented

by

Kai Yang

to

The Graduate School

in Partial Fulfillment of the

Requirements

for the Degree of

Doctor of Philosophy

in

Materials Science and Engineering

Stony Brook University

August 2014

Stony Brook University

The Graduate School

Kai Yang

We, the dissertation committee for the above candidate for the

Doctor of Philosophy degree, hereby recommend

acceptance of this dissertation.

Miriam H. Rafailovich – Dissertation Advisor

Professor of Department of Materials Science and Engineering

Dilip Gersappe - Chairperson of Defense

Associate Professor of Department of Materials Science and Engineering

Thomas A. Butcher

Professor of Department of Chemical and Molecular Engineering

Anantha N. Desikan

President at ICL-IP America Inc.

This dissertation is accepted by the Graduate School

Charles Taber

Dean of the Graduate School

Abstract of the Dissertation

Thermal and Mechanical properties of Graphene/Polymer Nanocomposites

by

Kai Yang

Doctor of Philosophy

in

Materials Science and Engineering

Stony Brook University

2014

We have successfully fabricated the PP/GNPs nanocomposites that are thermally conductive, processable, and flame resistant. Thermal conductivity measurements indicated that the thermal coefficient scaled linearly with GNP loading, where a value of 2.0W/m*k was achieved at a loading of 40%. Tensile measurement indicated that the modulus increased, linearly with GNPs loading, while the IZOD impact and toughness after an initial decrease, remained constant for loading up to 50%. The torque required for extrusion increased only by 25% over this range indicating that the compound remained processable despite the high loading content. SAXS showed a large decrease in the amount of lamellar folding relative to the neat PP sample, while WAXS and DSC measurements, indicated a slight increase in the degree of crystallinity . These results are consistent with strong adsorption of the PP chains to the GNP, which, while maintaining crystallinity, disrupts the lamellar structure. Cone calorimetry showed that nanocomposites with 10% loading or higher exhibited a dramatic decrease in heat release and mass loss rates. The time to ignition initially decreased relative to the neat PP, then

increased and surpassed it by a factor of 2 at 40%. These results paralleled those from conductivity/frequency measurements indicating that percolation occurred. Hence thermal phonon dissipation was effective for a slowly approaching heat front while contact was required for a rapidly approaching front.

Dedicate To

My

Family

TABLE OF CONTENTS

LIST OF FIGURES

LIST OF TABLES

LIST OF ABBREVIATIONS

PP	Polypropylene
CNT	Carbon nanotube
DMA	Dynamic mechanical analysis
DSC	Differential scanning calorimeter
SAXS	Small Angle X-ray Scattering
WAXS	Wide Angle X-ray Scattering
CB	Carbon Black
GNPs	Graphene Nanoplates
k	Thermal Conductivity
MWNTs	Multi-wall carbon nanotubes
SEM	Scanning electronic microscopy
TGA	Thermal Gravimetric Analysis
TEM	Transmission Electronic Microscopy
AFM	Atomic Force Microscopy
MDH	Magnesium Hydroxide
ATH	Aluminum Hydroxide
H5	Graphene Nanoplatelets with 5micro diameter
H25	Graphene Nanoplatelets with 25micro diameter
UL94	Underwriters Laboratories 94
QTM500	Quick Thermal Conductivity Meter 500

HRR	Heat Release Rate
PHRR	Peak Heat Release Rate
MLR	Mass Loss Rate
ΔH_f^0	Theoretical crystallization enthalpy of the polymer matrix if it was 100% crystalline
Φ	Function of loading
X_C	Crystallinity
T_{max}	Inflection Point

ACKNOWLEDGMENTS

I wish to address my sincerely respect to those contributed to my research in Ph.D degree study. Without them, I could not become who I am today and here I would like to show my appreciation to them.

The first to be acknowledged should definitely be Dr. Miriam H. Rafailovich, my dissertation advisor, who is not only expressing me the extensive knowledge on science and engineering, but also showing the enthusiasm as a scientist at every single day. During the past five years of a fruitful study on various topics, Dr. Rafailovich encouraged me to handle challenging problems and provided me an incredible opportunities to study the frontal of industrial applications. I sincerely appreciated for the chance to be her PhD student.

I also wish to thank Dr. Thomas Butcher, who provided me the opportunity to work in Brookhaven National Laboratory with great instructive enlightening and help in access to various instruments to realize my ideas.

I must also thank Dr. Jonathan Sokolov, for generous assistance and bearing with me to visit Miriam and him every single Saturday night at the last few month.

I also extend thanks to my other committee members, Dr. Anantha Desikan, for his suggestions and served as my dissertation committee.

It is also my pleasure to extend my gratitude to Dr. Takashi Kashiwagi for his valuable comments on my research and introducing me the science knowledge about flame retardant mechanism.

I also feel that I should appreciate my cooperators in various research topics for their instructive enlightening and help in access to various instruments. They are Ms. Rebecca Trojanowski, Mr. Steve Bennett, Dr. Lihua Zhang and Mr. Kim Kisslinger in Brookhaven National Laboratory; Mr. Alessio Gerald, Mr. Kali Suryadevara, Dr. Levchik Sergei and Dr. Seongchan Pack in Israel Chemical Limited-Industrial Products America Inc.; Dr. Maya Koga, Dr. Jim Quinn and Dr. Molly Gentleman in Stony Brook University. Without your support, I could not finish my research.

I also would like to thank my colleagues at Garcia MRSEC, Dr. Christine Falabella, Dr. Ying Liu, Dr. Chung-Chueh Chang, Dr. Perumal Ramasamy, Dr. Tatsiana Mironava, Dr. Cheng Pan, Sisi Qin, Liudi Zhang, Nahyum Cho, Yingjie Yu, Hongfei Li, Shan He, Ke Zhu, Zhenhua Yang, Yichen Guo, Linxi Zhang, Zhihao Chen, Yan Xu, Fan Yang, Kao Li, Kuan-Che Fang, Longtao Han and Juyi Li for their help and discussions.

I specially thank all my undergraduate students and high school students, for understand and supporting my research during my PhD. Finally, I would like to thank my family for their support and encouragement throughout my entire life.

Chapter 1. Introduction

1.1 Background

As heat exchanger construction material, polymers offer the advantages, relative to metals, of corrosion resistance, low cost, and low weight but suffer from low thermal conductivity. T'Joen et al reviewed the potential application of polymer heat exchangers to building cooling equipment applications [1]. In the buildings area, condensing boilers achieve very high efficiency by recovering heat from flue gas before it is discarded. The recovery of latent heat from the water vapor in the humid gas is a very important part of the total heat recovery but the condensate formed is corrosive-leading to the need for expensive alloys in the heat exchanger. In a study completed in 1989 [2], the application of a range of plastics for condensing heat exchangers in gas-fired furnaces was evaluated.

Polymer nanocomposites using carbon nanotubes, carbon black and graphene as the second phase which has been used for improving thermal conductivity[3], electronical conductivity[4], flame retardancy[5] and mechanical properties[6]. A wide range of polyolefin, including polypropylene[7, 8], polyethylene[9, 10], polystyrene[11, 12] and polycarbonate[13, 14] have been reinforced with carbon materials. Polymers with upper use temperature limits as high as 285°C were evaluated and it was concluded that several candidate materials could stand up to the condensate environment. Polypropylene is now the material used for vent pipe applications with oil-fired condensing boilers due to its high corrosion resistance[15],mechanical

properties and ease of processing. Some of these are configured for preheating combustion air, essentially serving as polymer condensing heat exchangers although with very low effectiveness. The development of high thermal conductivity polymer composites for the condensing boiler application could reduce the initial cost and improve the life of these heat exchangers, lead to expanded adoption of this high efficiency equipment.

Numerical simulations of the heat exchange parameters in a typical boiler found that the efficiency was always limited by the component with the lowest thermal coefficient, which in a metal heat exchanger is the gas-side convective coefficient.[16, 17] In the case of metal heat exchangers, the thermal coefficient of the metal body was approximately $k \geq 10 W/(m \cdot K)$, but that of the flue gas was only $k \approx 2.0 W/(m \cdot K)$. Hence the materials of the heat exchange unit could easily be replaced by a nanocomposite with a coefficient slightly larger than $2.0 W/(m \cdot K)$ without loss of efficiency in the performance of the unit.

Here we show results of nanocomposites formed with PP and nanoparticles which in themselves are thermally and electrically conductive, but among which only one type, Graphene Nanoplates(GNPs), was actually suitable for engineering a nanocomposites that meets the multiple and sometime conflicting conditions described.

1.2 Outline of Chapters

In chapter 2, we used a C.W. Brabender instrument to blend polymer pellet with different kind of fillers including aluminum hydroxide, magnesium hydroxide, short muti-wall carbon

nanotube, carbon black and graphene. The mixer was allowed to cool at room temperature and then pelletized and molded in a hot press at T=180°C into the different shapes required for the various thermal conductivity, mechanical tests and flame retardant tests. We found that a critical concentration for single metal additive like ATH or MDH to work is 30%wt. However, the mechanical properties dropped dramatically lead to the difficulty in the processing. On the other hand, carbon additives perform better in the tensile test and the thermal conductivity could be achieved as high as 0.57W/m*K with 20%wt loading for CNT. The flame retardant properties indicated to be good for PP/ATH/CNT (40/50/10 wt%) and PP/ATH/MDH/CNT(40/30/20/10 wt%) since they could achieve UL-94-V0 vertical burning test. And heat release rate and flameout time proved that the addition of ATH/MDH/CNT could greatly improve the flame retardancy.

In chapter 3, we have shown that two different kind of GNPs H5 and H25 could be the best additives in the Polypropylene to produce nanocomposites and the substitution of low amount of CNT could not boost the thermal conductivity for equivalent loading of the additives. Transmission electron microscopy had been conducted to prove that both types of particles exfoliate into single sheets in toluene and the H25 particles are much larger than H5. Raman spectroscopy was also introduced to demonstrate H5 samples appear to consist of one or two layers whereas the H25 have multiple layers. Multiple layers require exfoliation and higher shear which make it more difficult to disperse within the polymer matrix. Series thermal conductivity as function of the concentration of GNPs H5 and H25 have been done and the thermal conductivity, equivalent to that of the carrier gas in the heat exchanger unit, k=2.0 W/m*k, can be obtained with a minimum filler concentration of 40wt% and 50wt% for H5 and H25 respectively. We showed the torque measurement from the blending process to analysis the

degree of processing ability since the heat exchange coils require high ductility in order to extrude and process. Both PP/GNPs nanocomposites proved to have higher torque in the blending when they have high concentration. And H5 indicated lower torque which lead to easier for processing. In addition to it, tensile and Izod impact test were conducted to further illustrate the good ductility. Scanning electron microscopy and transmission electron microscopy were used to analysis the dispersion of the GNPs in the Polypropylene matrix and the result indicated that the H5 provide the better exfoliation for PP/GNPs nanocomposites.

SAXS characterization of the samples was performed and the results showed that while a sharp decrease was observed in lamellar ordering for graphene concentrations 10% or higher, WAXS data showed the degree of crystallinity remained high. Measurements of relative peak areas indicated that the graphene surfaces nucleated the alpha phase of PP, with a preferred (100) and (111) orientation. This result was consistent with DSC and TGA measurements which indicated no change in the melting temperature. Hence no significant disruption of the crystalline structure occurred with increased GNPs loading.

The response of the nanocomposites to an approaching heat front was measured using cone calorimetry. Nanocomposites with 10% loading or higher showed a dramatic decrease in heat release and mass loss rates, as well as oxygen consumption. Video images indicated the formation of a flexible char layer in these samples which reflected the incoming heat front, while reducing the flow of gases, and reducing the temperature of the sample.

The time to ignition of the nanocomposites initially decreased relative to the neat PP, reaching a minimum at a loading of 1%, and then increasing back to the PP value at 10%, and

surpassing it by a factor of 2 at 40%, indicating that the higher loading also rendered the nanocomposites flame retardant.

Conductivity measurement vs frequency as a function of GNP loading were performed and the transition for non-conducting to conducting response was found at a loading of 10%. These results indicated that thermal phonon dissipation was effective for slowly increasing temperatures, where steady state conditions are reached, while for rapidly approaching heat, effective dissipation had the same direct particle-particle contact percolation condition requirements as electrical conduction.

1.3 The development of suitable design for polymer heat exchanger

Condensing Boilers achieve very high efficiency levels by recovering heat from the flue gas before it is discarded. The recovery of latent heat from the water vapor in the humid gas is a very important part of the total heat recovery but the condensate formed is corrosive – leading to the need for expensive alloys in the heat exchanger. This study is focused on the potential replacement of these alloys in the condensing section of home heating boilers with polymeric materials. The requirements for selecting the polymer are fairly rigorous and cannot be satisfied by any polymer alone; the polymer must withstand relatively high temperatures (T~250°C) and be resistant to degradation in the presence of the sulfuric acid environment found in condensates produced from conventional oil combustion. Furthermore, even though the

polymer is not in contact with fire, its proximity to an open flame and to the ignition electronics found in boilers, OSHA and other building code regulations require that the materials must be flame retardant, and conform to UL94-V0 requirements. Since no single polymeric material can satisfy these criteria, the focus of this research was to develop organic-inorganic polymer blend nanocomposites, where the mechanical, chemical, and thermal properties could be tailored to meet the specific requirements for optimal boiler construction.

The design of the polymer heat exchanger has been listed in **Figure 1.1 and 1.2**. From the Figure we could conclude that the design of the double coil shape structure require good mechanical properties for the processing and the flue gas temperature is relative high which leads to the request of certain degree of flame retardant. Moreover, the principle have been proved that the efficiency was always limited by the component with the lowest thermal coefficient, which in a metal heat exchanger is the gas-side convective coefficient. The temperature of the heat exchanger material had been tested and the result showed in **Figure 1.3 and 1.4**.

Specific classes of polymers are known to be resistant to acid corrosion. These polymers include polypropylene, polycarbonate, Teflon, and other flouro-polymers. The major drawback of these materials is their high degree of immiscibility, which makes it difficult to tailor their properties for specific applications through blending. For example, polycarbonate, which has good thermal and corrosion resistance is too brittle, while polypropylene (PP), polyvinylchloride (PVC), or Teflon, which have the desirable impact toughness, deform easily when heated and therefore does not satisfy the UL-94 flame retardant criteria without further modification. We had previously demonstrated that it was possible to achieve compatibilization of a large group of polymers using exfoliated nano-clays.[18] This enabled us to adopt an approach where different

polymers are blended together, with specific flame retardant formulations to achieve the proper mechanical and thermal properties.

1.4 Carbon based nanoparticles

1.4.1 Graphene

Carbon is one of the most common elements in the world since it's a component of most molecules. The hybridized atomic orbitals of carbon could have infinity possibility of molecule structures. The nanoscale carbon based nano size materials have attracted great interest for next generation of materials for different application as thermal, electrical, building applications. The structure and dimension of the carbon based nanofillers are the key factors in the development, including round sphere shape carbon black (CB), tube like carbon nanotubes and Graphene nanoplatelets. Among all these carbon nano materilas, graphene has not been widely used in recent research before 2004 since researchers believe that graphene structure is not stable with less than 6000 carbon atoms. Nevertheless, in 2004, Andre Geim and Konstantin Novoselov at the University of Manchester published their groundbreaking experiments regarding the two-dimensional material graphene which help them won the Nobel Prize in Physics in 2010.[19] Graphene research has expanded quickly since the substance was first isolated in 2004. Graphene Nanoplates(GNPs) represent a new class of carbon nanoparticles with multifunctional properties. The platelet structure provides a high surface area and very thin but wide aspect ratio which makes these particles could compete with carbon black(CB) and CNTs for the preparation of polymer nanocomposites with excellent thermal, electrical, mechanical and

flame retardancy properties. Research was informed by theoretical descriptions of graphene's composition, structure and properties, which had all been calculated decades earlier. High-quality graphene also proved to be surprisingly easy to isolate, making more research possible.

The thermal conductivity of the graphene single sheet is considered to be around 6000W/m*K. Balandin A A et al reported a noncontact thermal conductivity measurement carried on a Raman spectrometer and reported an ultra-high thermal conductivitity of suspended monolayer graphene at room temperature as 4.8-5.3 $\times 10^3$ W/m*K[20], which provides a wide possibility of application to improve thermal conductivity of nanocomposites. However, thermal conductivity of graphene is also greatly affected by the surrounding environment. On silicaon substrate, graphene had been found to have the thermal conductivity around 600W/m*K which is decrease by the factor of ten due to phonon scattering between substrate and graphene platelets. [21]

Researchers have found that graphene platelet thermal conductivity is directly related to the lateral direction in the platelet of isolated graphene sheet.[22, 23] On the other hand, phonon transfer in the graphene platelet is mainly contribute to Van der Waals force, which is weaker than chemical bonds. [24-26]

The mechanical properties of graphene was measured by Atomic Force Microscopy that a Young's modulus of 1TPa indicated that graphene is a rigid and brittle material.[27] The force-displacement behavior is interpreted within a framework of nonlinear elastic stress-strain response, and yields second- and third-order elastic stiffnesses of 340 N/m and –690 N/m, respectively.[28] These high strength and modulus could be the key factors in developing nanocomposites with graphene.

The high surface area of graphene also provided outstanding electrical conductivity as high as 6000S/cm which is the encouraging results to illustrate the exciting potential for high performance, electrical energy storage devices based on this new class of carbon material.[29-31] The formation of a conducting channel throughout the polymer matrix caused an abrupt change in electrical conductivity could help boost the electrical conductivity of multiple polymer matrix.[32]

Because of the formation of compact, dense and uniform char during combustion, graphene could also be used as a flame retardant filler in the polymer nanocomposites.[33, 34] The char is observed which forms an elastic shell surrounding the sample that inflates during combustion controlling the release of the burning gases.

1.4.2 Carbon Black

Carbon Black is widely used as a pigment or colorant, a reinforcing filler to improve stability, an antioxidant to prolong the lifetime of polymer and a conductive filler. In some way, CB is an amorphous form of carbon and when used as a conductive filler, where three properties including structure, particle size and surface are important factors. High electrical properties is illustrated when a continuous conducting path is formed at the concentration of CB as high as 25wt%. Basically the interaction between polymer and CB is the not achieved until higher weight ratio was reached.[35, 36] The addition of CB into polymer normally increase the modulus of the polymer composites first at low loading but decrease at the higher loading. [37]

The conductive particles could disperse in the matrix to obtain percolation threshold to achieve good electrical conductivity. For one single polymer system, the electrical conductivity is directly related to the percolation of CB in the polymer matrix. However, if the blend has two

kind of polymer, the electrical conductivity of CB filled polymer blends is determined by two factors. One is concentration of CB in the filler rich phase and the other is phase continuity of this phase. These double percolations affect conductivity of conductive particle filled polymer blends.[38, 39]

1.4.3 Carbon Nanotubes

Carbon Nanotubes (CNTs) is considered to be one dimension version of graphene, which could provide exponential thermal and electrical conductivity together with high mechanical properties.[40] It is proved that the shear force in the mixing process is important factor in electrical conductivity for carbon nanotubes with Polypropylene. And the higher of concentration of CNT would be exhibited better thermal coefficient. [41] More researches have been done about designing a model for thermal conductivity. Gaxiola *et al* reported that the Nielsen thermal conductivity model could be used to analysis the through-plane and in-plane thermal conductivity for carbon nanotubes, graphene and carbon black. And synthetic graphite together with carbon nanotubes could be used as the primary filler in fuel cell bipolar plates.[42] The percolation thresholds in the polymer/CNT had been reported by Kovacs *et al*, in which the low particle concentrations blending prefer to have randomly distributed filler particles from the percolating paths, and the particle could move by external fields, shearing or diffusion. [43]

Numerous studies had been done about the maximum electrical conductivity that the polymer could achieve. For PU, 2000 S/m could be done with 15wt% of multi wall CNT which is reported by Koerner *et al*.[44] Blanchet *et al* reported that 3000 S/m can be achieved using same concentration (15wt%) of single wall CNT.[45] And Skakalova *et al* found an electrical conductivity of 10000 S/m containing 10wt% $SOCl_2$ treated single wall CNT. [46] Moreover,

Bauhofer et al mentioned some critical factors in polymer/CNT electrical conductivity that the type of the polymer and mixing techniques have the higher impact in conductivity and percolation rather than type of the CNT.[47]

1.5 Brief Summary

As described above, this study is mainly focusing on the development of the nanocomposites in the application of polymer heat exchanger, automobile and aircraft materials in the systems which maintain reasonable mechanical properties and achieve flame retardant and high thermal and electrical conductivity. In summary, the study include but not limit to:

1. A method to blend the polymer and filler together and maintain good mechanical properties which could be easily cast into double coil shape polymer heat exchanger material.
2. A deep understanding on the affections of filler shape from the simulation of thermal conduction and surface morphology on polymer nanocomposites conductivity.
3. Analysis the structure and properties of different types of graphene nanoplatelets and developed the proper weight ratio of PP/GNPs nanocomposites which could fit the requirement of heat exchanger.
4. A systematic study for the nuclear effect of the GNPs in the Polypropylene matrix and the crystallinity of nanocomposites.
5. Knowledge of mechanical properties of PP/GNPs nanocomposites, which not only facilitate GNPs' application in heat exchanger but also promote its widespread

application in thermal energy storage devices, thermal and electrical conductive nanocomposites, etc.

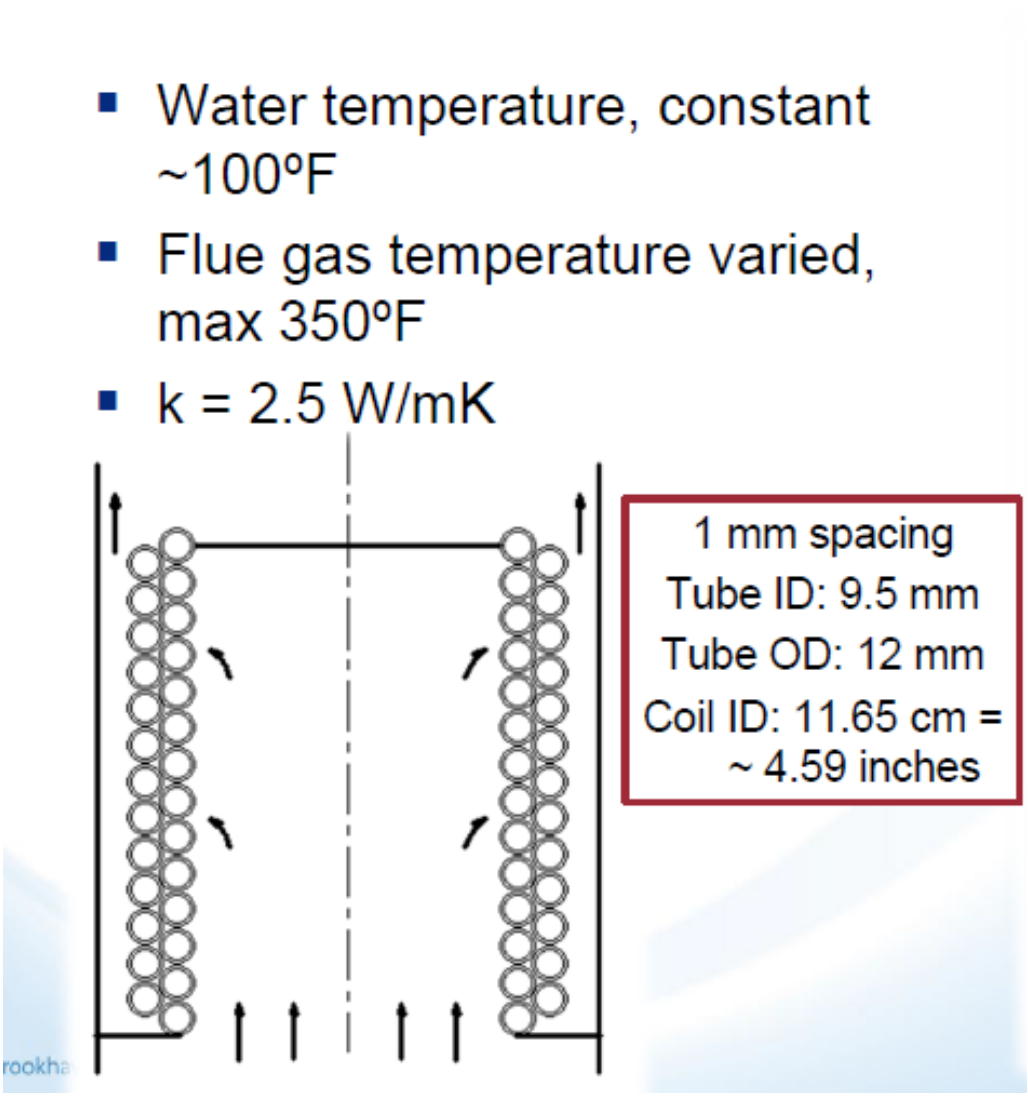

Figure 1.1 The Model of Polymer heat exchanger

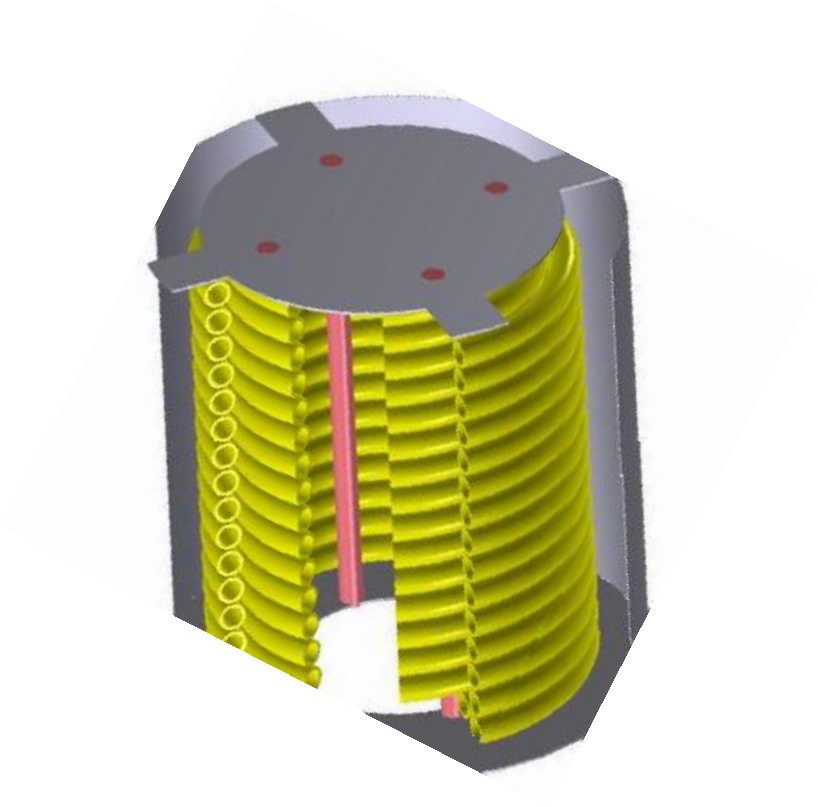

Figure 1.2 The 3-D structure of polymer heat exchanger

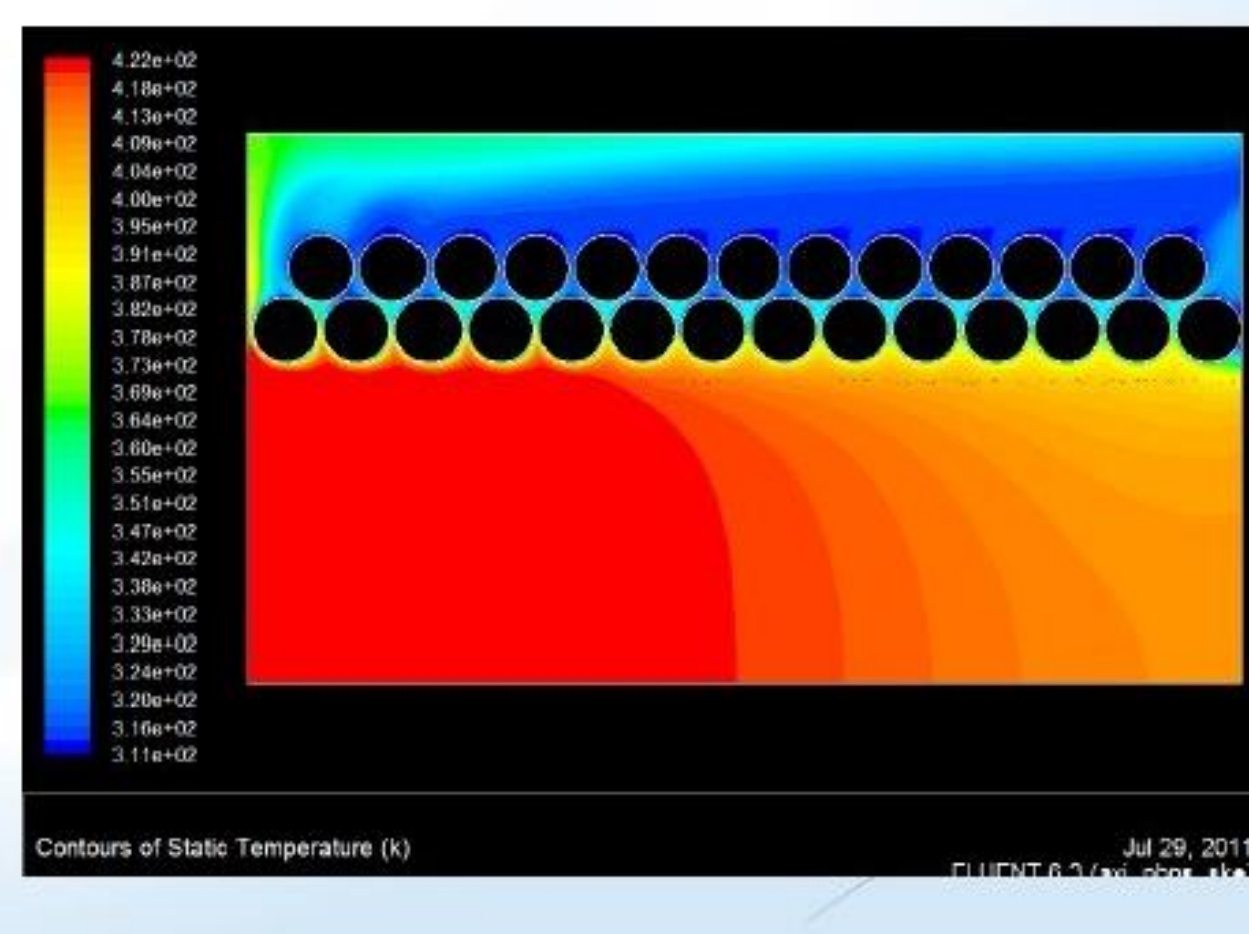

Figure 1.3 The simulation of heat diffusion in the double coil heat exchanger.

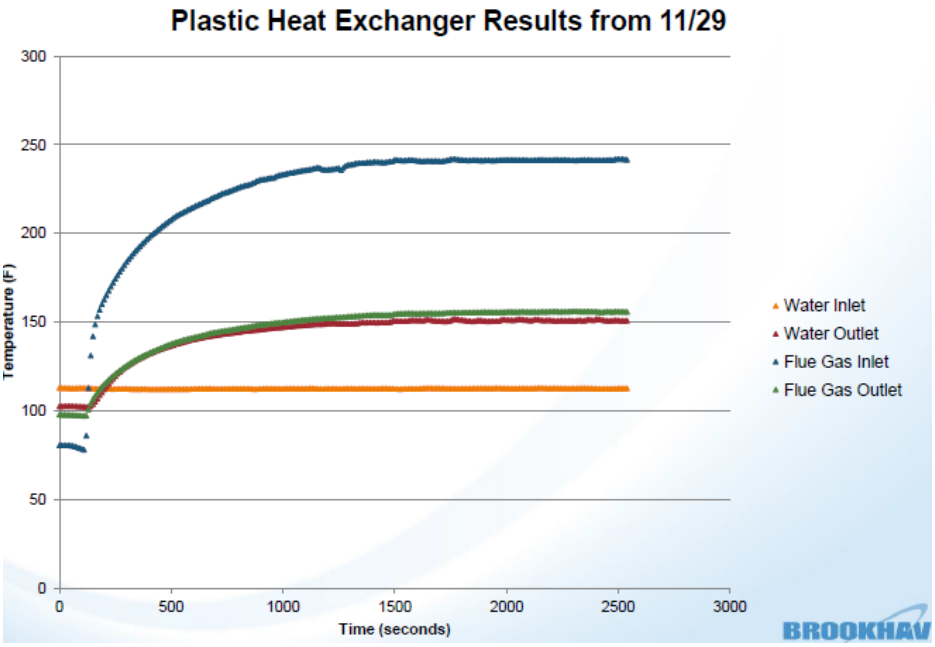

Figure 1.4 The temperature of inlet and outlet flue gas and water as a function of time in polymer heat exchanger.

Chapter 2. THERMAL CONDUCTIVITY AND FLAME RETARDANCY OF METAL BASED FILLERS WITH POLYPROPYLENE NANOCOMPOSITE

2.1. Introduction

Biofuels are currently being introduced as "green" replacements for fossil fuels in numerous applications including replacements for home heating in oil burners. One major drawback of these fuels is their high acidity, which makes them corrosive and limits their usefulness in metal boilers or storage tanks. Consequently there has been intense research in finding a suitable, non-corrosive, and yet thermally conductive and malleable material for replacing the metal heat exchangers and storage tanks. Polypropylene, (PP) a crystalline polyolefin elastomer has been proposed due to its high corrosion resistance, toughness and ease of processing. On the other hand, PP is also extremely flammable, and has a poor thermal conductivity coefficient typical of most polymers, k=0.2 W/(m·K). In order to overcome these difficulties numerous attempts at compounding PP with various nanoparticles were reported that produced compounds which were either thermally conductive or flame retardant. Yet in order to be useful for the production of heat exchange units, the compound must have a higher thermal coefficient, while be simultaneously flame resistant and processable.

Despite the apparent simplicity, it still required nearly an order of magnitude increase of the polymer thermal coefficient. Numerous nanoparticles exist, i.e. nanotubes, carbon black, graphene, or metallic particles like aluminum hydroxide, magnesium hydroxide, Zinc oxide and copper micro particles, which have been shown to increase the electronic conductivity[27, 48-63], but increasing the thermal conductivity has proven far more difficult[64-72]. Electronic conductivity can be accomplished when the percolation threshold of the particle is reached and the conducting components are at least in point contact.[73] Point contact, on the other hand, is insufficient for phonon transfer which is required for thermal conductivity. Phonon transfer is a more complicated process which requires proper coupling between the nanoparticle structure and the polymer matrix over much larger contact areas.

In this chapter, we show the PP nanocomposites perform excel thermal conductivity as high as 1.1W/m*k and meet the multiple and sometime conflicting conditions described.

2.2. Experimental Section

2.2.1. Materials

The matrix polymer used was Polypropylene (Resin 3825, Total Petrochemical, Houston, TX), the melt flow of which is 30g/10min and density is 0.905g/cc. The multi-walled carbon nanotubes (MWCNTs) and Graphene were provided by Cheap Tubes Inc. The lengths of the MWCNTs used in this study were 0.5-2.0µm which have a diameter of 30-50nm. Copper Microparticles (Copper powder, <75um, 99%; Sigma Aldrich) were used as an additive to improve the thermal conductivity. Carbon black was provided by Cabot Corporation. The series number is Sterling V N660 and SD is 4403015. Magnesium oxide (Vertex 100) and aluminum oxide (6810) were provided by J.M. Huber Corporation.

2.2.2 Fabrication of PP/GNPs nanocomposites

A C.W. Brabender instrument, type Intelli-Torque Plasti-Corder **Fig 2.1** was used to blend the nanocomposites. The blender was equipped with two screw-type roller blades in a heating chamber. The polymer pellets were first added to the chamber at a rotation speed of 20 rpm and temperature of 180°C. The ATH/MDH, GNPs or MWCNT were then gradually inserted and mixed at the same rpm for 2 min. The thermal conductivity agents were gradually added into the chamber, while blending. The entire mixture was then blended at 100rpm for 15 min under nitrogen gas flow, which prevented degradation of the mixture from heat-induced oxidation. The

mixing torque at 15min is recorded and the mixture was allowed to cool at room temperature and then pelletized and molded in a hot press instrument **Fig 2.2** at T=180°C into the different shapes required for the thermal conductivity, mechanical tests and flame tests.

2.2.3 Thermal Conductivity measurement

Thermal Conductivity tests were measured using Quick Thermal Conductivity Meter (QTM500) **Fig 2.3** at 23°C. Molded samples of dimension 64mm×64mm×10mm were tested and the results quoted represent the statistical average of the measurements from 5 identical specimens.

2.2.4 Tensile Test

Nanocomposites were molded in the dog-bone shape to perform tensile test using Instron Tensile Tester (Model: 5542) **Fig 2.4** with 500N load cell and pressure grip. The measurement was performed at a rate of 1mm/min and the tensile strength, tensile strain and impact toughness were analyzed from the acquired data. Specimens were molded from the hot press and tested according ASTM D638.

2.2.5 UL-94 Vertical Burning Test

A vertical burning chamber purchased from Underwriters Laboratories Inc. was used to assess flammability. Samples of dimensions 125 mm x 13 mm x 1.5 mm were molded and

tested using the protocol established by ASTM D3801/ISO 1210 UL 94 V0. The test to probe flame retardancy was conducted by first clamping the samples approximately 10mm from the top edge and suspending them, with the long axis pointing down, from a ring stand. A compressed methane gas burner with a gas flow rate of 105 mL/min was then placed 20 mm beneath the lower edge of the samples. A flame, 20 ± 2 mm, high was applied to the sample for 10 sec. and then t_1, the time that it took to extinguish the flame was measured. The flame was then reapplied and t_2, the time to extinguish the flame again was measured. If either t_1 or t_2 was less than 10 sec., then the sample was classified as V0 in the UL-94 test. The classification details of the UL-94-V0 test is listed on **Table 3.1**. Furthermore, it was also recorded whether the nancomposites dripped and /or ignited a wad of cotton placed under the holder.

2.2.6 Cone Calorimetry Test

The heat release rate (HRR) and mass loss rate (MLR) of each sample were tested using cone calorimetry at Israel Chemistry Limited Industrial Products (ICL-IP, Ardsley, NY). The samples were made by molding the composite into a 75mm×75mm×5mm square. Thin aluminum foil was used to wrap all sides of samples except for the upper face to avoid the burning splash. The samples were then exposed in ambient atmosphere, to an external radiant flux of 50kW/m2, perpendicular to the sample surface and the HRR and MLR were measured as a function of exposure time. The standard uncertainty of the measured heat release rate (HRR) was ±10%. The cone calorimetry test was conducted according to the ISO 5660 protocol.

2.2.7 Morphology of Nanocomposites

In order to analyze the internal structure of the PP nanocomposites, scanning electron microscopy (SEM), was used to characterize the morphology of the samples.): The distribution of ATH, MDH andCNT was imaged using JEOL 7600F Analytical high resolution SEM at the center for Functional Nanomaterials (CFN), Brookhaven National laboratory, Upton, NY. Cross section PP/GNPs, CNT specimens were placed on a conductive, double sided, carbon adhesive tab and imaged at 5 kV accelerating voltages using a secondary electron imaging (SEI) detector. Ten nanometers of gold were coated on the surface of the specimens in order to make the specimens conduct.

The elemental distribution of Al, carbon, Mg was imaged using an energy dispersive X-ray spectroscopy (EDXS) attachment on the SEM. The SEM/EDXS measurements were conducted on Izod impact samples. The residues of cone calorimetry test in air atmosphere was also tested using SEM. Ten micrometers of gold nanoparticles were coated on the surface of the samples in order to make the specimens conduct.

2.3 Results and Discussions

2.3.1 Thermal Conductivity of the Nanocomposites

We first produced a series of Polypropylene nanocomposites with different particles such as CNT, ATH, Graphene, CB and MDH, which are all known for their high thermal and electrical conductivity. The thermal conductivity of the PP/ATH is tabulated in the **Table 2.2**, in which the thermal coefficient remain same as 0.30W/m*k for both 90/10 and 80/20 weight ratio. As soon the loading increase to 30%, the ATH begin to perform a higher impact factor in the system. And the result of 0.45W/m*k is far below the required value which is close to 2.0W/m*k. In that case, single additive like ATH and MDH are not enough as a strong agent for the thermal conductivity in our case.

Because of that, carbon black, graphene and carbon nanotubes begin to attract our attention since numerous studies have been done about their ability to increase thermal and electrical conductivity of the polymer. We produce a series test of the thermal conductivity of polypropylene with 20% of the filler ratio, which include 20% of single filler of carbon black, CNT and Graphene and 10%+10% for each of the fillers. The result tabulate in **Table 2.3**, from which we could clearly tell that for the pure additive system, CNT and graphene exhibit much higher result as 0.65W/m*k and 0.58W/m*k, respectively. And the combination of the fillers lead to an interesting result that all three kind of combination have a relatively same thermal conductivity as 0.45W/m*k at 23°C. This could be explained as the barrier effect come from the

mixing of the filler is high enough to overcome even the better mechanism for the heat transfer process.

To fully understand the mechanism of these result, a simulation of thermal conductivity has been employed to analyze the effect of the filler shape. In **Figure 2. 6**, we could conclude as follow, when the thermal conductivity of the filler is relative small as 0.05W/m*k, the filler will block the heat transfer in the composites which lead to a decrease of the overall thermal conductivity. Comparing to the spherical filler like carbon black, the tube filler like CNT will complicate the trail of the heat diffuse in the composites and thus the heat transfer would be harder and require longer time. On the other hand, as the k value of the filler is large enough as only 0.5W/m*k, the tube filler will have a much more positive role in the heat transfer and perform better than sphere ones. These result which consistence with our thermal conductivity test indicated that the Graphene and CNT is a much better choice for boosting thermal conductivity for polymer composites.

Combine the experiment we did before for ATH and carbon based fillers, we formulate the nanocomposites as PP/ATH (50/50wt), PP/MDH/ATH (50/30/20wt), PP/ATH/MDH/CNT (40/30/20/10wt) and PP/ATH/CNT (40/50/10wt). The thermal conductivity of them are tabulated in **Table 2. 4**, where we find that the thermal coefficient of k=1.0 W/m*k could be achieved with the concentration of PP/AHT/MDH/CNT (40/30/20/10wt) and PP/ATH/CNT (40/50/10wt).

2.3.2 Mechanical properties of the PP nanocomposites

Tensile test is one of the most important properties for the mechanical properties of a material. Therefore, we first test the PP/ATH composites with different filler loading from 10% to 30%. The curve of the tensile test is shown in **Figure 2.6(a)** and the ultimate tensile stress is shown in **Figure 2.6(b)**. From the curve we could conclude that the tensile properties of 10% and 20%wt loading of the ATH will not greatly affect the mechanical properties like tensile stress, tensile strain and toughness. On the other hand, the loading of 30%wt greatly reduce all mechanical properties, but it still in the range of processable for polymer. Form the thermal conductivity test we shown before, the ATH really need more than 30% to become relevant for the thermal coefficient. So we will try to blend more than 30% ATH with some other additives since it will maintain the relative right mechanical properties.

We also conduct the tensile test for PP with carbon fillers. In the **Figure 2.7**, we plotted the impact toughness, ultimate strain and ultimate tensile stress. Both PP/Graphene (80/20) and PP/ Graphene/CB (90/10/10) have the Impact toughness higher than 45MPa. But the rest of the samples could not get the toughness higher than 40MPa. The very interesting effect is that the CB itself perform really bad since its toughness is as low as 25MPa, however, CB seems to have a good synergy with Graphene plate since the round shape CB could fill the vacancy of the Graphene plate and form a much more stable structure. The tensile stress and strain showed the same trend, that graphene, CNT as the single filler and graphene with carbon black could perform the best in all the possible concentration. Consider the thermal coefficient of the blends are all lower than graphene and CNT, we could conclude that the best combination of tensile properties and thermal conductivity would be achieved if fillers like Graphene or CNT are used in the nanocomposites.

2.3.3 Morphology of Microstructure in Nanocomposites

As mentioned previously, the main object is to produce high thermal conductivity and flame retardant of the polypropylene nanocomposites while maintain reasonable mechanical properties for processing. Therefore, CNT, Graphene, ATH, MDH, CB were selected as the fillers for the nanocomposites. To further analyze the mechanical properties and thermal conductivity result, morphology of the nanocomposites need to be conducted.

In **Figure 2.8**, we compare the surfaces of pure polypropylene and its nanocomposites. From the **Figure 2.8 (a)**, we could see that in the case of PP/ATH/CNT (40/50/10), the bright region correspond to the ATH particles which have a higher Z than the matrix and scatter more electrons. In **Figure 2.8 (b)**, the PP/ATH/MDH/CNT (40/30/20/10) was tested to check the dispersion MDH and ATH. To further analysis the component of bright region, the EDXS was conducted on four different points which named as a, b, c and d. The **Figure 2.8 (c) to (f)** represent the elements on the related region. From the figure we could tell that point a, b are represent the MDH and point c and d are represent the ATH. From the figure we could tell, the ATH and MDH would prefer to form the particle have the size of 1 micron and disperse homogeneously in the polymer matrix. For both system, the filler particles separate pretty well even at the high loading and effect of adding this amount of ATH or MDH is probably the reason for low mechanical properties. In **Figure 2.9**, we also did an elemental mapping for PP/ATH/MDH/CNT (40/30/20/10) sample. From the mapping, we could clearly see the dispersion of carbon is very uniform. The oxygenium is separate well since it is the element in both ATH and MDH. The most interesting factor is Magnesium disperse much better than

Aluminum and prefer to form much smaller pieces. On the other hand, aluminum is the main factor of bright bulk particles in the nanocomposites. From the mapping, we conclude the dispersion of MDH is better than ATH and the mechanical properties would probably be affected more by ATH since its particle size is much bigger and hard to form homogeneous system.

2.3.4 Flame Retardant Properties of nanocomposites

In **Figure 2.10**, we show the cone calorimetry data for PP nanocomposites. From the figure we can see that in contrast to pure polypropylene, the addition of ATH and MDH have a significantly improve on the flame retardant properties. The details are further tabulate in **Table 2.5**. From the table, we could see that virgin polymer has the Heat Release Rate as 459kW/m^2, the PP/ATH/CNT and PP/ATH/MDH/CNT nanocomposite have the HRR decreased to 156kW/m^2 and 182kW/m^2 respectively, compare to pure PP, and the flameout time increase by the factor of three. The Peak Heat Release Rate (PHRR) decrease even more by a factor of four. The Time to Ignition (TTI) decrease from 33 second to 38s and 39s too. All these result indicated that the addition of ATH/CNT or ATH/MDH/CNT have tremendously affect the flame retardant properties of the PP, which is also confirm by the UL-94 Vertical Burning Test. From the **Table 2.6**, we could see that the PP/MDH/ATH (50/30/20) has already achieved UL-94-V1. However, after add CNT in the nanocomposites, both PP/ATH/MDH/CNT (40/30/20/10) and PP/ATH/CNT (40/50/10) performed really well in the test and achieved UL-94-V0, which is the best result that the fire extinguished in 10s and no dripping observed. Since adding 10% CNT could increase the UL-94 result from the V1 to V2, we believed that the CNT as a char forming

agent has an important effect in the burning process. We will further analysis the char in the following chapter to figure out the reason for the increasing flame retardant properties after adding these fillers in the nanocomposites.

2.3.5 Analysis of Char

Pure Polypropylene will not form char during the burning process. A formation of rigid chars when CNT are added to either homopolymer or polymer blend is one of the most important factors in the reduction of HRR which is proved by numerous researchers.[74-76] The rigid char will provide a thermal barrier which will dissipates heat from the burning gases and the external heat flux. The tube-like structures, will enhance the thermal dissipation through the point contact and improved the thermal conductivity to further help the diffusion of the heat which lead to an increase of TTI since the heat is spread out much faster and the particular temperature is much harder to achieve though the process.

In **Figure 2. 11**, we show the SEM images of the char samples. From the **Figure 2.11(a)** we could see that the char of PP/ATH/MDH/CNT is clearly porous from the burning process since the diffusion requirement for the gas phase from the burning surface to the heat source. From the **Figure 2.11(b) to (d)**, two different flame retardant nanocomposites show a similar reaction, which proved by the EDXS that the $Al(OH)_3$ and $Mg(OH)_2$ degraded to Al_2O_3 and MgO, respectively. However, the synergy from the mixing of $Al(OH)_3$ and $Mg(OH)_2$[77] is not observed since the PP/ATH/CNT perform better and provide lower HRR and PHRR and higher Flameout time. The time to ignition increase mainly affect by the addition of Aluminum Hydroxide and Magnesium Hydroxide, the CNT in the system mainly contribute to the char

forming progress and the char effectively withhold the dripping to achieve UL-94-V0 in vertical burning test.

2.4 Conclusion

We have shown that the addition of certain particles like CB, CNT, Graphene, ATH and MDH could enhance thermal conductivity of polypropylene. The thermal coefficient could be achieved 0.65W/m*K and 0.58W/m*K by CNT and Graphene. The effect of mix CB, CNT and Graphene is not efficient in the PP blends, where single kind Carbon base filler proved to provide more consistent dissipation path which is consistence with the simulation result. The addition of ATH could hardly increase thermal coefficient until the loading of 30%wt. Combine these two factors, we developed PP/ATH/CNT and PP/ATH/MDH/CNT nanocomposites as the candidate for the polymer heat exchanger. PP/ATH/CNT and PP/ATH/MDH/CNT nanocomposites performed good thermal coefficient that as high as 1.0W/m*K and 1.1W/m*K, respectively. These result, which could not be accomplished by the single carbon nanotubes or metal based fillers, is comparable to the requirement of the polymer heat exchanger and other usage in automobile.

The mechanical measurement showed that the toughness and tensile strength decrease dramatically after the amount of ATH increased to 30%. The single filler as Graphene and CNT proved to have at least 20% high tensile strength and tensile strain, the toughness could achieve even higher to 30% increase compare to other filler combination indicate the Graphene and CNT could be a better single filler rather than the mixture of them.

Through SEM and EDAX characterization, we found that even though high amount of particles were blended in the matrix, a high degree of exfoliation could be obtained with ATH, MDH and CNT particles.

Cone Calorimetry measurement was conducted for the nanocomposites to analysis the flame retardant properties. Nanocomposites with PP/ATH/MDH/CNT and PP/ATH/CNT showed a dramatic decrease in heat release rates and pass UL-94-V0 test. The time to ignition of the nanocomposites decreased compare to virgin PP and the flameout time have surpassed the PP by a factor of 3, indicating that the addition of the ATH/MDH/CNT rendered the flame retardant of the nanocomposites.

The images of the char residue indicated the formation of a rigid char layer formed in these burning process of the nanocomposites which reduced the flow of gases and keep the samples from the heat sources while maintain low temperature to keep nanocomposites flame retardant.

Figure 2.1 A C.W. Brabender instrument, type Intelli-Torque Plasti-Corder

Figure 2.2 Hot Press instrument from Carver.

Figure 2.3 Quick Thermal Conductivity Meter (QTM500)

Figure 2.4 Instron Tensile Tester (Model: 5542)

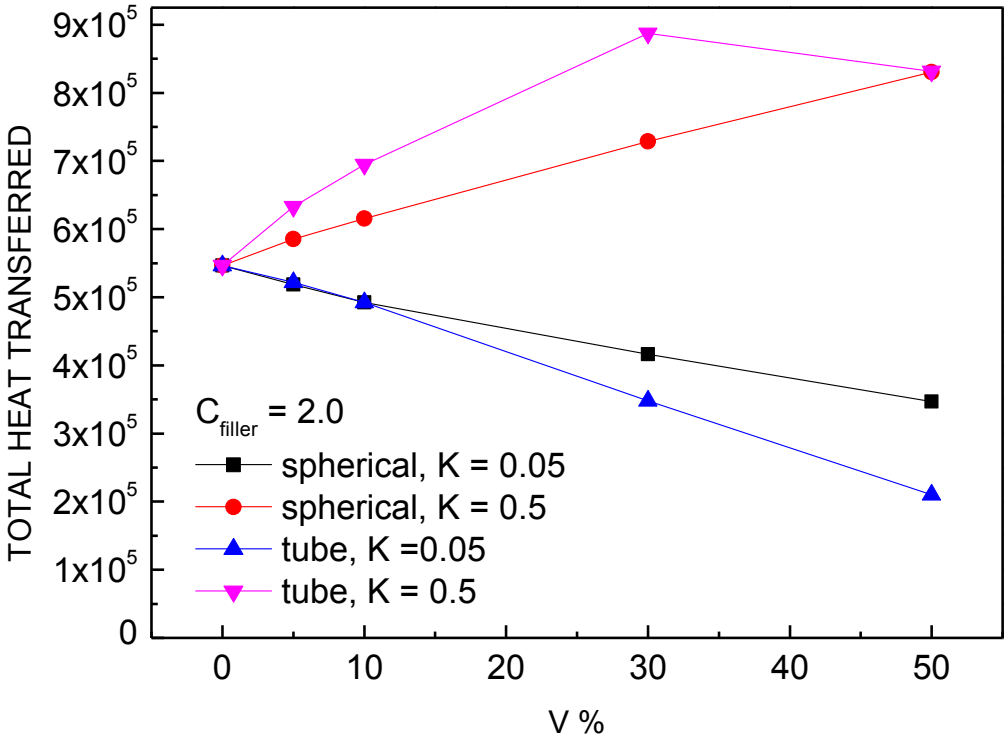

Figure 2.5 The simulation of heat transfer in polypropylene matrix of different shape of the fillers as a function of volume ratio of the filler.

(a)

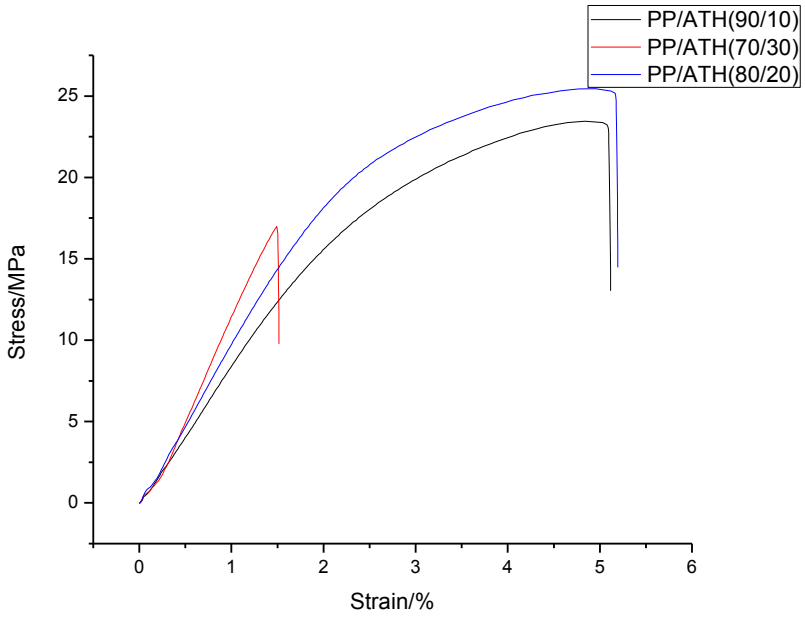

(b)

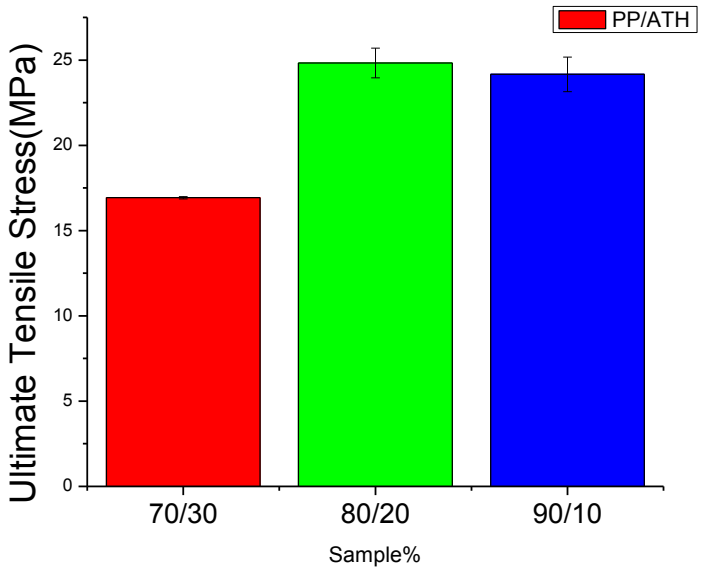

Figure 2.6 (a) Tensile curve of PP/ATH composites with loading from 10% to 30%; (b) the ultimate tensile strength of the tensile test of PP/ATH composites.

(a)

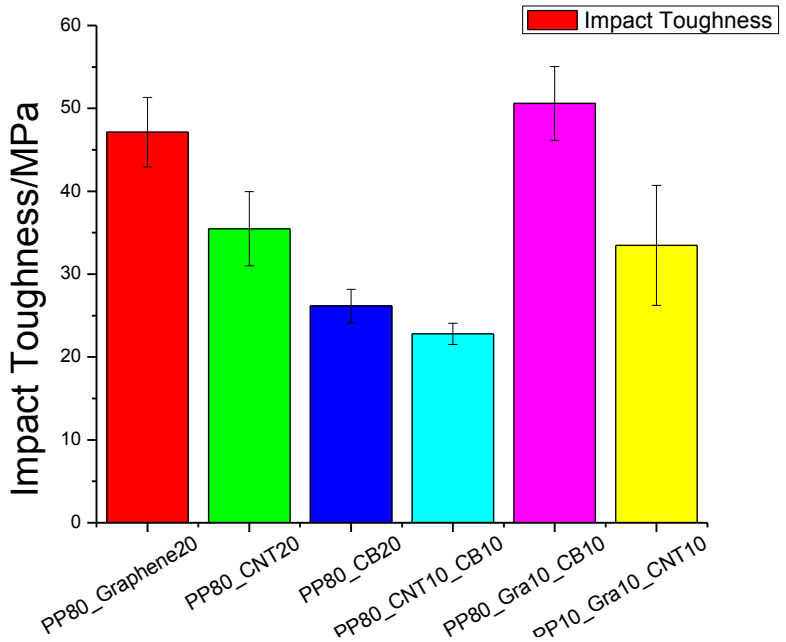
Impact Toughness
Impact Toughness/MPa
60
50
40
30
20
10
0
PP80_Graphene20
PP80_CNT20
PP80_CB20
PP80_CNT10_CB10
PP80_Gra10_CB10
PP10_Gra10_CNT10

(b)

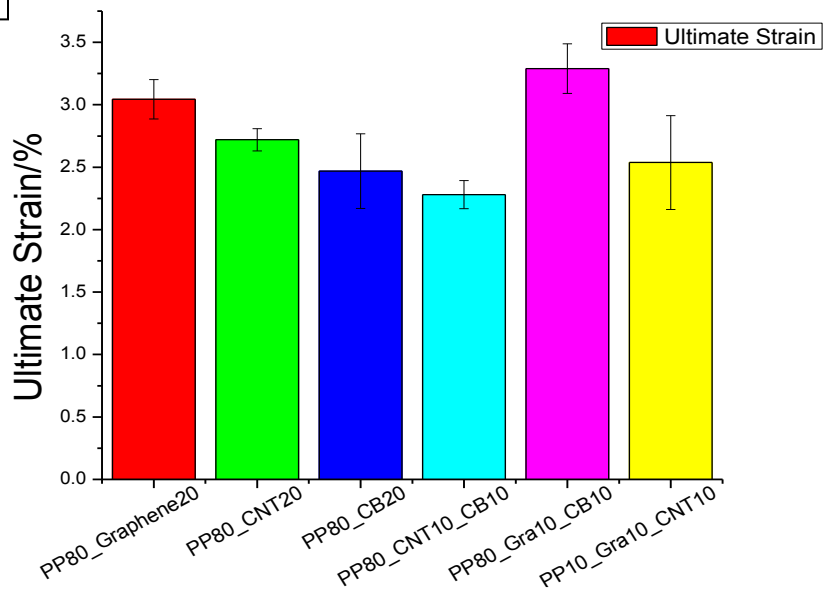
Ultimate Strain
Ultimate Strain/%
3.5
3.0
2.5
2.0
1.5
1.0
0.5
0.0
PP80_Graphene20
PP80_CNT20
PP80_CB20
PP80_CNT10_CB10
PP80_Gra10_CB10
PP10_Gra10_CNT10

(c)

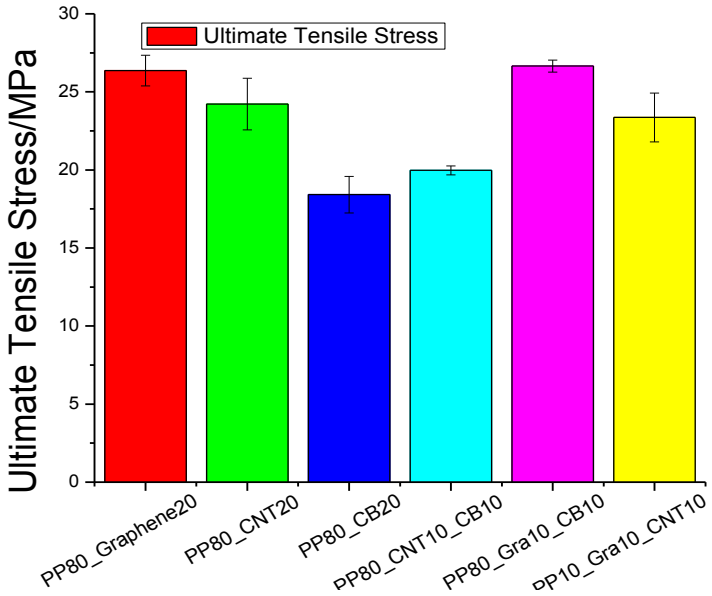

Figure 2.7 (a) Impact toughness from the tensile test of PP with carbon additives. (b) Ultimate tensile strain of the PP nanocomposites; (c) Ultimate tensile stress of the PP nanocomposites.

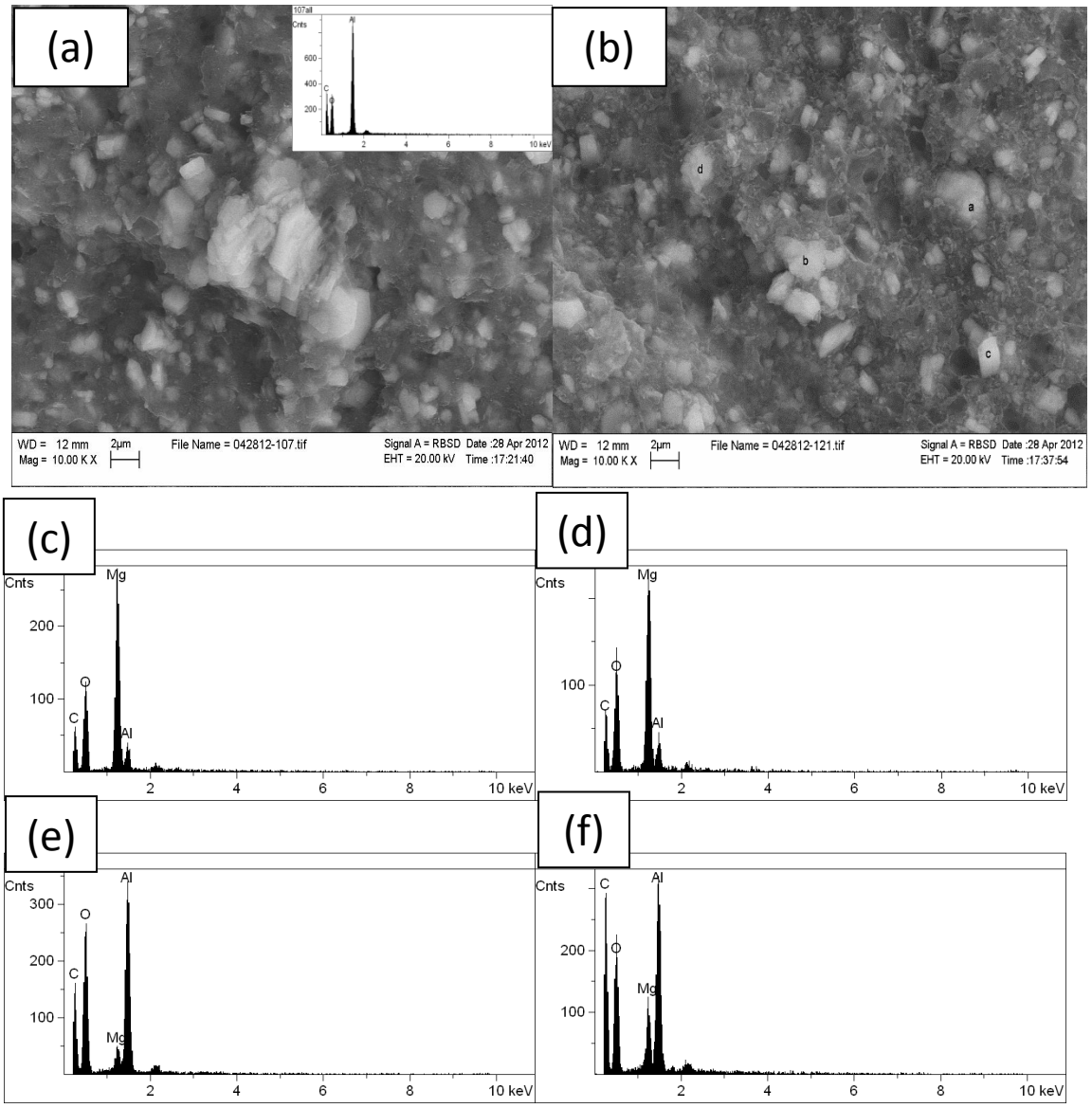

Figure 2.8 SEM images for PP nanocomposites with the concentration of (a) PP/ATH/CNT (40/50/10); (b) PP/ATH/MDH/CNT (40/30/20/10); (c)-(f) EDXS of PP/ATH/MDH/CNT (40/30/2010) for the four different region.

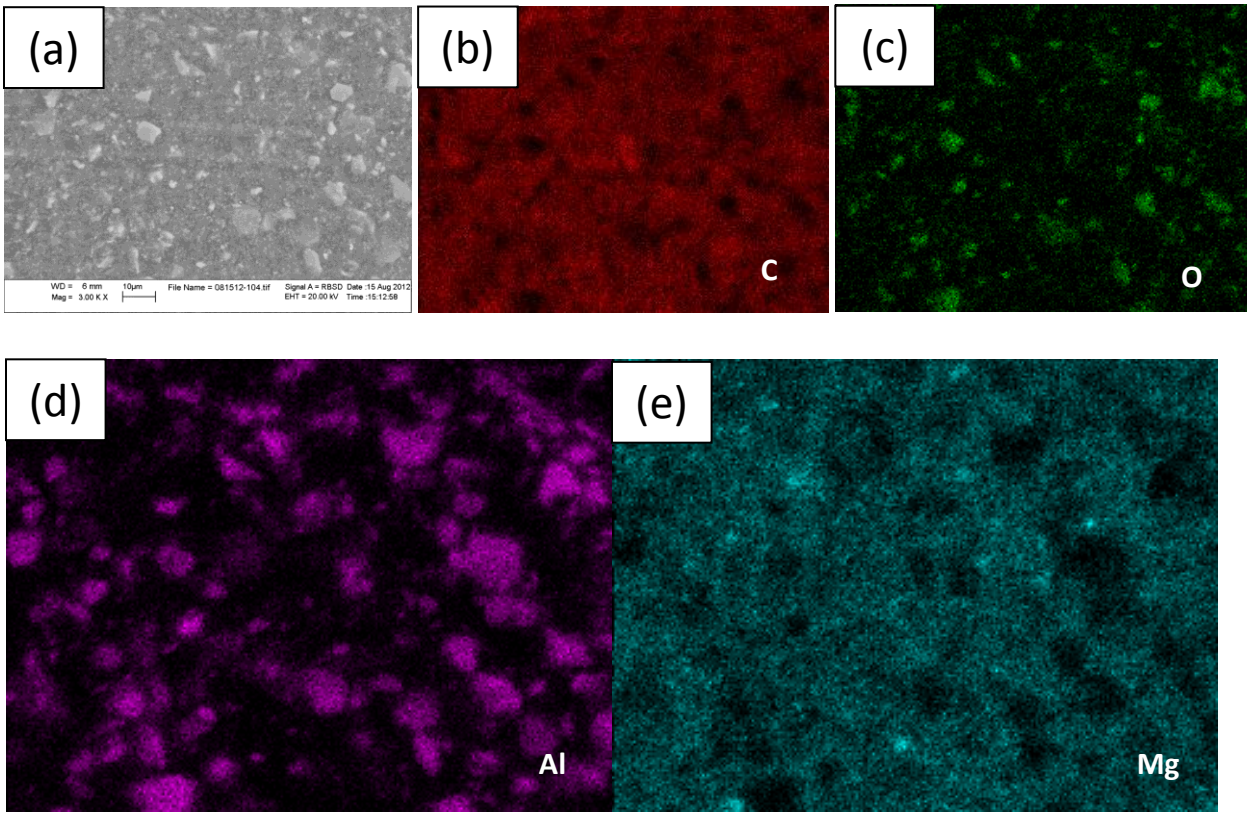

Figure 2.9 Mapping and SEM image of PP/ATH/MDH/CNT (40/30/20/10): (a) is the SEM image, (b)-(e) is the mapping of Carbon, Oxygenium, Aluminum and Magnesium.

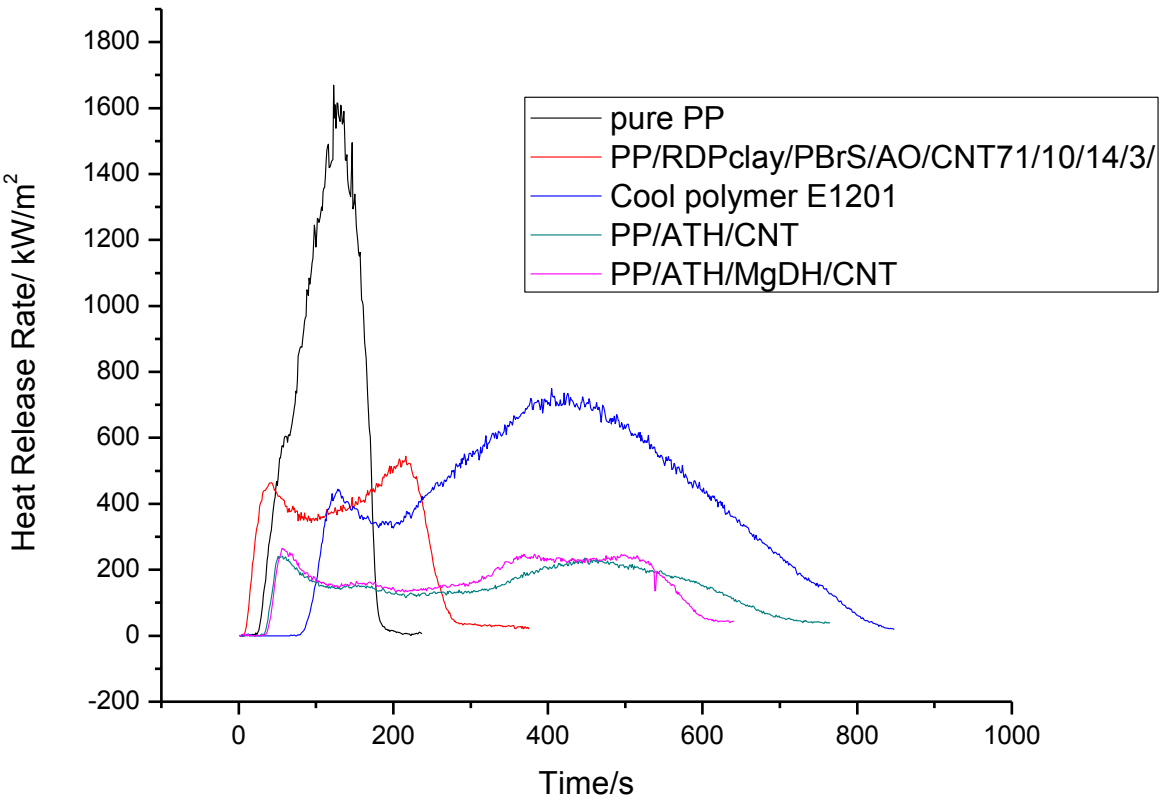

Figure 2.10 The effects of addition ATH and MDH on Heat release rate in Polypropylene matrix at 50kW/m2.

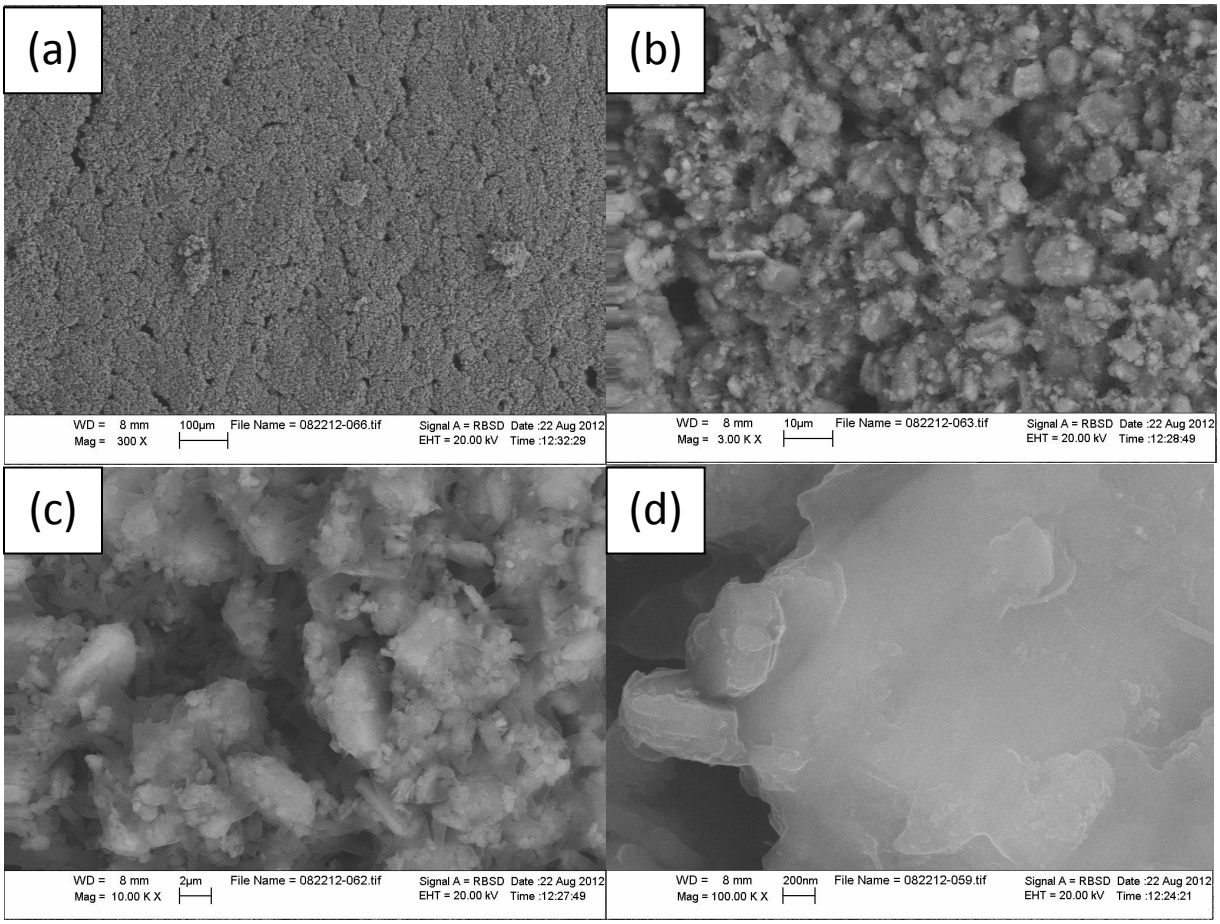

Figure 2.11 SEM images of Char samples of: (a-b) PP/ATH/MDH/CNT and (c-d) PP/ATH/CNT.

UL-94

Ranking	Description
HB	Slow burning on a horizontal specimen; burning rate <76 mm/ min for thickness <3 mm
V2	Burning stops within 30 s on a vertical specimen, drips of flaming particles are allowed
V1	Burning stops within 30 s on a vertical specimen; drips of particles are allowed as long as they are not inflamed
V0	Burning stops within 10 s on a vertical specimen; drips of particles are allowed as long as they are not inflamed

Table 2.1 Classifications according to the UL-94 vertical burning standard

Sample	Weight Ratio (%)	Thermal Conductivity(W/m*k) at 23°C
Pure Polypropylene	100	0.22
PP/ATH	90/10	0.30
PP/ATH	80/20	0.30
PP/ATH	70/300	0.45

Table 2.2 The thermal conductivity of PP/ATH composites

Sample	Weight ratio (%)	Thermal Conductivity(W/m*k) at 23°C
Pure PP	100	0.22
PP/CB	80/20	0.36
PP/CNT	80/20	0.65
PP/Graphene	80/20	0.58
PP/CB/CNT	80/10/10	0.46
PP/CNT/Graphene	80/10/10	0.44
PP/Graphene/CB	80/10/10	0.46

Table 2.3 Thermal conductivity test of different ratio of Polypropylene nanocomposites with carbon black, graphene and CNT.

Sample	Weight Ratio (%)	Thermal Conductivity(W/m*k) at 23°C
Pure PP	100	0.22
PP/ATH	50/50	0.62
PP/MDH/ATH	50/30/20	0.71
PP/ATH/MDH/CNT	40/30/20/10	1.1
PP/ATH/CNT	40/50/10	1.0

Table 2.4 Thermal conductivity test of the combine fillers polypropylene composites.

Sample Name	Weight Ratio (%)	Time to Ignition(s)	HRR(kW/m^2)	PHRR(kW/m^2)	Flameout(s)
PP	100	33	459	1055	190
PP/ATH/CNT	40/50/10	38	156	242	731
PP/ATH/MDH/CNT	40/30/20/10	39	182	265	606
PP/AHT/MDG/Graphene	50/25/20/5	45	127	175	528

Table 2.5 Cone Calorimetry test for PP nanocomposites.

Sample Name	Weight Ratio (%)	UL-94 Level
Pure PP	100	Fail
PP/CNT	96/4	Fail
PP/MDH/ATH	50/30/20	V1
PP/ATH/MDH/CNT	40/30/20/10	V0
PP/ATH/CNT	40/50/10	V0

Table 2.6 UL-94 Vertical Burning Test for PP nanocomposites.

CHAPTER 3. *Thermal and Mechanical Properties of Graphene/Polymer Nanocomposites*

3.1 Introduction

Biofuels are currently being introduced as "green" replacements for fossil fuels in numerous applications including transportation and home heating. One major drawback of these fuels is their high acidity, which makes them corrosive and limits their usefulness in metal boilers or storage tanks. Consequently there has been intense research in finding a suitable, non-corrosive, heat resistant, and yet thermally conductive and malleable material for replacing the metal heat exchangers and fuel storage tanks [3, 4, 6, 15, 64, 78-80]. Polypropylene, (PP) a crystalline polyolefin elastomer has been proposed due to its high corrosion resistance[81], toughness and ease of processing. On the other hand, PP is also extremely flammable, and has a poor thermal conductivity coefficient typical of most polymers, k=0.2 W/(m·K). In order to overcome these difficulties numerous attempts at compounding PP with various nanoparticles were reported that produced compounds which were either thermally conductive [67, 69, 82] or flame retardant [5, 83, 84]. Yet in order to be useful for the production of heat exchange units, the compound must have a higher thermal coefficient, while simultaneously being flame resistant and processable.

Numerical simulations of the heat exchange parameters in a typical boiler found that the efficiency was always limited by the component with the lowest thermal coefficient, which in a metal heat exchanger is the gas-side convective coefficient.[16, 17]. In the case of metal heat exchangers, the thermal coefficient of the metal body was approximately $k \geq 10 W/(m \cdot K)$, but that of the flu gas was only $k \approx 2.0 W/(m \cdot K)$. Hence the materials of the heat exchange unit could easily be replaced by a nanocomposite with a coefficient slightly larger than 2.0 W/(m·K) without loss of efficiency in the performance of the unit.

Despite the apparent simplicity, it still required nearly an order of magnitude increase of the polymer thermal coefficient. Numerous nanoparticles exist, i.e. nanotubes, carbon black, graphene, or metallic particles, which have been shown to increase the electronic conductivity [48-51], but increasing the thermal conductivity has proven far more difficult. Electronic conductivity can be accomplished when the percolation threshold of the particle is reached and the conducting components are at least in point contact[73]. Point contact, on the other hand, is insufficient for phonon transfer which is required for thermal conductivity. Phonon transfer is a more complicated process which requires proper coupling between the nanoparticle structure and the polymer matrix over much larger contact areas.

Here we show results of nanocomposites formed with PP and nanoparticles which in themselves are thermally and electrically conductive, but among which only one type, Graphene Nanoplates (GNPs), was actually suitable for engineering a nanocomposites that meet the multiple and sometime conflicting conditions described. Using a series of complementary techniques, i.e. small angle and wide angle x-ray scattering (SAXS, WAXS), dielectric spectroscopy, and thermal conductivity measurements, we propose a model to for the internal structure of the nanocomposites consistent with the observed structures.

3.2 Experimental Section

3.2.1 Materials

The Graphene Nanoplatelets (GNPs) were purchased from XG Sciences. The GNPs have an average thickness of approximately 15 nanometers and a typical surface area of 50 to 80 m^2/g. H5 and H25 were used as the average particle diameters of 5 microns and 25 microns. The particles were characterized using FTIR, Raman and TEM.

The multi-walled carbon nanotubes (MWCNTs) were provided by Cheap Tubes Inc. The lengths of the MWCNTs used in this study were 0.5-2.0μm which have a diameter of 30-50nm.

Copper Microparticles (Copper powder, <75um, 99%; Sigma Aldrich) were used as an additive to improve the thermal conductivity.

The matrix polymer used was Polypropylene (Resin 3825, Total Petrochemical, Houston, TX), the melt flow of which is 30g/10min and density is 0.905g/cc.

Compounding: A C.W. Brabender instrument, type Intelli-Torque Plasti-Corder was used to blend the nanocomposites. The blender was equipped with two screw-type roller blades in a heating chamber. The polymer pellets were first added to the chamber at a rotation speed of 20 rpm and temperature of 180°C. The GNPs or MWCNT were then inserted and mixed at the same rpm for 2 min. Either the GNPs or the MWCNTs were gradually added into the chamber, while blending. The entire mixture was blended at 100rpm for 15 min under nitrogen gas flow, which prevented degradation of the mixture from heat-induced oxidation. The mixing torque at 15min is recorded and the mixture was allowed to cool at room temperature and then

pelletized and molded in a hot press at T=180°C into the different shapes required for the thermal conductivity, mechanical tests and flame tests.

3.2.2 Thermal Conductivity

Thermal Conductivity tests were measured using Quick Thermal Conductivity Meter (QTM500) at 23°C. Molded samples of dimension 64mm×64mm×10mm were tested and the results quoted represent the statistical average of the measurements from 5 identical specimens.

3.2.3 Thermal and Mechanical Properties

Tensile Properties: Nanocomposite samples were molded into dog bone shapes, 1.5mm thick and 6.4 cm long, for use with the Instron Tensile Tester (Model: 5542) equipped with a 500N load cell and hydraulic pressure grip. The measurement was performed at a rate of 1mm/min and the young's modulus, tensile strength, tensile strain and impact toughness were analyzed from the acquired data. Specimens were molded from the hot press and tested according ASTM D638.

IZOD Impact: Notched Izod Impact tests were measured using TMI Impact tester (model 43-02) at23°C, 50%RH with 5.5J pendulum. The samples with dimensions 64mm×12.7mm×3.2mm were used according to ASTM D256. The statistical average of the measurements of 10 specimens was taken to obtain a reliable data with appropriate standard deviation.

Thermal gravimetric analysis (TGA): TGA was carried out on a TA Instruments Q50 analyzer to determine the decomposition process. A sample with mass between 10-15mg was put

in the crucible in the furnace and heated from 30 to 600°C at a rate of 10°C/min under 20mm/min nitrogen atmosphere.

Dynamic mechanical analysis (DMA): The DMA test was performed on a DMA Q800 from TA Instruments in the single cantilever mode at a fixed frequency of 1 Hz. The samples were molded in the dimensions 40mm×10mm×2mm. The measurement temperature range was from -30°C to 110 °C with a heating rate of 3°C/min; the storage modulus and tan δ were recorded as a function of temperature.

Differential Scanning Calorimetry (DSC): Thermal properties were studied using a TA Instruments Q2000 under a 20mm/min nitrogen atmosphere. Samples of about 10mg were heated at a rate of 10°C/min from -30 to 180°C. The degree of crystallinity was calculated using the following equation:

$$\chi = \frac{1}{1-\text{wt}\%}\frac{\Delta H_c}{\Delta H_f^0}$$

Where χ the percentage of crystallinity in the polymer matrix, wt% is the weight ratio of the GNPs, and ΔH_f^0 is the theoretical crystallization enthalpy of the polymer matrix if it was 100% crystalline.

3.2.4 Morphology of the Nanocomposites

Raman Spectroscopy: Raman spectroscopic measurements were carried out using a Raman microscope (Renishaw, inVia, UK) in the range of 3000 to 1000 cm^{-1}.

Synchrotron X-ray Characterization: WAXD and SAXS measurements were carried out at the Advanced Polymers Beamline (X27C, λ = 0.1371 nm) in the National

Synchrotron Light Source (NSLS), Brookhaven National Laboratory (BNL). Aluminum oxide (Al2O3) and a silver behenate (AgBe) standard were used to calibrate the detector distance for WAXD and SAXS, respectively. A 2D MAR CCD X-ray detector (MAR-USA) with a resolution of 1024X1024 pixels (pixel size = 158.44μm) was used to acquire 2D-WAXD and 2D-SAXS images. For SAXS, the exposure time was 120s and the sample to the detector length was 1689mm. For WAXS, the exposure time was 300s and the sample to the detector length was 169mm.

2D-WAXS and SAXS patterns were integrated with proper orientation correction to obtain their corresponding scattering profiles as a function of $|q| = 4\pi \sin\theta/\lambda$, where q is the first-order scattering vector, λ is the wavelength of X-ray beamline (0.137nm), and 2θ is the scattering angle. For integrated 1D-WAXD curves, a multipeaks Gaussian fitting was used to obtain the areas of crystalline and amorphous peaks.

The overall crystallinity X_C was calculated by

$$X_C = \frac{\sum A_{cryst}}{\sum A_{cryst} + \sum A_{amorp}}$$

Where $\sum A_{cryst}$ and $\sum A_{amorp}$ are crystalline and amorphous phases, respectively.

Scanning Electron Microscopy (SEM): The distribution of GNPs, CNT was imaged using JEOL 7600F Analytical high resolution SEM at the center for Functional Nanomaterials (CFN), Brookhaven National laboratory, Upton, NY. Cross section PP/GNPs, CNT specimens were placed on a conductive, double sided, carbon adhesive tab and imaged at 5 kV accelerating voltages using a secondary electron imaging (SEI) detector. Ten nanometers of gold were coated on the surface of the specimens in order to make the specimens conduct.

Transmission Electron Microscopy (TEM): TEM images of the GNPs particles were obtained by placing drops of the particles, suspended in toluene, on Cu TEM grids, and air dried. TEM of the nanocomposites was conducted on thin sections obtained from the nanocomposites. Sections were cut with a diamond knife mounted in a Reichert-Jung Ultracut E Ultramicrotome. The sections were floated onto Cu mesh grids from the surface of deionized (DI) water and left to air dry. FEI Tecnai 12 BioTwinG^2 TEM was used to observe the sections and digital images were obtained from an AMT XR-60 CCD digital camera system.

3.2.5 Combustion Properties

Vertical Oxidative Flame Test: A vertical burning chamber purchased from Underwriters Laboratories Inc. was used to assess flammability under oxidative atmosphere. Samples of dimensions 125mm×13mm×5mm were molded and tested using the protocol established by ASTM D3801 UL94 V0. Ten specimens were preconditioned with 50% relative humidity for 48h at 23°C. A flame of 20±2mm was applied to the sample for 10s and then t_1, the time the sample took to self-extinguish was measured. The flame was reapplied for another 10 s and t_2 the time to extinguish the flame was measured. The criteria for achieving V0 could require that either t_1 or t_2 be less than 10s. The results reported are the average of 5 samples for each type of sample.

Limited Oxygen Index (LOI): Limited Oxygen Index (LOI) was conducted by Stanton Redcroft FTA Flammability Unit. Sample of dimensions 100mm×6.5mm×3mm were molded and tested according to ASTM D2863.

Heat and Mass Loss Rates: The heat release rate (HRR) and mass loss rate (MLR) of each sample were tested using cone calorimetry at Israel Chemistry Limited Industrial Products

(ICL-IP, Ardsley, NY). The samples were made by molding the composite into a 75mm×75mm×5mm square. Thin aluminum foil was used to wrap all sides of samples except for the upper face to avoid the burning splash. The samples were then exposed in ambient atmosphere, to an external radiant flux of 50kW/m^2, perpendicular to the sample surface and the HRR and MLR were measured as a function of exposure time. The standard uncertainty of the measured heat release rate (HRR) was ±10%. The cone calorimetry test was conducted according to the ISO 5660 protocol.

3.2.6 Gas Permeability

The O_2 permeability was measured with ASTM Standard D 1434-82(2009)e, procedure V and a Custom Scientific Model CS-135. The values of the O_2 transmission rate were obtained at 23°C and 15.0 psi.

3.2.7 Dielectric Measurements

Conductivity measurements were made using Dielectric measurement setup purchased from Wayne Kerr Electronics, UK (Precision Impedance Analyzer 6500 B series. The measurements were made in the frequency range 100Hz- 1MHz at 23°C. The samples were hot pressed at 180°C between two brass electrodes. The electrodes were 20mm in diameter and 1-2 mm thick.

3.3. Result and Discussion

3.3.1 Characterization of the GNPs

3.3.1.1 Transmission Electron Microscopy (TEM)

We first characterized the GNPs particles. TEM images of the GNPs particles were obtained by placing drops of the particles, suspended in toluene, on Cu TEM grids, and air dried. The images are shown in **figure 3.1**. From the figure we can see that both types of particles exfoliate into single sheets in toluene and that the H25 particles are much larger than the H5 particles, or approximately, 25microns and 5 microns respectively.

3.3.1.2 Raman Spectroscopy

RAMAN spectra were obtained from the GNPs using excitation of 514nm. From the **Figure 3.2a** we find that the first peak (D band) at 1346cm^{-1} and 1355cm^{-1} for H5 and H25, respectively, could be ascribed to the disorder or defect structure of GNPs. The second peak (G band) at 1569cm^{-1} and 1578cm^{-1} is due to the sp^2 carbon vibration in the graphitic lattice.[85] The intensity ratio (I_D/I_G) of the H5 was about 0.08 and the ratio of H25 was 0.12. The third peak (2D band) at 2693 for H5 cm^{-1} and 2712 cm^{-1} for H25 corresponds to the overtone of the D band which is sensitive to the number of graphene layers. Malard [86] reported that for samples with multiple layers the peak develops a shoulder, such as the one observed for H25. For samples with one or two layers, a symmetric peak, such as the one observed for H5 at 2693 cm^{-1} occurs.[87] This analysis is consistent with the TEM images shown above where the H5 samples appear to consist of one or two layers whereas the H25 have multiple layers. Multiple layers

require exfoliation and higher shear which make it more difficult to disperse within the polymer matrix. Standard peaks corresponding to 514nm excitation in GNPs are clearly visible in both samples, confirming that they have the expected GNPs conformation. From these data we can conclude that the particles have relatively small defect components, with H5 having the lowest Id/Ig quotient.

3.3.2 Thermal Conductivity of nanocomposites.

We first produced a set of PP nanocomposites with different nanoparticles such as Cu, CNT, and carbon black, which are all known to have a high thermal and electrical conductivity. The thermal conductivity measured for nanocomposites samples, 10mm thick, is tabulated below for compositions containing 5-30% particles. From the table we can see that the spherical particles, such as CB and Cu, have only a minimal effect on the thermal conductivity, even at loadings in excess of 30%. In the case of MWCNT, from the table1, we can see that even for the highest concentrations, which are far above the percolation thresholds, the highest coefficient that can be reached is k=0.57W/m*k, which is still far below the required minimum value of k=2.0W/m*k. From the table we can see that the compounds with GNPs particles had the highest thermal coefficients for concentrations around 20%; H25 has a coefficient of k=0.83 W/m*k at a loading of 25%, while H5 achieved a value of k=1.12W/m*k at a loading of 20%. Hence GNPs appeared to be the most promising approach to increase the thermal coefficient.

We therefore also tested PP/GNPs nanocomposites of higher concentration in order to determine at which loading the required value of k=2.0 W/m*k could be reached. The data is tabulated in **Table 3.2 and 3.3** for both H5 and H25.

In **Figure 3.3** we plot the thermal conductivity for these two particles as a function of loading, Φ, where we find a direct linear relationship given by the following two equations for H25 and h5 respectively.

Equation 3.1: $y= 3.65 \Phi +0.21$ (for H25) $R^2=0.985$

Equation 3.2: $y=4.77 \Phi +0.16$ (for H5) $R^2=0.999$

The slope of the curve for H5 is somewhat steeper than H25 indicating that H5 could produce a higher reading for the thermal coefficient with lower GNPs loading in the PP matrix studied. From the figure we can also see that the thermal conductivity, equivalent to that of the carrier gas in the heat exchange unit, k=2.0 W/m*k, can be obtained with a minimum filler concentration of 40% and 50% for H5 and H25 respectively.

In order to compare more directly whether CNT and GNPs nanoparticles achieved equivalent results, we substituted 5% CNT for 5% H5 in PP nanocomposites having a total of 30% and 40% filler concentration. From the table we find that in both cases the composite with only H5 had slightly higher coefficients than those with 5%CNT, confirming that for equivalent loading the GNPs particles performed better than CNT. Furthermore, despite the much larger aspect ratio of the CNTs, no synergy was established such as the one reported by [88] for mixtures of clays and CNTs.

3.3.3 Mechanical Properties

3.3.3.1 Torque measurement from C.W.Brabender

The tensile properties are another essential component in choosing the appropriate material. Heat exchange units need large surface areas in order to increase their efficiency in interacting with their environment. These can be achieved by forming heat exchange coils, which require high ductility in order to extrude and process the nanocomposite. Hence we monitored the torque required to process the different nanocomposites. In **Figure 3.4**, we show the torque of the twin screw extruder as a function of the GNPs concentration, where we can see that a roughly linear increase occurs as a function of concentration, but the absolute values even at 50% are still reasonable. It is interesting to note though that in this case, the slope of the increase is larger for the H25 than the H5 compounds, indicating that the increased dispersion observed for H5 is also responsible for higher ductility at larger loading.

3.3.3.2 Tensile Test

Tensile tests were therefore performed only on samples containing H5, as a function of filler concentration. The results are shown in **Figure 3.5** and the parameters of the curves are tabulated in **Table 3.4**. From the figure we find that a large decrease in tensile toughness and occurs at a concentration of 1% and decreases linearly up to a loading of 10%, after which a plateau is reached and minimal further change occurs even at a loading of 50%. The tensile and storage moduli, on the other hand, both have are nearly constant values for loading less than 10% and increase almost linearly for concentrations up to 50%. Hence reasonable mechanical

properties and processability could be obtained at a loading of 40%, which is the minimum required to obtain the desired thermal coefficient of k=2.0W/m*k.

3.3.3.3 IZOD impact test

The IZOD impact parameter was also measured and the results are shown in **Figure 3.6(a).** From the figure we see that it follows the same trend as the toughness shown in **Figure 3.6(b)**. The IZOD impact parameter initially decreases linearly, to 40% of the PP homopolymer value at an H5 concentration of 10%wt, and then the value plateaus and remains constant for loading up to 50%wt. Hence the filler concentration, $\Phi \approx 0.40$, which produces the PP nancomposite with the desired thermal coefficient, has nearly the same IZOD factor and toughness as the formulation containing only $\Phi \approx 0.10$ filler. This is consistent with the results shown in figure 4 where the torque required to mix this formulation is only 30% higher than that required for the $\Phi \approx 0.10$ mixture. Hence this formulation has both acceptable mechanical properties, as well as being easily processed.

3.3.4 Morphology of structures in Nanocomposites.

3.3.4.1 Transmission Electron Microscopy (TEM)

TEM cross sections from nanocomposites containing 40% filler are shown in **Figure 3.7**. In **Figures 3.7a** and **3.7b** we show images from compounds made with H5 and H25 respectively. From the figure we can see that the H5 GNPs is exfoliated and dispersed well within the PP matrix. On the other hand the H25 series does not mix well, and is seen to form multi-layer

tactoids. This effect is mainly due to the size of H25 which is much larger and agglomerates easily. In **Figure 3.7c** we show the morphology of a sample containing 5%CNT and 35% H5. The two types of particles were mixed in order to determine whether a synergy could be established where the CNTs would bridge the H5 platelets thereby establishing new conduction pathways and enhancing the thermal conductivity of the nanocomposite. Despite the fact that the CNTs and the GNPs were initially mixed together before addition to the Brabender extruder, the TEM images of the sample indicate that they phase segregated within the compound. Hence regions with distinct platelet morphologies similar to the one shown in **Figure 3.7a** were observed to coexist with regions containing only CNTs such as the one shown in **Figure 3.7c**. The morphology observed is consistent with the reduction in the thermal conduction coefficient observed previously when 5% CNT was substituted for 5% H5 in the sample contain total concentration of 40% nanofiller, and confirms the observation that CNTs are less efficient at thermal conduction than the H5 GNPs.

3.3.4.2 Scanning Electron Microscopy (SEM)

SEM images were obtained from the fracture surfaces following the IZOD impact test. **In Figure 3.8** we compare the surfaces of nanocomposites containing 20% H5 and H25 platelets. In the case of the H5 nanocomposites we see that the platelets are well aligned and dispersed uniformly within the polymer across the interface. In the case of the H25 sample, regions with high platelet concentrations are seen within areas of much lower concentrations, consistent with the agglomerated morphology observed with TEM. When compared to the unfilled polymer surface, both nanocomposites surfaces had higher concentrations of micro cracks, consistent with the large decrease in toughness shown in **Figure 3.6**. Yet when compared to each other, fewer

cracks were observed in the H5 sample, consistent with the improved processing parameters observed in **Figure 3.4**.

3.3.5 Thermo mechanical characterization

3.3.5.1 Dynamic mechanical analysis (DMA)

In **Figure 3.9** and **Table 3.5** we show the storage and loss moduli of the PP/H5 nanocomposites as a function of temperature for different GNP concentrations. From the figure and table we see that the storage modulus decreases rapidly with increasing temperature, while the peak in the tan delta traces indicate that the glass transition of the nanocomposites remains relatively contestant at T=14°C, or the value of unfilled PP, for all GNP filler concentration studied. This indicates that the PP chains do not adsorbed strongly to the GNP, and hence no suppression of segmental motion occurs which would increase the glass transition. The storage modulus at room temperature is plotted in **Figure 3.9(c)** where we find that it observes the same linear increase with GNP loading as the tensile modulus, with the two quantities having a relative same result. In **Figure 3.9(d)** we also plot the storage modulus at T=100°C as a function of filler concentration. From the figure we find that in this case the modulus increases more rapidly, or as a power law in concentration. Hence the addition of the GNP is more effective of improving the mechanical properties at elevated temperature than in ambient. This factor can be beneficial in preventing dripping when the material is exposed to flame, as is discussed below.

3.3.5.2 Thermal gravimetric analysis (TGA)

TGA analysis was performed to further understand the degradation process of polymer nanocomposites under different weight ratio of GNPs. Pure GNPs are extremely thermally stable

with less than 4% mass loss for temperatures of at least 500°C. In the case of the nanocomposites addition of GNPs slightly improves the thermal stability relative to PP. The results of TGA analysis, where we plot the temperatures of the maximum weight loss rate (inflection point,T_{max}) and the weight loss onset temperature($T_{10\%}$) are summarized in **Figure 3.10** and **Table 3.6**. From the table we can see that the decomposition temperatures increase from approximately 380°C for pure PP to on 414°C with the addition of 10% GNPs, but increasing the concentration of GNPs does not increase further the decomposition temperature. This enhancement of the thermal stability of the PP/GNP results from the interaction between the PP matrix and the GNP. The surface of the GNP absorbs the free radicals produced in the decomposition of PP and restricts the mobility of the polymer molecules, which retards the degradation of the PP/GNP.[89, 90] The majority of the PP/GNPs have the same T_{max} indicates that the addition of GNPs mainly acts as a physical barrier in the polymer nanocomposites up to a composition of 50/50. Above that concentration the high loading of GNPs adversely affects the compatibility of the polymer and additive, resulting in a reduction of T_{max}.

3.3.5.3 Differential Scanning Calorimetry (DSC)

The DSC traces for the PP/GNPs nanocomposites, obtained at a heating rate of 10 degrees per minute, are shown in **Figure 3.11** and summarized in **Table 3.7**. Compared with the pure Polypropylene polymer matrix, the melting temperatures of the nanocomposites were relative same for different concentration of GNPs (H5). Hence the influenced of the GNPs (H5) on the melting point was minimal, indicating that the surface interaction between the GNP and the matrix was not strongly attractive. From the DSC curves we can also estimate the influence of the GNP on the degree of crystallinity, where we can see that the degree of crystallinity is

decreased with increasing H5 GNP concentration. Hence the GNPs do not serve as increased crystalline nucleation sites, blocking the growth of crystalline structures in the nanocomposite. This phenomenon is also consistent the lack of strong interactions which would results in adsorption of the PP chains to the GNP.

3.3.6 Synchrotron X-ray Characterization.

It is known that the crystal structure of the matrix has a key role in determining the properties of polymer-based composites. WAXS spectra was obtained on all the samples in order to investigate the crystal structure of the bulk samples. (**Fig 3.12**) From the figure we can see that the peaks corresponding to the alpha structure are clearly visible, but have different relative peak area. A fitting procedure was applied to all the WAXS patterns in order to measure the degree of crystallinity. According to the method proposed by Hindeleh and Johnson[91], experimental WAXS spectra were produced by convolution of Lorentzian functions. In **Table 3.8** we showed the degree of crystallinity as a function of GNPs weight ratio from 0.7 Å-1<q< 2.1 Å-1, where we find that the degree of crystallinity remains high and relatively constant for all the samples. Hence the addition of graphene does not affect the crystallinity of PP even at loadings as high as 40%. The peaks observed in **Figure 3.12** correspond primarily to the α-phase, which was previously shown to nucleate readily on the platelet surfaces at lower concentrations. No peak was observed, even at the highest loading for β crystal (300), to indicate the presence of a β-phase, as reported by Xu, Chen et al [92]for a pp nancomposite with low graphene volume fraction subjected to high shear rates. From the figure we can see though that the relative

amplitudes of the peaks area differ significantly from the spectra of PP homopolymer, where the ratio of intensities between the (110) and (111) orientation are 18.5% and 11% respectively.

In Table 8 and in figure 12 ,when graphene is added, we can see that the intensity of the (110) and (111) peaks increases to 28% and 17% compare to 18.5% and 11%, respectively for virgin polymer, while that of the (040), (130) and (041) peaks decreases with increasing graphene concentration, such that for the sample with 40% loading we find values of 6%, 9% and 10.5%, as opposed to 16%,13.5% and 16% for the unfilled sample. The (311) of the β-phase configuration overlaps with the (111) peak of the alpha configuration, but since we do not see the predominant peak at (300), this orientation is not probable. Hence from this data we can conclude that the graphene surfaces nucleate a somewhat different orientation of α phase. This feature becomes more pronounced as the GNP concentration increases and a larger volume fraction of the PP matrix is crystalized on the platelet surfaces. Hence this effect was not apparent in previous studies performed at concentrations below 10%.

SAXS spectra in Figure 13 were obtained in order to determine the effect of the graphene on the lamellar orientation. From the figure we can see that for the unfilled system a clear peak is observed corresponding to a lamellar spacing of $q=0.04Å^{-1}$. Xu, Chen et al reported on the presence of this peak at a loading of less than 10%, but from our data we find that when the loading increases to 10% , the amplitude of this peak is greatly decreased and at concentrations of 30% or higher it is nearly undetectable. These results indicate that the internal crystal structure can be very different for blends with high degree of loading. In this case most of the polymer is adsorbed in thin layers onto the platelet surfaces, which now constitute a significant fraction of the total volume. As has been shown previously [30] the platelet surfaces are very effective at nucleation of in plane crystal structure of the adsorbed polymer chains, and hence the

high degree of crystallinity measured by WAXS or DSC. On the other hand, the lamellar structure, which requires chain folding and long ranged order is disturbed by the presence of the GNP. Since the platelets do not have a preferred orientation, in the absence of shear, within the matrix, no longer ranged correlations are present which would produce a peak in the SAXS spectrum, as illustrated in **Figure 3.14**. It is interesting to note that the reduction in ductility normally associated with the introduction of nanoparticles, may be partially offset in this system by the increased ductility which results from disruption of the long ranged lamellar ordering. Therefore, after the initial reduction at low GNP loading, where the lamellar structure is still predominant, toughness remains relatively high and constant at higher concentrations where scattering from the ordered phase disappears.

3.3.7 Gas permeability properties

It has been previously demonstrated that high aspect ratio nanoparticles dispersed within a matrix, such as exfoliated clays, can block the diffusion of gas molecules and hence reduce the gas permeability of the nanocomposites[93-95]. Here we tabulate the results of the permeability for the PP/GNP compounds having 10 and 40% loading. From **Table 3.9** we see that the permeability is unchanged even at the highest loading. This effect is interesting since from **Figure 3.7 and 3.8** we find that the GNPs (H5) are exfoliated within the compound. The fact that the permeability is unaffected may be due to the open lattice structure of the GNPs which does not impede diffusion of small molecule gases. This open lattice may also be a factor in the enhanced thermal conductivity, since the open structure also allows penetration of the polymer molecules thereby facilitating phonon conductivity.

3.3.8 Flame Retardance

3.3.8.1 Deformation and oxygen consumption

The thermal conductivity of a material involves the steady state process of heat energy transfer, while flame retardance involves the ability of the system to dissipate heat rapidly from an approaching intense heat source. Heat exchange units are frequently positioned near open flame areas where the heating of the gases occur. It is therefore important to understand the response of the materials to both steady state and intense pulse heat sources. For instance, we must also determine the extent to which that the materials used are flame retardant, even though the temperature in the heat exchange unit itself is far lower than the ignition temperature of the polymer nanocomposite.

Flame retardance can be quantified in terms of the time it takes to extinguish a flame, without dripping, after a ten second exposure. If either t_1 or t_2 was less than 10s, then the sample was classified as V0 in the UL-94 test. Hence flame retardance requires the ability to both dissipate an intense heat pulse quickly in order to reduce temperatures below combustion, while at the same time decrease the reduction in modulus with temperature to prevent dripping.

The results for nancomposites with different GNPs/polymer ratios exposed to an open flame for ten seconds are tabulated in **Table 3.10**. From the table we find that even though PP drips profusely, dripping stops very quickly at concentrations of 10% or higher, even though concentrations of 40% or higher are required for rapid extinction of the flame.

From **Figure 3.9** we find that the major effect of the grapheme filler is to increase the viscosity at higher temperatures, which reduces dripping. The filler concentration of 10% where dripping stops also corresponds to the value where the increase in modulus at 120°C relative to that of pure PP, becomes significant. In order to further explore the mechanism for reducing the flameout time we measured the Limited Oxygen Index, which determines the rate of oxygen consumption during burning. The results are tabulated in **Table 3.11** where we find a small but steady increase in the amount of oxygen required for burning, which is consistent with a slower rate of combustion, but no dramatic change in the combustion reaction. Hence GNPs does not appear to be catalyzing a different reaction pathway. Rather, as loading increases, GNPs provides a barrier to oxygen penetration, while increasing the thermal dissipation of the heat, thereby reducing the rate of burning.

3.3.8.2 Cone Calorimetry

The reaction of a material to a rapidly approaching heat flux is best measured using cone calorimetry. Here we examined the rate of gasification in air of PP/GNPs nanocomposites as a function of weight ratio. In **Figure 3.15**, Video images of the combustion process reveal that for the higher loading samples, a char is observed which forms an elastic shell surrounding the sample the inflates during combustion controlling the release of the burning gases. Images of the chars are shown in **Figure 3.16**, where we can see that the PP homopolymer burns completely without char formation. Addition of H5 initiates char, which forms a solid shell for composites with loading of 10% or higher. The mass of the char residue in each case is consistent with the H5 fraction, hence the chars are mostly likely composed almost entirely of GNPs. GNPs is known to absorb and re-radiate the heat in the approaching front, thereby reducing the effective flux reaching the sample, and decreasing the combustion rate [10]. This can be seen from the

effect of the char on the heat and mass loss rates of the samples, plotted in **Figure 3.17**. The mass of char residue after the cone calorimetry is exactly same with the amount of GNPs which is consistent with TGA result that confirmed the char is mainly GNPs. The peak heat release rate (PHRR) of Polypropylene homopolymer is as high as 2045kW, the heat release rate (HRR) reaches a value around 659kW/m^2, while the mass loss rate is 15g/s. Addition of H5 reduces the PHRR continuously to nearly half its original value at a concentration of 5%, but only a minimal decrease in the Heat Release Rate (HRR) or mass loss (MLR) rates is observed. A significant change in the HRR and MLR profiles is observed at a concentration of 10%, where the HLR and MLR are reduced to 400kW/ m^2 and 10g/s.

The largest reduction occurs in the PHRR, indicating that combustion is greatly reduced. This is consistent with the decrease in oxygen consumption for 18.3% to 19.5% which also occurs at this concentration. Inspection of the morphology of the chars in **Figure 3.16** shows that for samples containing less than 10% H5 filler, the char is porous, while the char containing higher filler concentrations has a uniform, solid appearance. Hence, in addition to improved thermal conduction, the solid char surface also blocks diffusion of oxygen to the hot gases in the interior, impeding the rate of combustion.

The flame out time is strongly correlated to the mass loss rate. From **Table 3.12** and **Figure 3.17**, we see that an abrupt increase from 184sec for pure PP to 350sec for samples with 10% or higher loading of H5.The flame out time, as well as the HLR and MLR do not change significantly with further increase in H5 loading, as would be expected if the phenomena were a result of a percolated structure formed by the filler particles. This structure would at once increase heat conduction, while decreasing gas flow and hence reducing the rate of mass loss. Both of these effects would contribute strongly to the flame retardant behavior observed.

3.3.8.3 Time to Ignition

Cone calorimetry also measures the time to ignition of the sample from an approaching heat front. The time to ignition is an additional measure of the ability of the sample to dissipate heat, before the combustion temperature is reached. In contrast to the MLR or HLR, ignition occurs before char formation and hence is not related to the char structure. Therefore, decreased ignition times are known to occur in nancomposites[96] even when flame retardancy is increased. The time to ignition for PP/H5 nanocomposites obtained from cone calorimetry are plotted in **Figure 3.18** as a function of GNPs concentration. From the figure we can see that the time to ignition is initially decreased relative to that of the PP homopolymer for H5 filler concentrations of 5% or lower. A large increase occurs at a filler concentration of 10%, where the value becomes slightly larger than that of pure PP, and in contrast to the MLR and HLR values, the times to ignition continue to increase sharply up to about 30% after which a plateau is reached.

3.3.9 Electrical Conductivity Test

In order to understand the influence of the GNPs on the electrical properties of the nanocomposites, dielectric measurements of the samples were performed as a function of H5 concentration. The results are shown in **Figure 3.19**, where we can see that for low filler concentrations (less than or equal to 5%) the conductivity decreases exponentially, with frequency, as expected for an insulator. At a concentration of 10% the functional form, namely the exponential decrease function is similar, except that the zero frequency extrapolation is an order of magnitude higher. For a filler concentration of 20% we find a mixed mode function,

where the response is initially a plateau, followed by an exponential decrease at higher frequencies (above 10^5). For loading higher than 20% the response is constant with frequency, as would be expected for a good conductor. The DC conductivities, obtained from the readings at 100Hz, are plotted in **Figure 3.19** as a function of filler concentration. From the figure we can see that for filler concentrations larger than 10%, the DC conductivity increases nearly exponentially with filler concentration. From here we can discern that the percolation threshold for the GNPs fillers occurs at approximately 10%. The intrinsic conductivity of the PP matrix is poor, enhancement only occurs via direct electron transfer between GNPs, which occurs at higher loadings. Tunneling through thin layer of polymer is also possible at concentrations just below the percolation threshold, which may explain the deviation from a linear function with increasing frequency starting at 10% and the bimodal behavior at 20% between the low and high frequency regions.

3.4 Discussion

Comparing the results from **Figure 3.2** with those of **Figure 3.19 and 3.20**, we find that the increase in the thermal conductivity constant does not show an onset of a plateau at a filler concentration of 10%. In fact, the thermal conductivity is well fit by **Equation 3.1 and 3.2** throughout the entire concentration range studies, underscoring the fact that electrical and thermal conductivity arise from different physical processes. Electrical conductivity is a property mostly dependent on the nature of the GNPs particles, and occurs via electron transport when the GNPs are in direct contact. The properties of the matrix enter peripherally when electron tunneling occurs as the platelets come in increasingly closer proximity approaching percolation. On the other hand the thermal conductivity is a function of the phonon transfer between the GNPs platelets and the polymer matrix, which is dependent on the GNPs / polymer coupling as opposed to the GNPs/GNPs coupling. [97]has shown that in the case of GNPs the propagation of phonons may be affected by the surrounding medium. They showed that the open two dimensional lattice structure couples strongly to its environment and the nature of the substrate affects interfacial properties. Evidence for the open structure and good coupling with the polymer structure, is indicated by the lack of interference with the gas transport properties in the matrix. Clay or metallic platelets, of similar dimension as the GNPs, with good dispersion or exfoliation within polymer matrices are well known to prevent diffusion of gases. The close packed rigid lattice structure of the clays or metals act as barriers to the gas penetration, deflecting the gas molecules. This close packed rigid structure also prevents good mechanical coupling and phonon transfer with the polymer matrix.

Figure 3.21 is a linear plot of the electrical conductivity shown together with the time to ignition as a function of filler concentration. From the figure we find that initially the time to

ignition decreases at the lowest filler concentration, and begins to increase slowly for increased loading. The value for pure PP is recovered at a loading of 10% and increases continuously thereafter. The decreased time to ignition is a common phenomenon in filled systems, and posses problems even when the filler decreases the heat release and mass loss rates, or otherwise improves other flame retardant properties. The phenomenon has been explained as being due to a rapid increase in the local temperature near the filler as the heat front approaches and the lower heat capacity of the filler causes a more rapid increase in the local temperature. The poor conductivity of the matrix does not allow the heat to dissipate, leading to the decrease in time to ignition. In this case restoring and even increasing the time to ignition does seem to correlate well with the electrical percolation concentration. This indicates that thermal conductivity within a filled system may be subject to two time constants. When the system is subject to small thermal gradients (i.e. 1 degree/minute) the thermal conductivity increases linearly with filler concentration, or with the number of filler polymer interfaces indicating that thermal conduction is moderated only by phonon conduction. On the other hand, when the sample is subjected to a rapidly approaching heat front, as is the case when the material is exposed to a flame, thermal conduction must occur on a time scale which is much larger than the phonon frequency in the matrix. In this case, the much more rapid conductivity properties of the electrically conducting particles dominate and actual contact between the particles is required to dissipate the heat. In this case, for low GNPs loading, heat will accumulate within the vicinity of the particle, accelerating combustion, till percolation is reached and a conducting pathway is created with particle/particle contacts.

3.5 Conclusion

We have successfully fabricated the PP/GNPs nanocomposites with well-dispersed GNPs (H5) and GNP (H25) via melt blending method. Thermal conductivity measurements on both types of nanocomposites indicated that the thermal coefficient scaled linearly with GNP loading, with H5 having a higher efficient per mass of GNP. A value of 2.0W/m*k was achieved at a loading of 40% and 50%, respectively for H5 and H25. This value, which could not be achieved with conductive particles or carbon nanotubes, is comparable to that of flu gas, and hence opens multiple uses for these compounds in heat exchange units or storage tanks for biodegradable, corrosive fuels.

In contrast to PP-clay nanocomposites, no change in gas permeability was observed even at the highest loading, indicating that the open graphene structure did not interfere with diffusion of small molecules. This large structure was also postulated to allow for interpenetration of the polymer chains leading to phonon coupling between the graphene and the polymer, thereby enhancing the thermal conductivity.

Using SEM, RAMAN and TEM characterization we determined that even though both types of particles were dispersed in the matrix, a higher extent of exfoliation was achieved with GNPs (H5) particles.

Tensile measurement indicated that the modulus increased, linearly with GNPs loading throughout the range tested (1-50% weight percent), while the IZOD impact and toughness decreased initially up to a loading of 10% and then remained constant for up to 50%. The torque required for extrusion increased only by 25% over this range indicating that the compound remains processable despite the high loading content.

SAXS and WAXS characterization of the samples was performed and the results indicated no change in lamellar structure relative to the neat PP sample, while the WAXS spectra indicated an increase in the degree of crystallinity for loading up to 10% followed by a slight decrease relative to the neat sample. This result was consistent with DSC and TGA measurements which indicated no change in the melting temperature. Hence no significant disruption of the crystalline structure occurred with increased GNPs loading.

The response of the nanocomposites to an approaching heat front was measured using cone calorimetry. Nanocomposites with 10% loading or higher showed a dramatic decrease in heat release and mass loss rates, as well as oxygen consumption. Video images indicated the formation of a flexible char layer in these samples which reflected the incoming heat front, while reducing the flow of gases, and reducing the temperature of the sample.

The time to ignition of the nanocomposites initially decreased relative to the neat PP, reaching a minimum at a loading of 1%, and then increasing back to the PP value at 10%, and surpassing it by a factor of 2 at 40%, indicating that the higher loading also rendered the nanocomposites flame retardant.

Conductivity measurement vs frequency as a function of GNP loading were performed and the transition for non-conducting to conducting response was found at a loading of 10%. These results indicated that thermal phonon dissipation was effective for slowly increasing temperatures, where steady state conditions are reached, while for rapidly approaching heat, effective dissipation had the same direct particle-particle contact percolation condition requirements as electrical conduction.

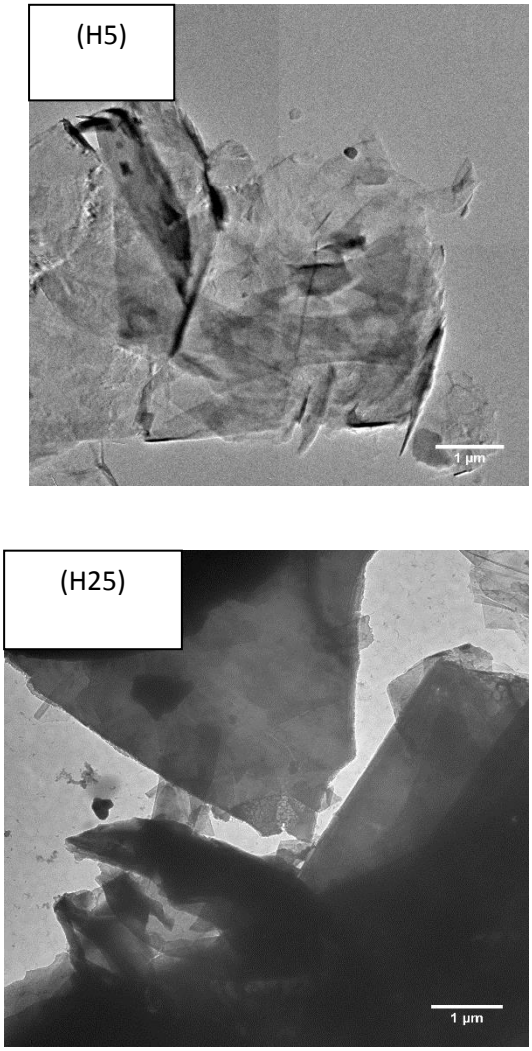

Figure 3.1 TEM images of GNPs (a) H5 and (b) H25.

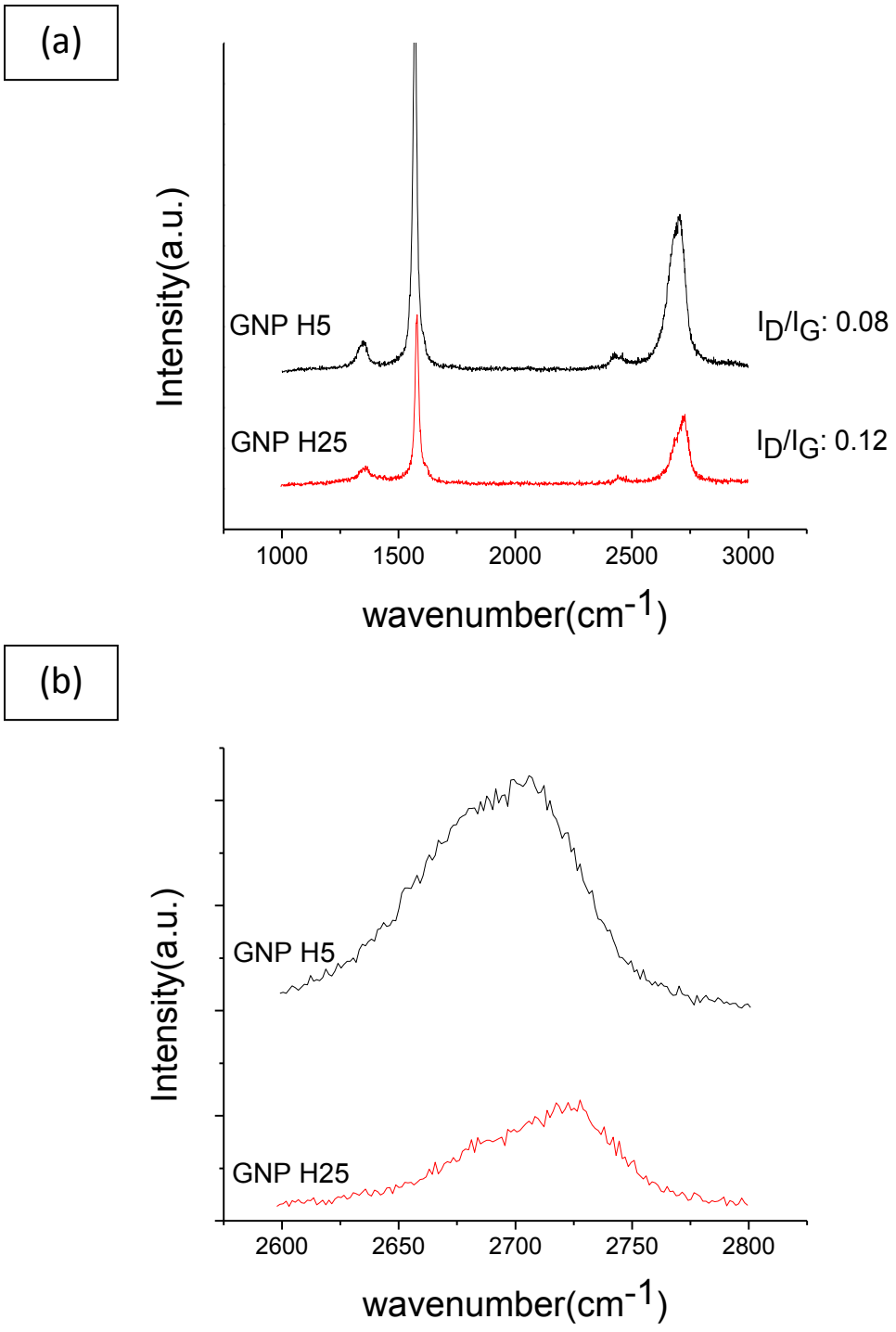

Figure 3.2 (a) Comparison of the raman spectra of GNPs H5 and H25 measured at 514nm. (b) Comparison of the 2D peaks in GNPs H5 and H25.

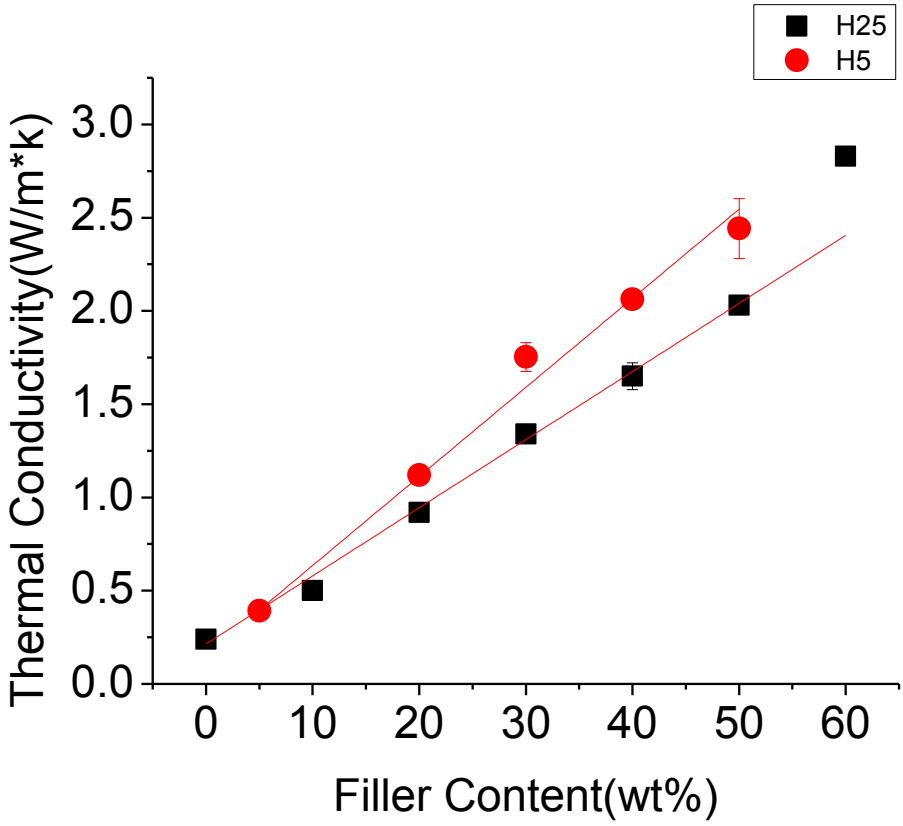

Figure 3.3 Thermal conductivity of two different type of GNPs blends with polypropylene.

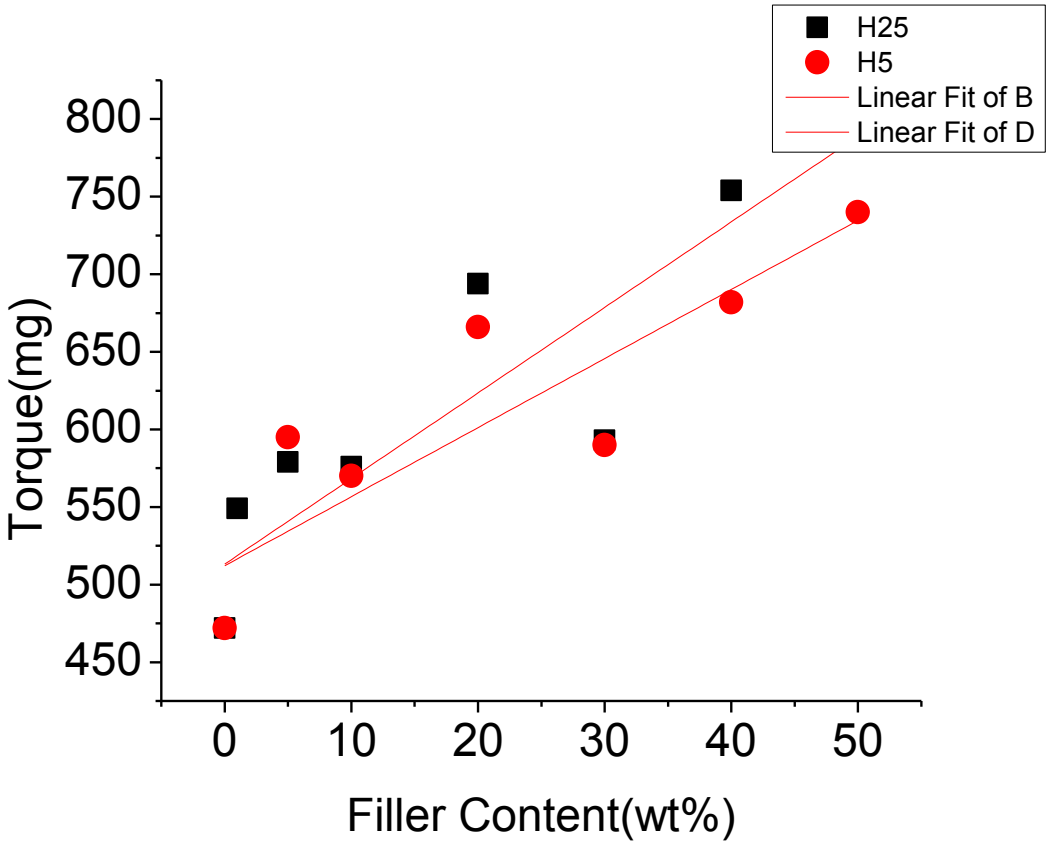

Figure 3.4 Torque measurement for PP/GNPs H5 and H25 nanocomposites.

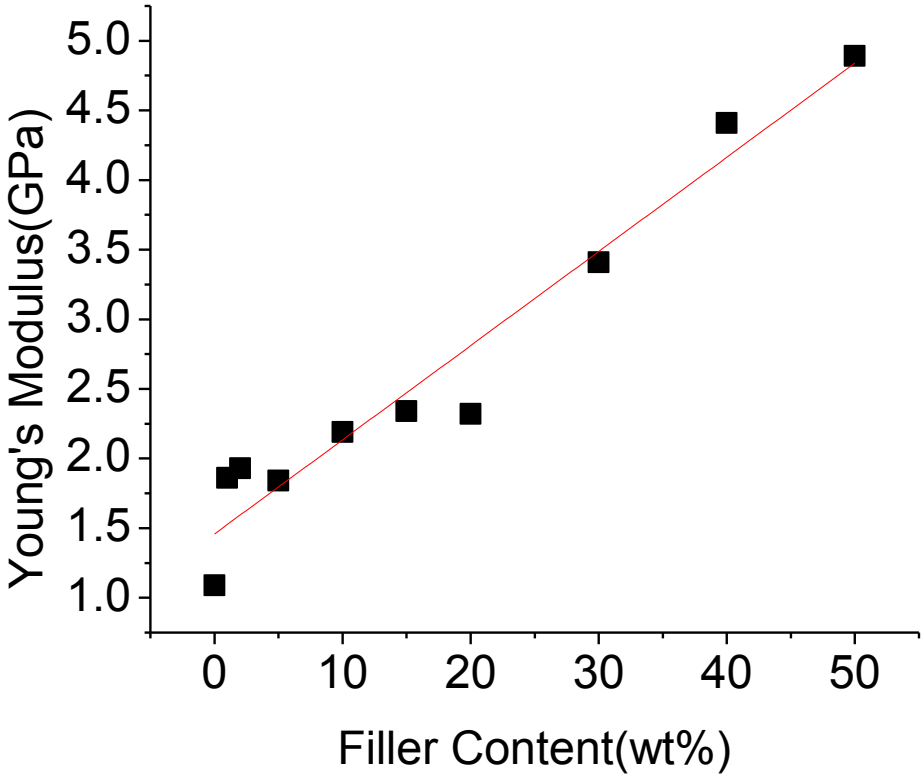

Figure 3.5 Young's modulus of PP/GNPs (H5) nanocomposites from tensile test at room temperature.

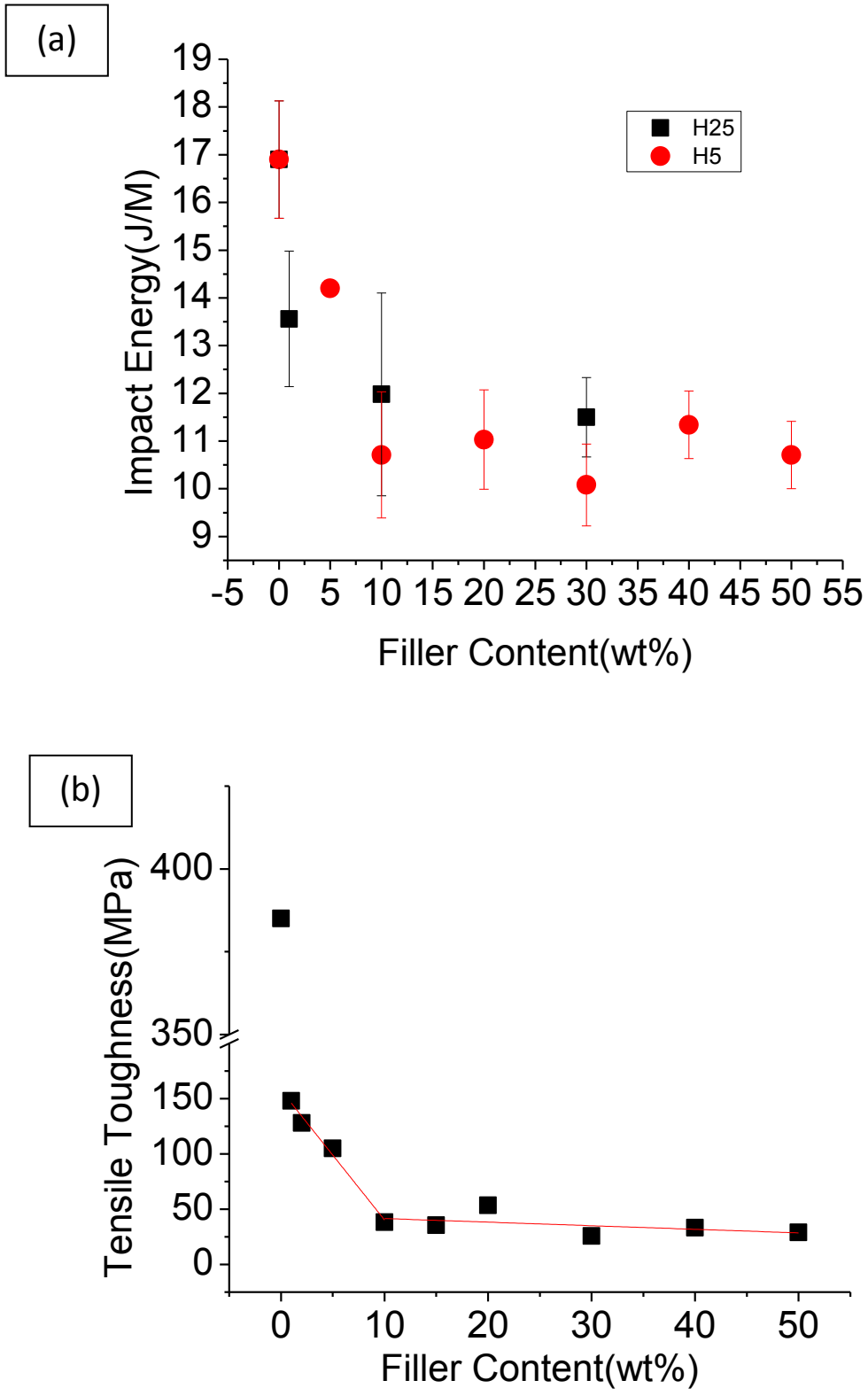

Figure 3.6 (a) Izod Impact Test for PP/GNPs nanocomposites; (b) Tensile Toughness of PP/GNPs nanocomposites.

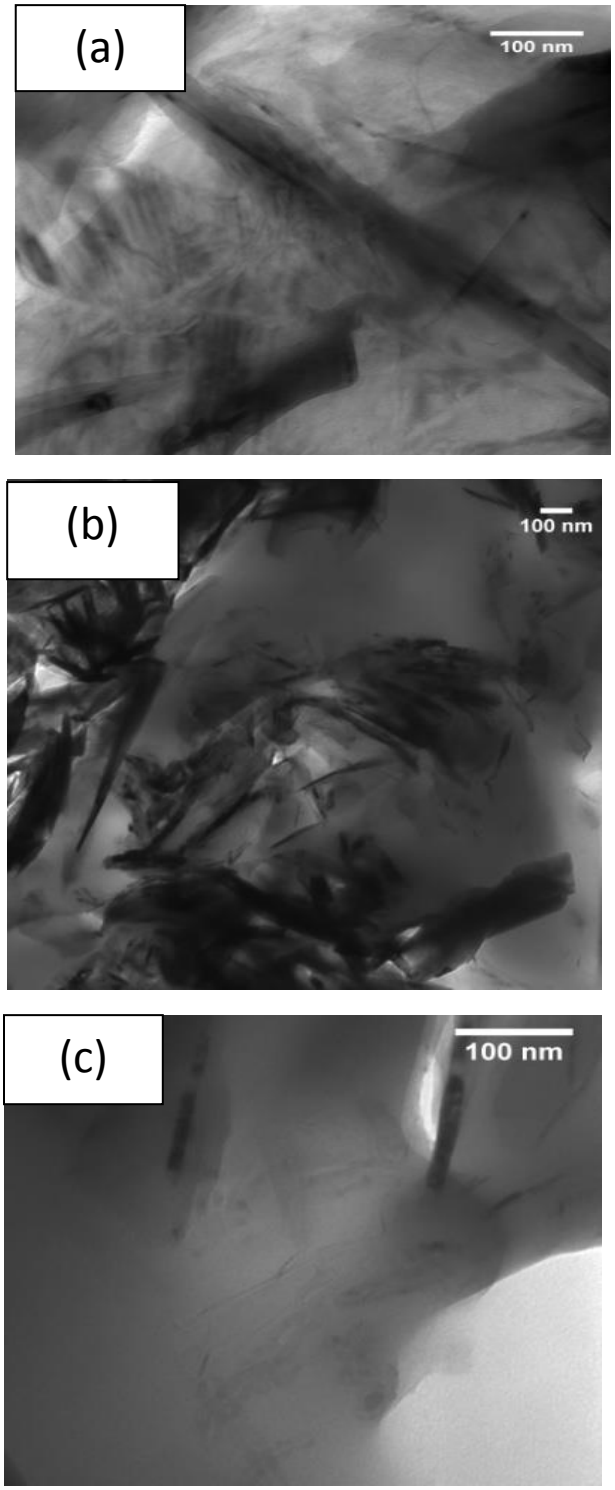

Figure 3.7 The TEM images of a cross section from (a) PP/GNPs (H5) (60/40wt); (b) PP/GNPs (H25) (60/40wt); (c) PP/GNPs (H5)/CNT (60/35/5wt).

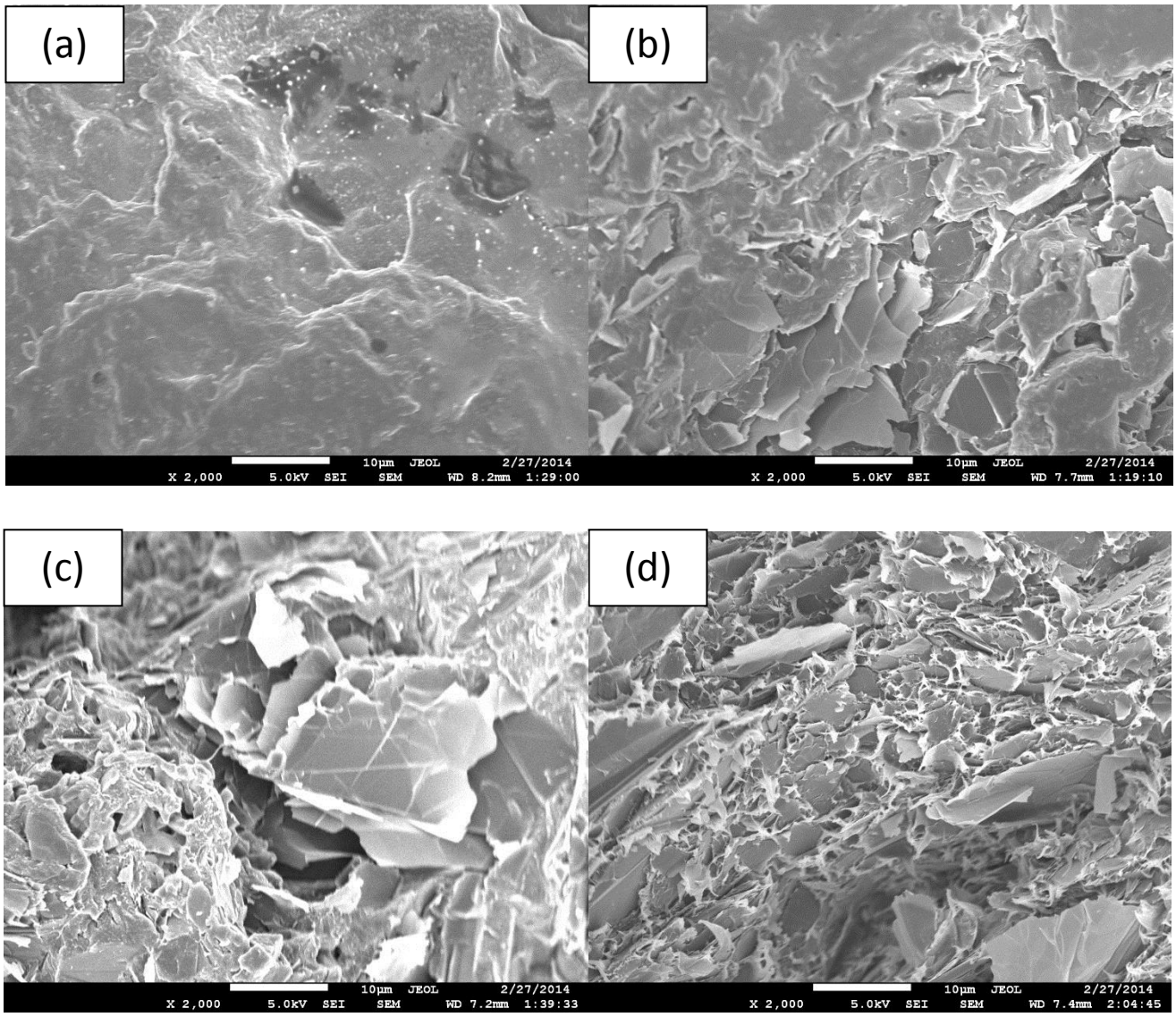

Figure 3.8 The SEM images of (a) Pure PP; (b) PP/GNPs H5 (80/20); (c) PP/GNPs (H25) (80/20); (d) PP/GNPs (H5) (60/40).

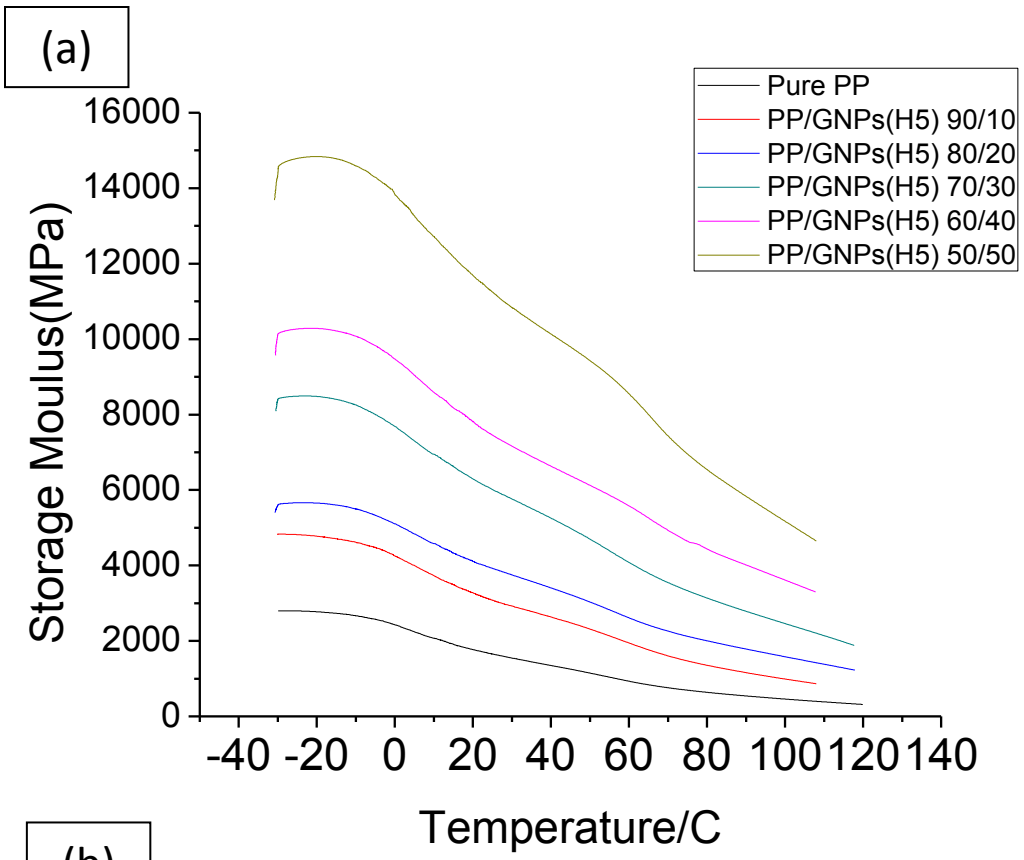
(a)
Pure PP
PP/GNPs(H5) 90/10
PP/GNPs(H5) 80/20
PP/GNPs(H5) 70/30
PP/GNPs(H5) 60/40
PP/GNPs(H5) 50/50
Storage Moulus(MPa)
16000
14000
12000
10000
8000
6000
4000
2000
0
-40 -20 0 20 40 60 80 100 120 140
Temperature/C

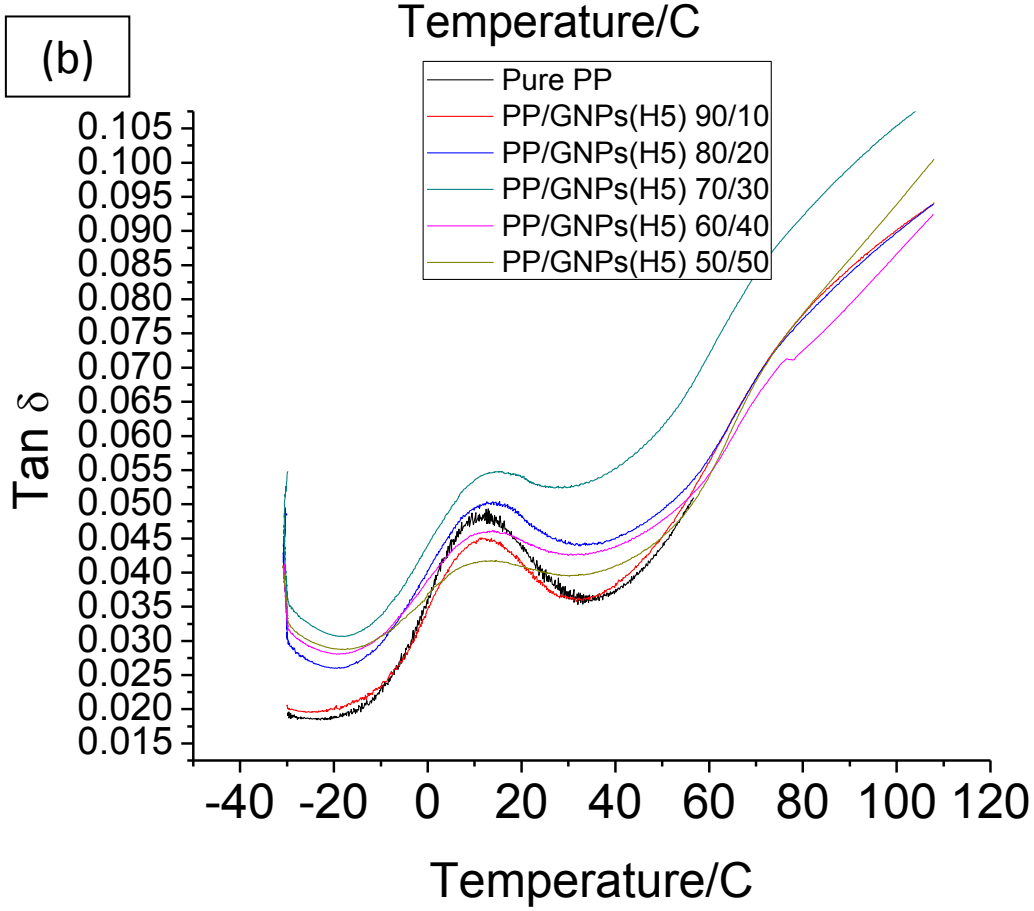
(b)
Pure PP
PP/GNPs(H5) 90/10
PP/GNPs(H5) 80/20
PP/GNPs(H5) 70/30
PP/GNPs(H5) 60/40
PP/GNPs(H5) 50/50
Tan δ
0.105
0.100
0.095
0.090
0.085
0.080
0.075
0.070
0.065
0.060
0.055
0.050
0.045
0.040
0.035
0.030
0.025
0.020
0.015
-40 -20 0 20 40 60 80 100 120
Temperature/C

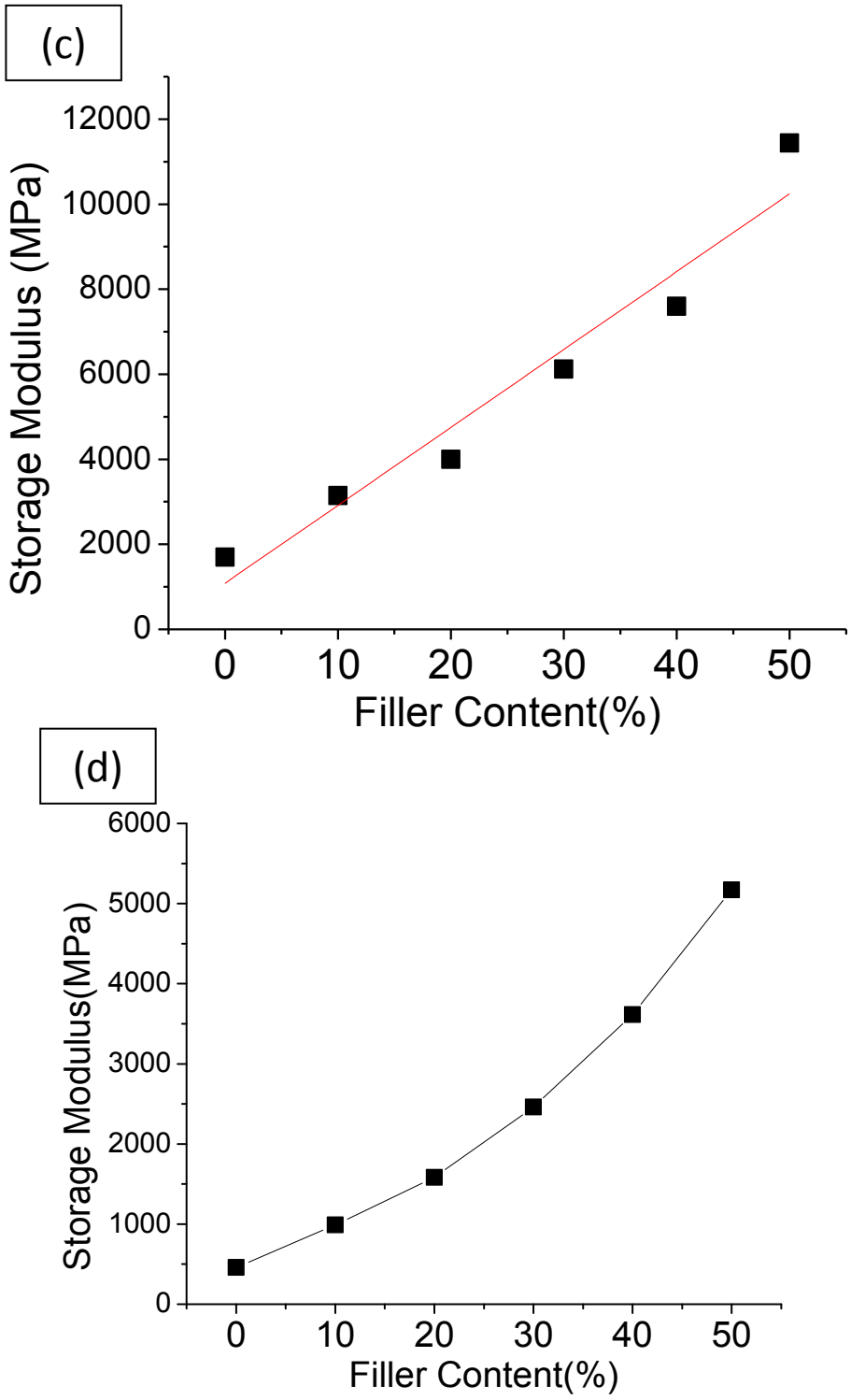

Figure 3.9 (a) Storage modulus of PP/GNPs (H5) nanocomposites as a function of temperature. (b) Tan delta of PP/GNPs nanocomposite; (c) Storage modulus at 23°C of the PP/GNPs (H5) nanocomposites; (d) Storage modulus of nanocomposites at 100°C.

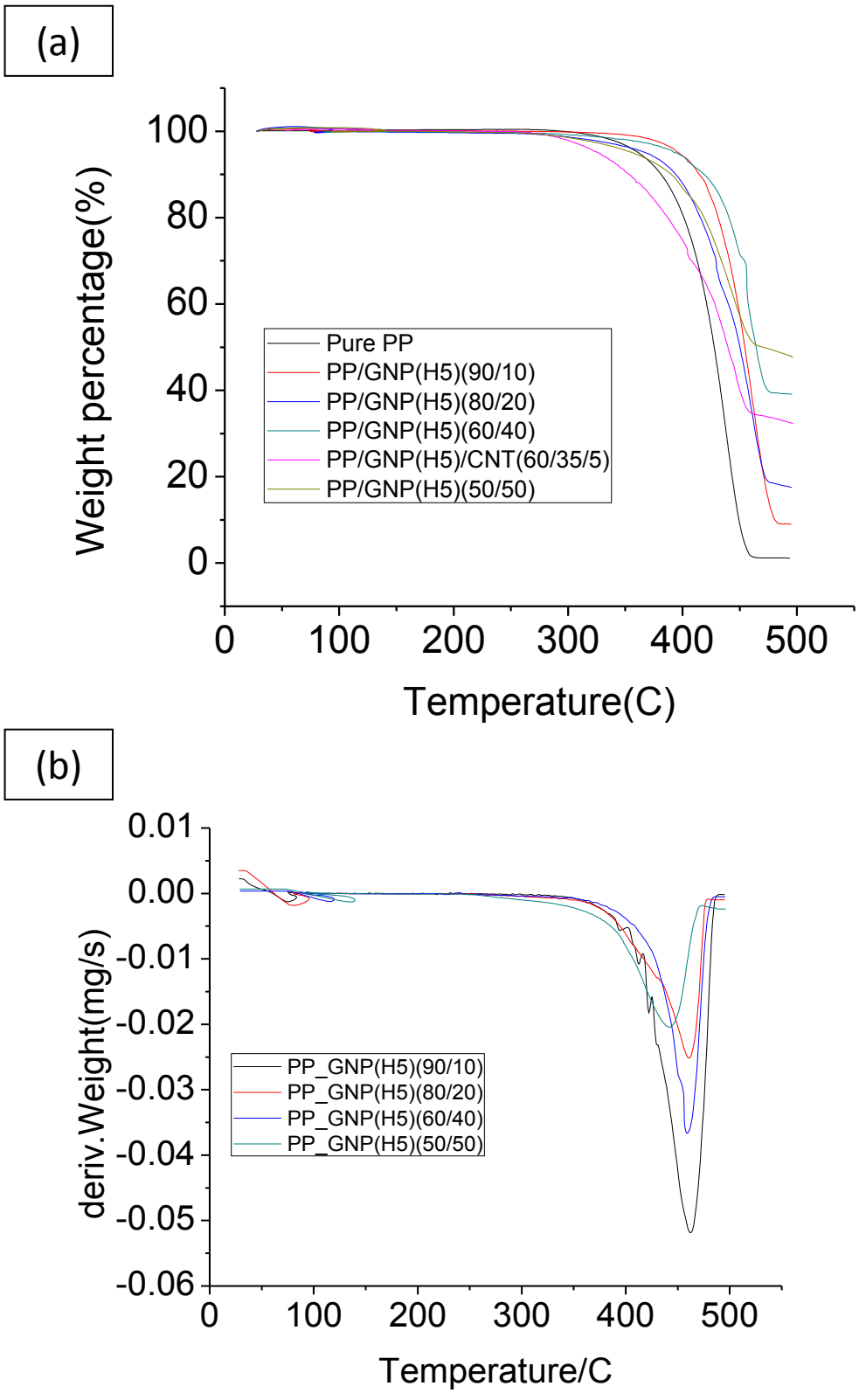

Figure 3.10 (a) TGA data of pure polypropylene and PP/GNPs nanocomposites; (b) Derivative weight loss curves of pure PP and PP/GNPs composites.

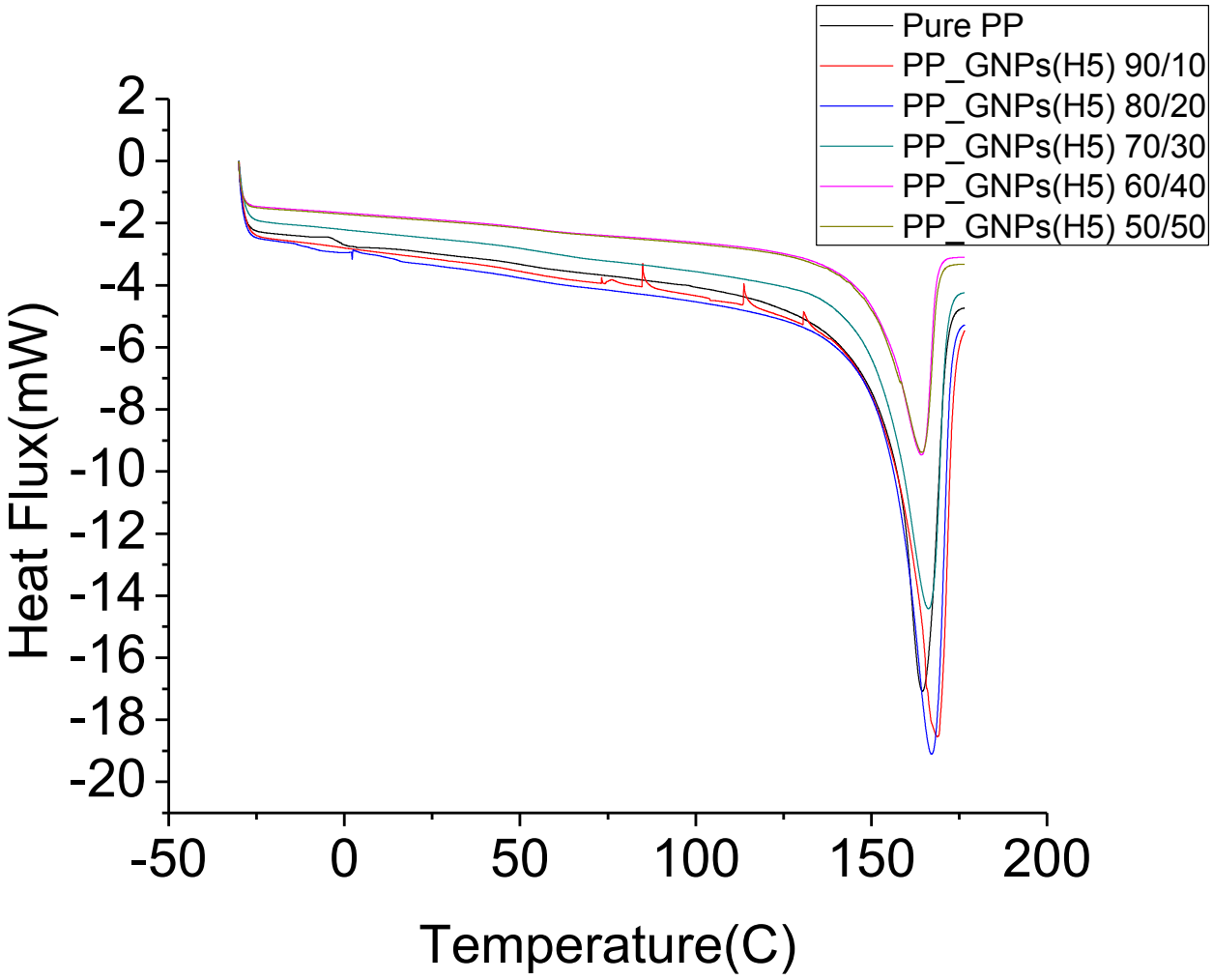

Figure 3.11 DSC data of pure polypropylene and PP/GNPs nanocomposites.

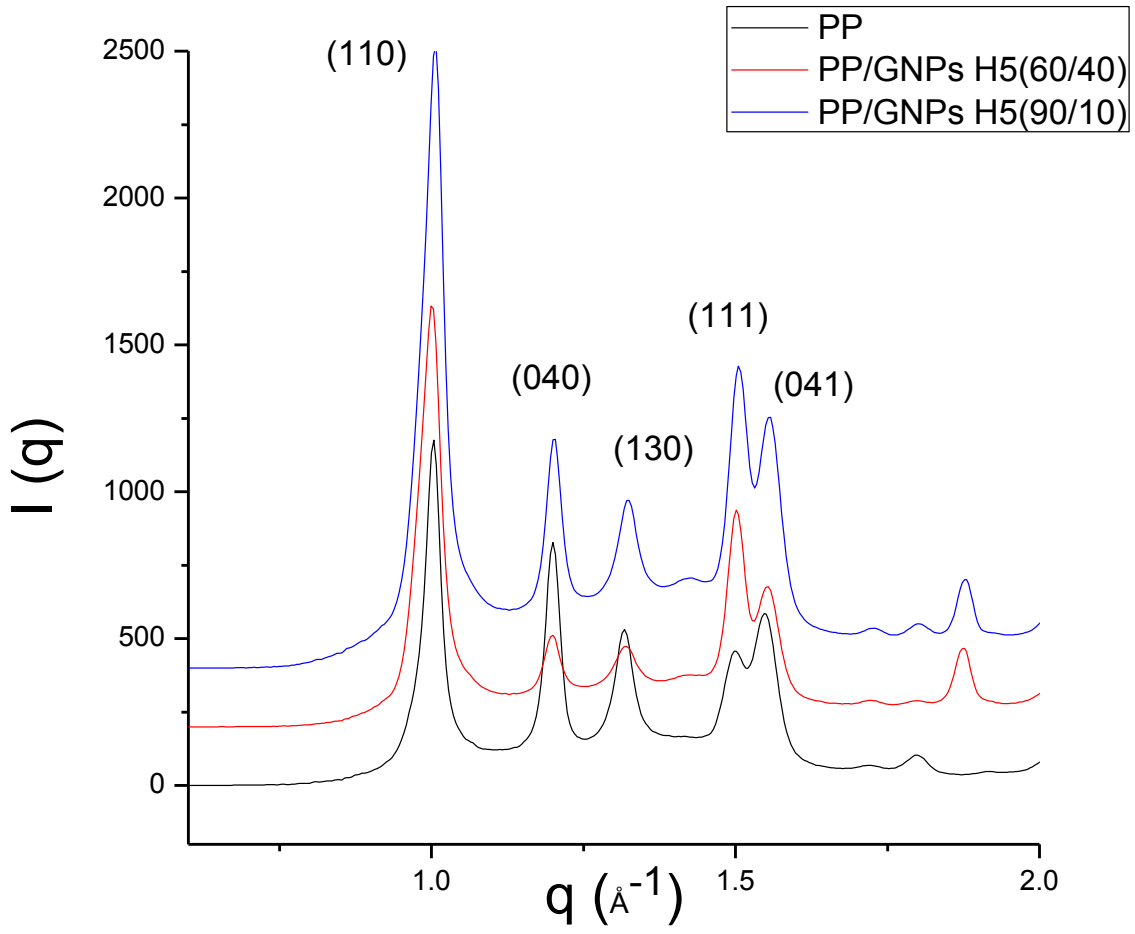

Figure 3.12 Wide Angle X-ray scattering data of PP/GNPs nanocomposites.

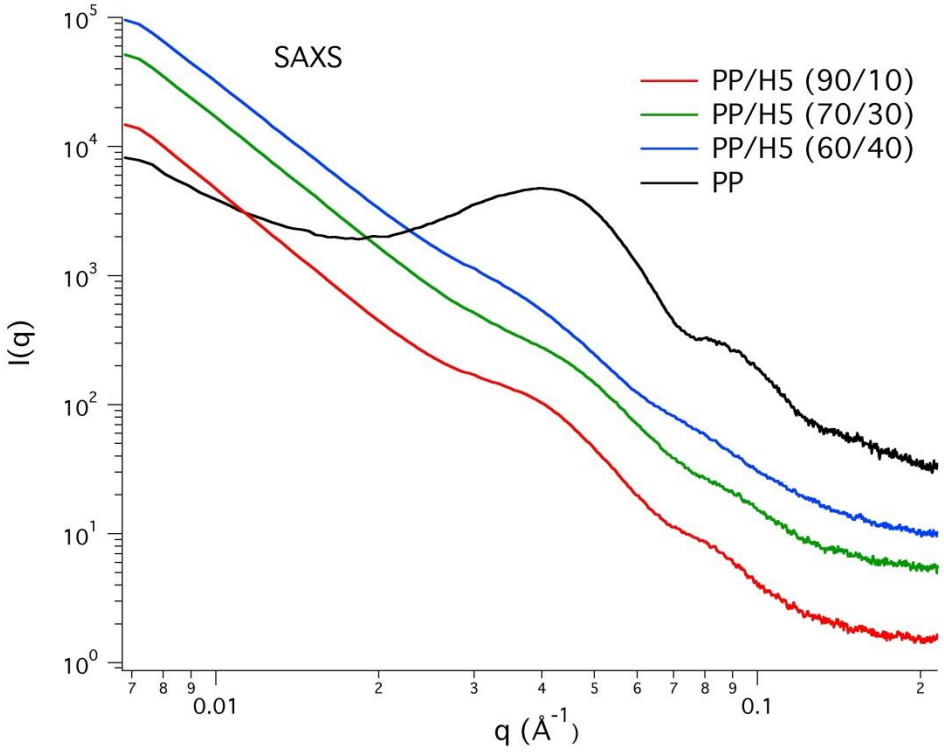

Figure 3.13 Small Angle X-ray scattering data of PP/GNPs nanocomposites.

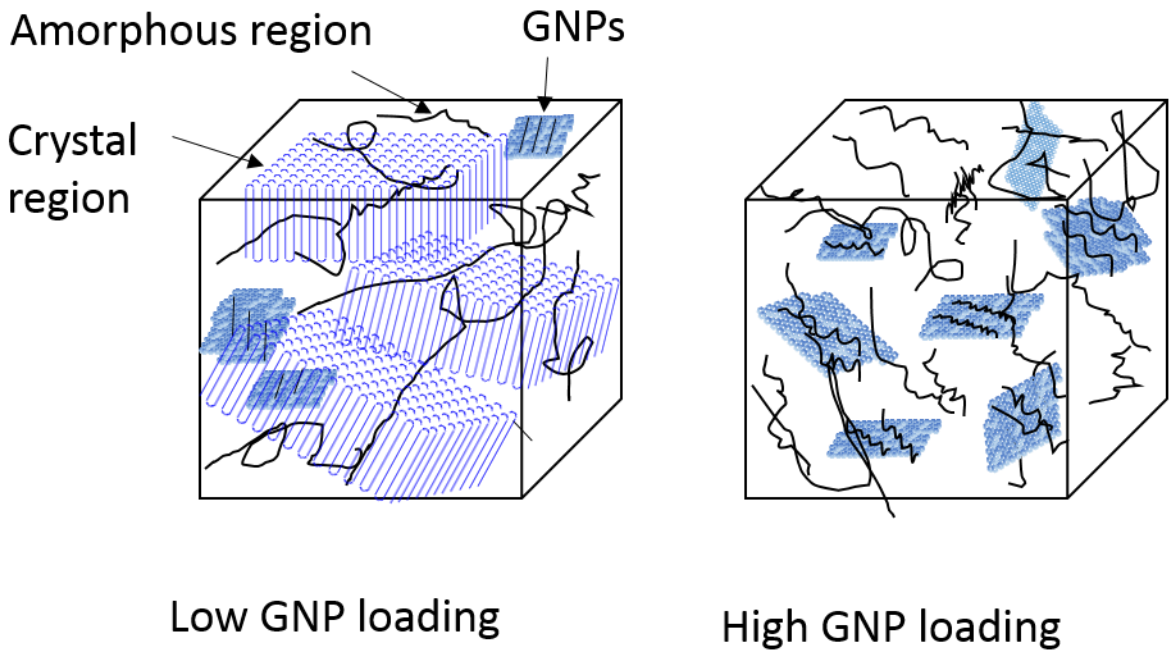

Figure 3.14 Schematic diagrams of crystallization structure of PP with GNPs.

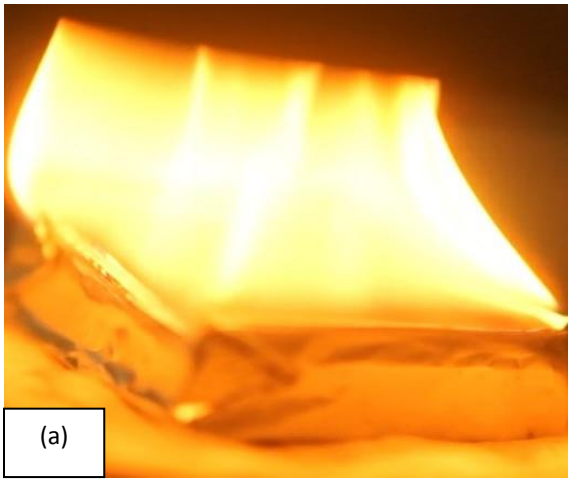
(a)

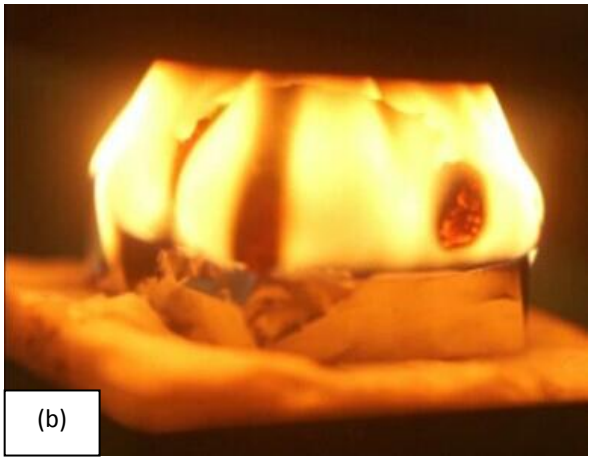
(b)

Figure 3.15 Images of burning process in Cone Calorimetry of (a) pure polypropylene and (b) PP/GNPs nanocomposites.

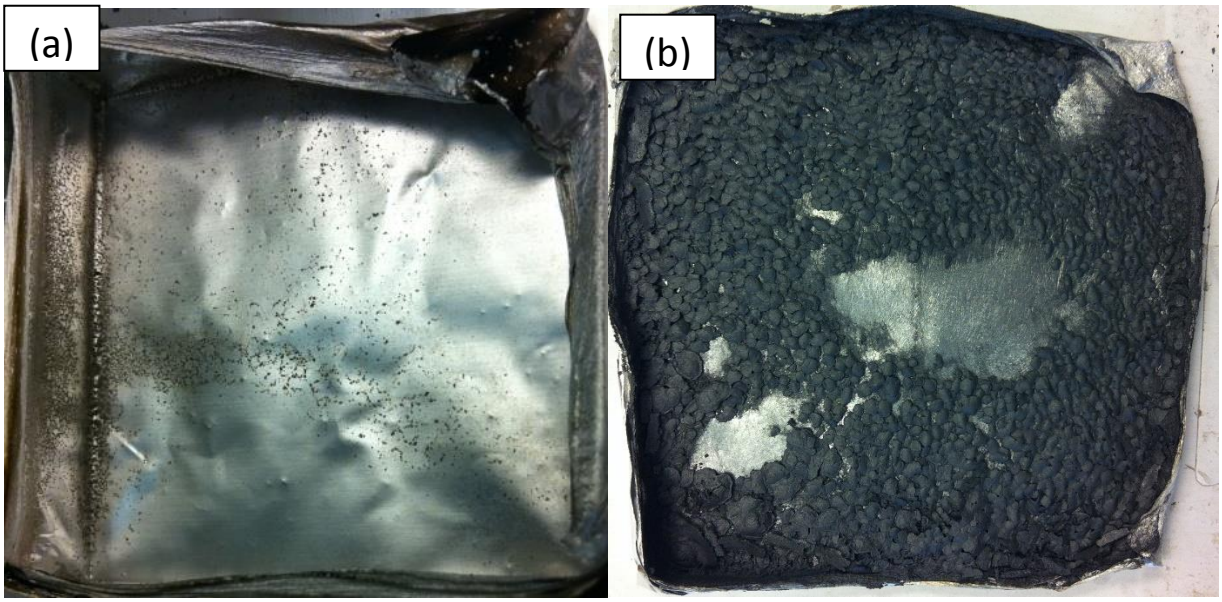

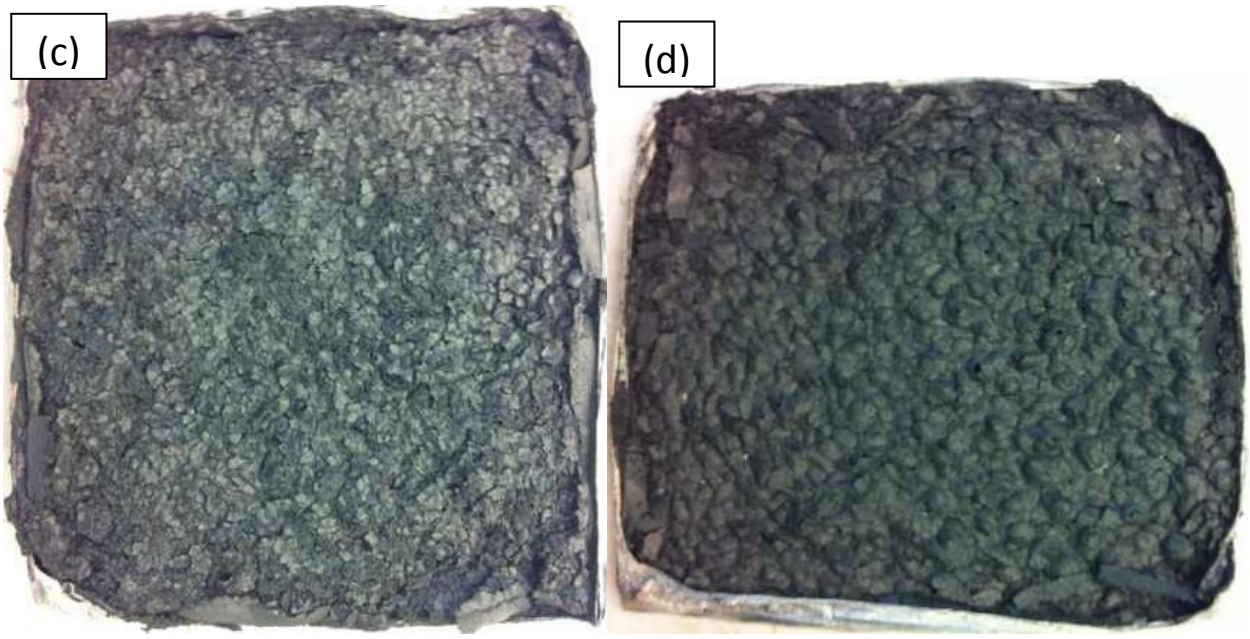
(c)
(d)

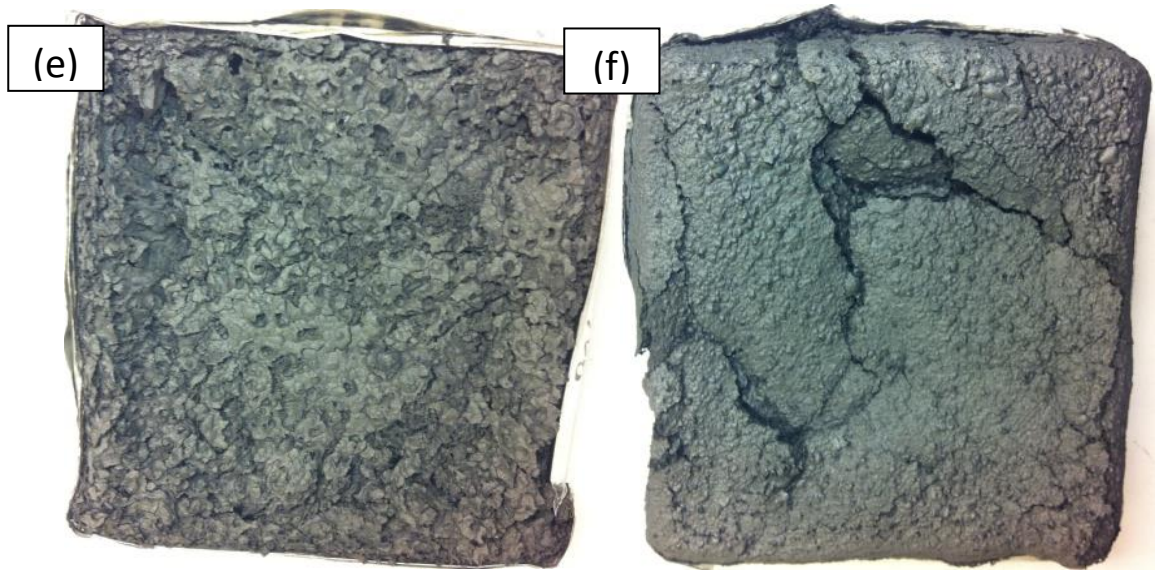
(e)
(f)

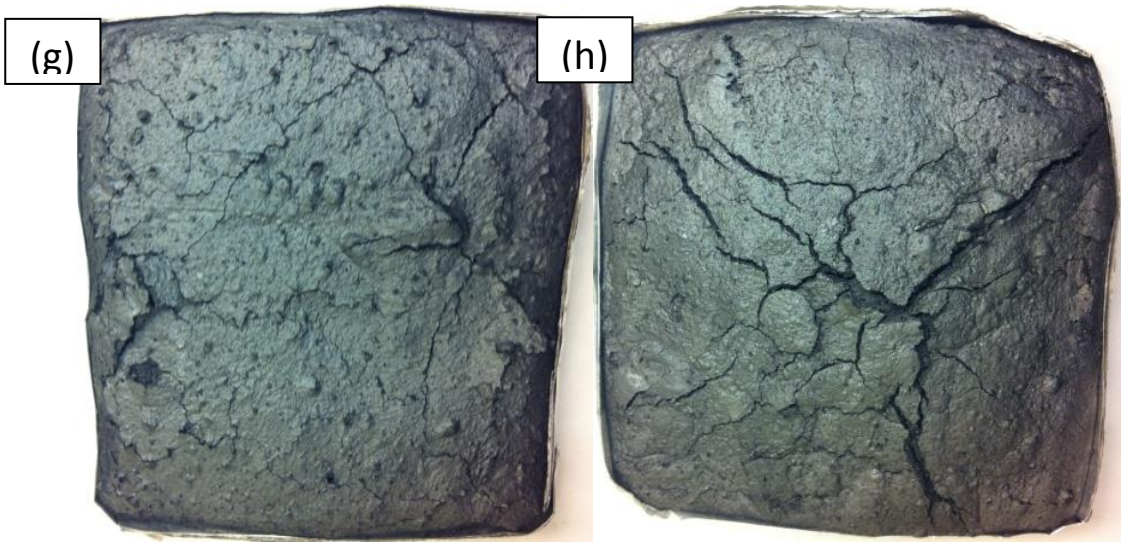

Figure 3.16 Photographs of the char residue after the cone calorimetry test. (a) Pure Polypropylene; (b) PP/GNPs H5 (99/1); (c) PP/GNPs H5 (98/2); (d) PP/GNPs H5 (95/5); (e) PP/GNPs H5 (90/10); (f) PP/GNPs H5 (80/20); (g) PP/GNPs H5 (70/30); (h) PP/GNPs H5 (60/40)

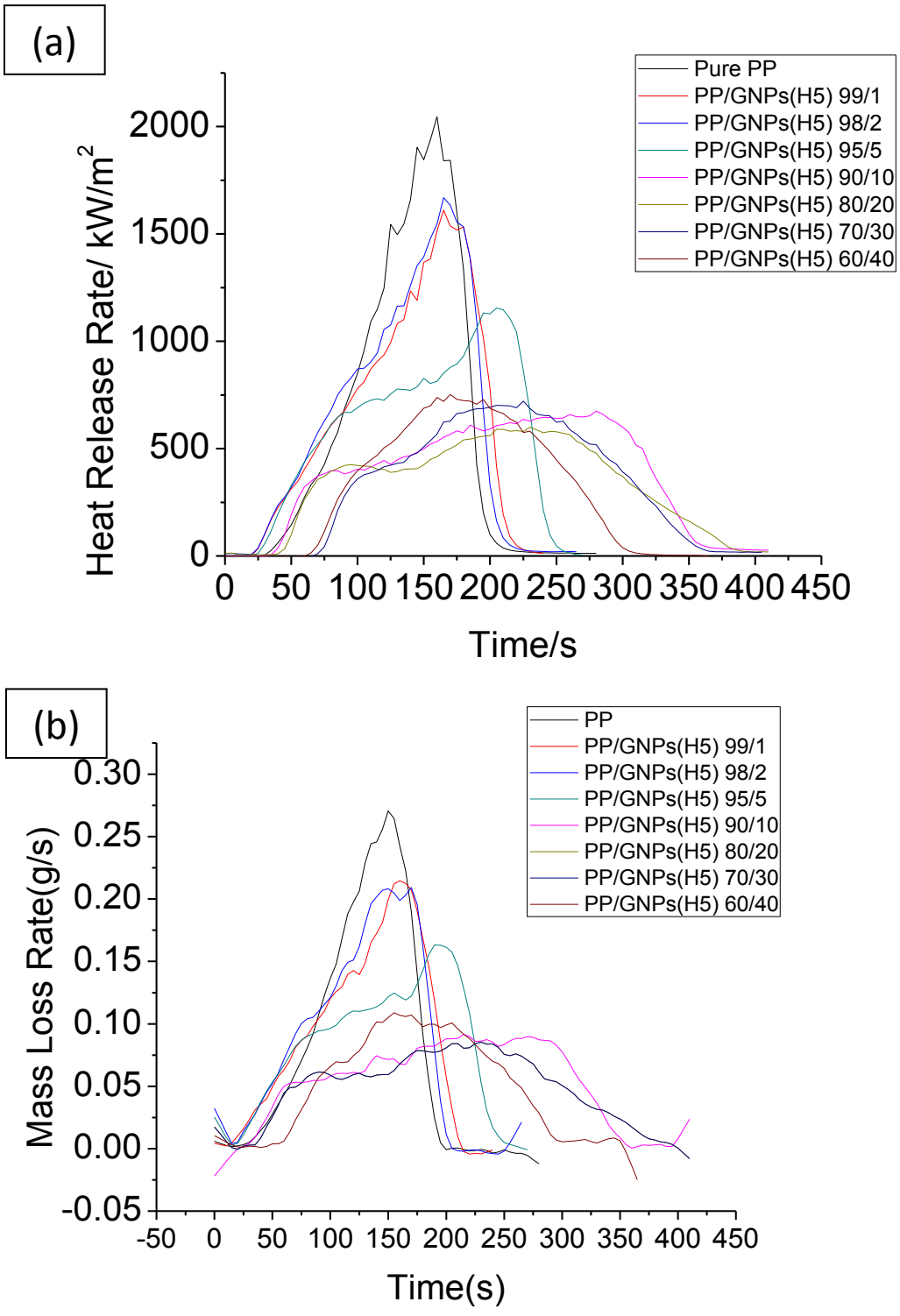

Figure 3.17 Overlays of heat release curves (a) and mass loss curves (b) of PP/GNPs nanocomposites performed in cone calorimeter at a heat flux of 50 kW/m2 in air atmosphere.

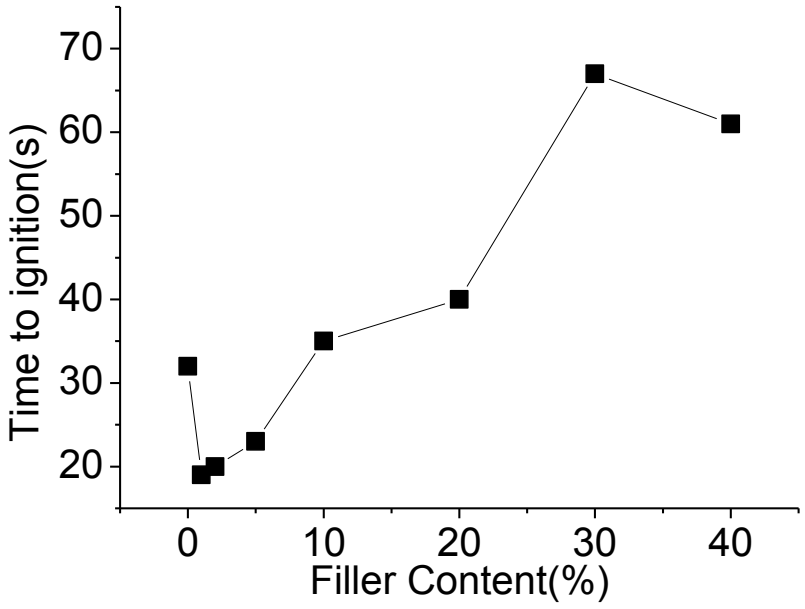

Figure 3.18 The TTI of PP/GNPs (H5) nanocomposites in Cone Calorimetry Test.

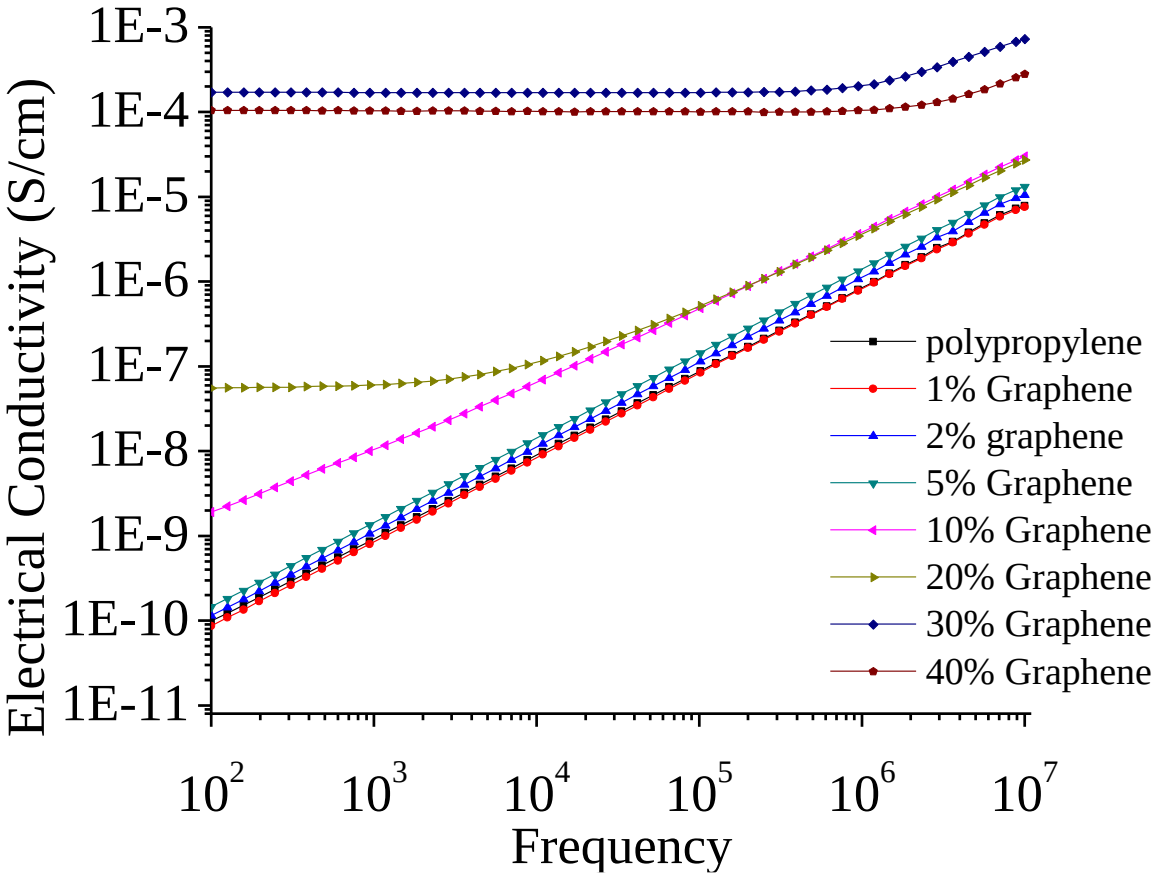

Figure 3.19 Frequency dependence of electrical conductivity for PP/GNPs nanocomposites with GNPs (H5) loading from 0-40wt%.

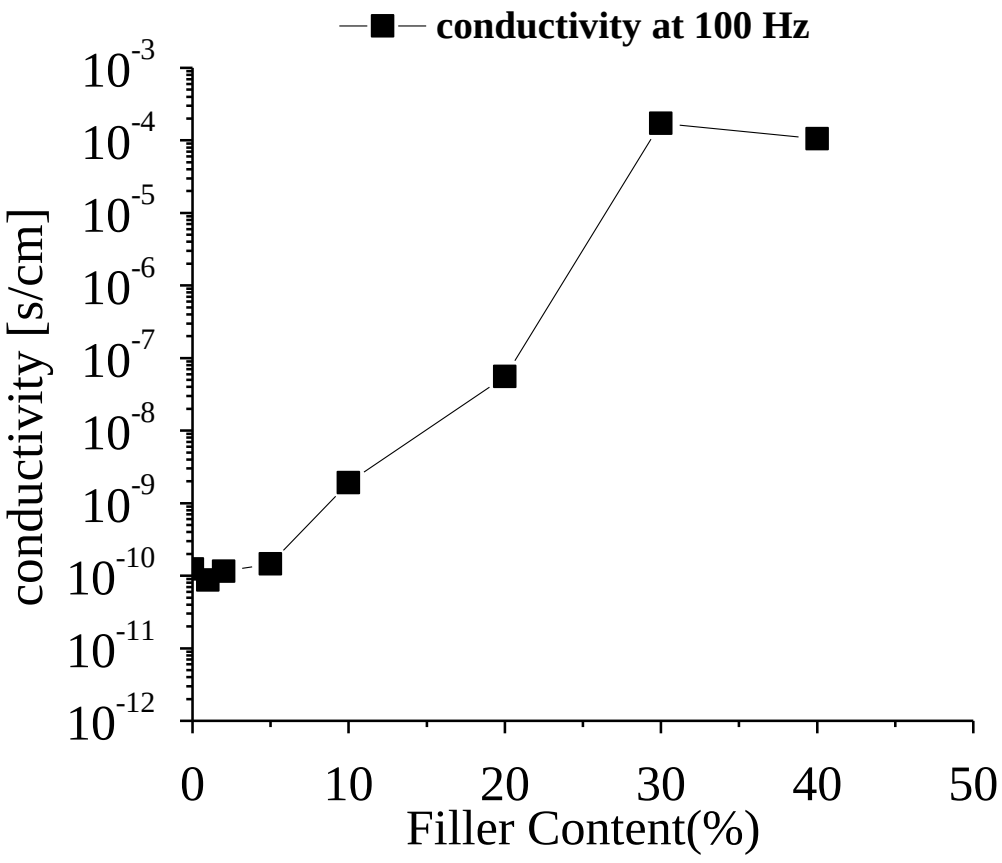

Figure 3.20 Electrical conductivity of GNPs (H5) at 100 Hz for PP/GNPs nanocomposites.

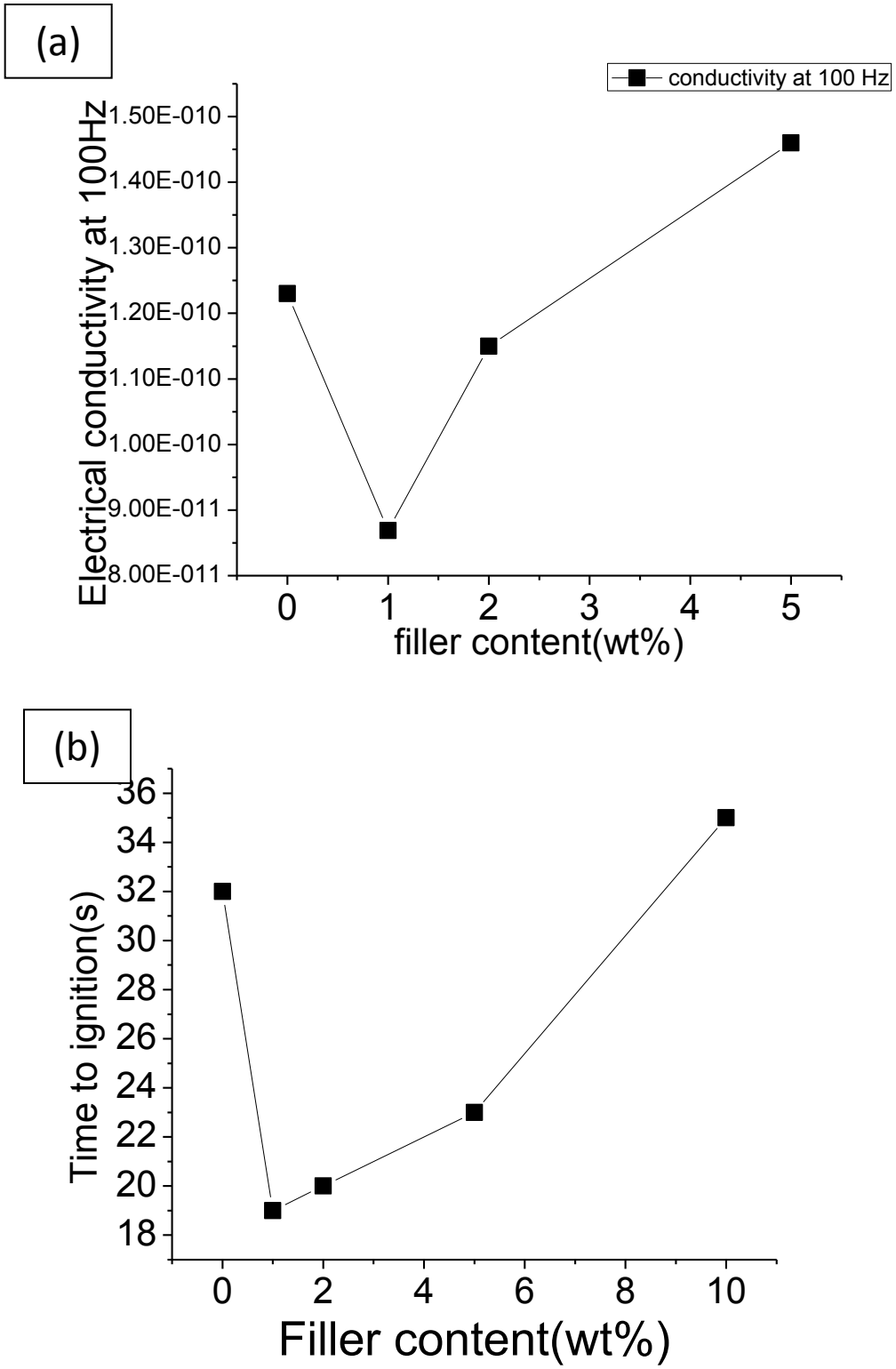

Figure 3.21 (a) Electrical conductivity of GNPs (H5) at 100 Hz; (b) Time to ignition for PP/GNPs nanocomposites.

Sample	(Filler Concentration, wt%)	Thermal conductivity(W/m*k)
PP	100	0.23
PP/GNPs(H25)	90/10	0.67
PP/GNPs(H25)	75/25	0.83
PP/GNPs(H5)	95/5	0.39
PP/GNPs(H5)	80/20	1.12
PP/CB	80/20	0.36
PP/CNT	80/20	0.57
PP/Cu	90/30	0.33

Table 3.1 Thermal Conductivity Test of Polypropylene Nanocomposites with GNPs, Carbon Black, Carbon nanotube, copper micro particles.

Sample	(Filler Concentration, wt%)	Thermal conductivity(W/m*k)
Pure Polypropylene	100/0	0.23
PP/GNPs(H25)	99/10	0.50
PP/GNPs(H25)	90/20	0.92
PP/GNPs(H25)	70/30	1.34
PP/GNPs(H25)	60/40	1.65
PP/GNPs(H25)	50/50	2.03
PP/GNPs(H25)	40/0	2.83

Table 3.2 Thermal Conductivity Test of Polypropylene Nanocomposites with GNPs (H25).

Sample	(Filler Concentration,wt%)	Thermal conductivity(W/m*k)
Pure Polypropylene	100/0	0.23
PP/GNPs(H5)	95/5	0.39
PP/GNPs(H5)	80/20	1.12
PP/GNPs(H5)	70/30	1.75
PP/GNPs(H5)/CNT	70/25/5	1.67
PP/GNPs(H5)	60/40	2.06
PP/GNPs(H5)/CNT	60/35/5	2.01
PP/GNPs(H5)	50/50	2.44

Table 3.3 Thermal Conductivity Test of Polypropylene Nanocomposites with GNPs (H5).

Sample	(Concentration, wt%)	Young's Modulus(GPa)	Tensile Stress(MPa)	Ultimate Strain (%)	Tensile Toughness(MPa)	Izod Impact Energy (J/M)
PP	100	1.09	30.7	16.1	385	16.9
PP/ GNPs(H5)	99/1	1.86	25.4	7.6	148	---
PP/ GNPs(H5)	98/2	1.93	25.9	6.5	128	---
PP/ GNPs(H5)	95/5	1.84	25.6	5.6	105	14.2
PP/ GNPs(H5)	90/10	2.19	20.5	2.9	38.3	10.7
PP/ GNPs(H5)	85/15	2.34	24.0	2.6	35.6	---
PP/ GNPs(H5)	80/20	2.32	27.7	3.3	53.4	11.0
PP/ GNPs(H5)	70/30	3.41	24.7	1.82	25.7	10.0
PP/ GNPs(H5)	60/40	4.41	29.9	1.91	33.3	11.3
PP/ GNPs(H5)	50/50	4.89	24.7	1.38	28.9	10.7

Table 3.4 Tensile and Izod properties of PP/GNPs (H5) nanocomposites.

Sample Name	Weight ratio (%)	Storage Modulus at 23°C (MPa)	Storage Modulus at 100°C(MPa)	Glass transition temperature(°C)
Pure PP	100	1697	459.2	14.2
PP/GNPs(H5)	90/10	3147	989.9	13.6
PP/GNPs(H5)	80/20	3998	1583	13.9
PP/GNPs(H5)	70/30	6119	2461	14.3
PP/GNPs(H5)	60/40	7594	3613	13.9
PP/GNPs(H5)	50/50	11435	5170	13.7

Table 3.5 Storage Modulus at different temperature and glass transition temperature for PP/GNPs (H5) nanocomposites.

Sample Name	Weight ratio (%)	$T_{10\%}$(°C)	T_{max}(°C)
PP	100	381	426
PP/GNPs(H5)	90/10	414	462
PP/GNPs(H5)	80/20	393	459
PP/GNPs(H5)	60/40	418	461
PP/GNPs(H5)	50/50	390	446
PP/GNPs(H25)	50/50	403	450

Table 3.6 TGA result of pure PP and PP/GNPs nanocomposites. $T_{10\%}$: temperature of 10% weight loss; T_{max}: inflection point.

Sample Name	Weight ratio/%	Melting Temperature/°C	Crystallinity/%
Pure PP	100	164.7	53.2
PP/GNPs(H5)	90/10	168.6	52.1
PP/GNPs(H5)	80/20	167.0	57.1
PP/GNPs(H5)	70/30	166.3	60.6
PP/GNPs(H5)	60/40	164.7	55.3
PP/GNPs(H5)	50/50	164.5	50.4

Table 3.7 Melting Temperature and crystallinity of PP/GNPs nanocomposites

Sample	Weight ratio/%	Degree of Crystallinity (%)	Area of the peak (%)				
			(110)	(040)	(130)	(111)	(041)
PP	100	78	18.5	16	13.5	11	16
PP/GNPs(H5)	90/10	73	23.5	10	10.5	14.5	12
PP/GNPs(H5)	60/40	75	28	6	9	17	10.5

Table 3.8 The crystallinity and the area of the corresponding peak for each individual orientation of PP/GNPs nanocomposites

Sample	Thickness(cm)	Oxygen Transmission rate(OTR)(cm^2/sec*atm)	Relative permeability
Pure PP	0.0782	3.7×10^{-8}	1.00
PP/GNPs(H5) 90/10	0.0829	3.7×10^{-8}	1.00
PP/GNPs(H5)60 /40	0.0815	3.5×10^{-8}	0.94

Table 3.9 Oxygen permeability of PP/GNPs nanocomposites

Sample	Weight ratio/%	Dripping	T_1(s)	T2(s)	UL-94 V0
PP	100	Yes	≥30	---	NG[a]
PP/GNPs(H25)	90/10	NO	≥30	---	NG
PP/GNPs(H25)	80/20	NO	≥30	---	NG
PP/GNPs(H25)	70/30	NO	≥30	---	NG
PP/GNPs(H25)	60/40	NO	1	3	V0
PP/GNPs(H25)	50/50	NO	1	3	V0
PP/GNPs(H5)	70/30	NO	≥30	---	NG
PP/GNPs(H5)	60/40	NO	2	2	V0
PP/GNPs(H5)	50/50	NO	1	3	V0

Table 3.10 Result of UL-94 Vertical Burning Test of PP/GNPs Nanocomposites

NG[a]: No grading and burnt up to the upper clamp at the stand.

*UL-94 V0 achieved since both t1 and t2 are lower than 10s.

Sample	Weight ratio/%	LOI (%)
PP	100	18.3
PP/GNPs(H5)	90/10	19.5
PP/GNPs(H5)	80/20	20.6
PP/GNPs(H5)	70/30	22.6
PP/GNPs(H5)	60/40	23.4

Table 3.11 Limited oxygen index of PP/GNPs Nanocomposites.

Sample #	Time to Ignition (sec)	Mass Loss Rate (g/s)	Heat Release Rate (kW/m^2)	Peak HRR (kW/m^2)	Flameout (sec)
Pure PP	32	15.33	659.07	2045.40	186
PP/GNPs H5 (99/1)	19	17.27	718.62	1611.44	203
PP/GNPs H5 (98/2)	20	15.61	657.38	1669.05	191
PP/GNPs H5 (95/5)	23	15.58	623.47	1155.33	235
PP/GNPs H5 (90/10)	35	9.96	410.00	674.55	348
PP/GNPs H5 (80/20)	40	9.14	361.04	600.06	377
PP/GNPs H5 (70/30)	67	10.35	393.46	720.96	359
PP/GNPs H5 (60/40)	61	10.07	374.96	752.54	295

Table 3.12 Results of Cone Calorimetry of PP/GNPs (H25) nanocomposites.

Reference

1. T'Joen, C., et al., *A review on polymer heat exchangers for HVAC&R applications.* International Journal of Refrigeration-Revue Internationale Du Froid, 2009. **32**(5): p. 763-779.
2. Bigg, D.M., G.H. Stickford, and S.G. Talbert, *APPLICATIONS OF POLYMERIC MATERIALS FOR CONDENSING HEAT-EXCHANGERS.* Polymer Engineering and Science, 1989. **29**(16): p. 1111-1116.
3. Peters, J.E., D.V. Papavassiliou, and B.P. Grady, *Unique Thermal Conductivity Behavior of Single-Walled Carbon Nanotube-Polystyrene Composites.* Macromolecules, 2008. **41**(20): p. 7274-7277.
4. Haggenmueller, R., et al., *Single wall carbon nanotube/polyethylene nanocomposites: Thermal and electrical conductivity.* Macromolecules, 2007. **40**(7): p. 2417-2421.
5. Kashiwagi, T., et al., *Thermal and flammability properties of polypropylene/carbon nanotube nanocomposites.* Polymer, 2004. **45**(12): p. 4227-4239.
6. Raza, M.A., A.V.K. Westwood, and C. Stirling, *Effect of processing technique on the transport and mechanical properties of graphite nanoplatelet/rubbery epoxy composites for thermal interface applications.* Materials Chemistry and Physics, 2012. **132**(1): p. 63-73.
7. Kalaitzidou, K., H. Fukushima, and L.T. Drzal, *Mechanical properties and morphological characterization of exfoliated graphite-polypropylene nanocomposites.* Composites Part a-Applied Science and Manufacturing, 2007. **38**(7): p. 1675-1682.
8. Hofmann, D., et al., *Functionalized Graphene and Carbon Materials as Additives for Melt-Extruded Flame Retardant Polypropylene.* Macromolecular Materials and Engineering, 2013. **298**(12): p. 1322-1334.
9. Pang, H., et al., *Segregated Conductive Ultrahigh-Molecular-Weight Polyethylene Composites Containing High-Density Polyethylene as Carrier Polymer of Graphene Nanosheets.* Polymer-Plastics Technology and Engineering, 2012. **51**(14): p. 1483-1486.
10. Liu, L., L. Zhang, and J. Lua, *Branched carbon nanotube reinforcements for improved strength of polyethylene nanocomposites.* Applied Physics Letters, 2012. **101**(16): p. 5.
11. Pang, H.A., et al., *The effect of electric field, annealing temperature and filler loading on the percolation threshold of polystyrene containing carbon nanotubes and graphene nanosheets.* Carbon, 2011. **49**(6): p. 1980-1988.
12. Roy, N., R. Sengupta, and A.K. Bhowmick, *Modifications of carbon for polymer composites and nanocomposites.* Progress in Polymer Science, 2012. **37**(6): p. 781-819.
13. Yoonessi, M. and J.R. Gaier, *Highly Conductive Multifunctional Graphene Polycarbonate Nanocomposites.* Acs Nano, 2010. **4**(12): p. 7211-7220.
14. Shen, B., et al., *Enhanced interfacial interaction between polycarbonate and thermally reduced graphene induced by melt blending.* Composites Science and Technology, 2013. **86**: p. 109-116.

15. Han, Z.D. and A. Fina, *Thermal conductivity of carbon nanotubes and their polymer nanocomposites: A review.* Progress in Polymer Science, 2011. **36**(7): p. 914-944.
16. Weidenfeller, B., M. Hofer, and F.R. Schilling, *Thermal conductivity, thermal diffusivity, and specific heat capacity of particle filled polypropylene.* Composites Part a-Applied Science and Manufacturing, 2004. **35**(4): p. 423-429.
17. Enomoto, K., et al., *Effect of filler orientation on thermal conductivity of polypropylene matrix carbon nanofiber composites.* Japanese Journal of Applied Physics Part 2-Letters & Express Letters, 2005. **44**(24-27): p. L888-L891.
18. Si, M., et al., *Compatibilizing bulk polymer blends by using organoclays.* Macromolecules, 2006. **39**(14): p. 4793-4801.
19. Novoselov, K.S., et al., *Electric field effect in atomically thin carbon films.* Science, 2004. **306**(5696): p. 666-669.
20. Balandin, A.A., et al., *Superior thermal conductivity of single-layer graphene.* Nano Letters, 2008. **8**(3): p. 902-907.
21. Seol, J.H., et al., *Two-Dimensional Phonon Transport in Supported Graphene.* Science, 2010. **328**(5975): p. 213-216.
22. Kato, H., T. Baba, and M. Okaji, *Anisotropic thermal-diffusivity measurements by a new laser-spot-heating technique.* Measurement Science & Technology, 2001. **12**(12): p. 2074-2080.
23. Khveshchenko, D.V., *Magnetic-field-induced insulating behavior in highly oriented pyrolitic graphite.* Physical Review Letters, 2001. **87**(20).
24. Charlier, J.C., et al., *Electron and phonon properties of graphene: Their relationship with carbon nanotubes*, in *Carbon Nanotubes: Advanced Topics in the Synthesis, Structure, Properties and Applications*, A. Jorio, G. Dresselhaus, and M.S. Dresselhaus, Editors. 2008, Springer-Verlag Berlin: Berlin. p. 673-709.
25. Dean, C.R., et al., *Boron nitride substrates for high-quality graphene electronics.* Nature Nanotechnology, 2010. **5**(10): p. 722-726.
26. Wei, N., et al., *Strain engineering of thermal conductivity in graphene sheets and nanoribbons: a demonstration of magic flexibility.* Nanotechnology, 2011. **22**(10): p. 11.
27. Stankovich, S., et al., *Graphene-based composite materials.* Nature, 2006. **442**(7100): p. 282-286.
28. Lee, C., et al., *Measurement of the elastic properties and intrinsic strength of monolayer graphene.* Science, 2008. **321**(5887): p. 385-388.
29. Stoller, M.D., et al., *Graphene-Based Ultracapacitors.* Nano Letters, 2008. **8**(10): p. 3498-3502.
30. Peres, N.M.R., F. Guinea, and A.H.C. Neto, *Electronic properties of disordered two-dimensional carbon.* Physical Review B, 2006. **73**(12): p. 23.
31. Kuilla, T., et al., *Recent advances in graphene based polymer composites.* Progress in Polymer Science, 2010. **35**(11): p. 1350-1375.
32. Mattevi, C., et al., *Evolution of Electrical, Chemical, and Structural Properties of Transparent and Conducting Chemically Derived Graphene Thin Films.* Advanced Functional Materials, 2009. **19**(16): p. 2577-2583.
33. Huang, G.B., et al., *How can graphene reduce the flammability of polymer nanocomposites?* Materials Letters, 2012. **66**(1): p. 187-189.
34. !!! INVALID CITATION !!!

35. Huang, J.C., *Carbon black filled conducting polymers and polymer blends.* Advances in Polymer Technology, 2002. **21**(4): p. 299-313.
36. Boehm, H.P., *SOME ASPECTS OF THE SURFACE-CHEMISTRY OF CARBON-BLACKS AND OTHER CARBONS.* Carbon, 1994. **32**(5): p. 759-769.
37. Huang, J.C. and C.L. Wu, *Processability, mechanical properties, and electrical conductivities of carbon black-filled ethylene-vinyl acetate copolymers.* Advances in Polymer Technology, 2000. **19**(2): p. 132-139.
38. Sumita, M., et al., *DISPERSION OF FILLERS AND THE ELECTRICAL-CONDUCTIVITY OF POLYMER BLENDS FILLED WITH CARBON-BLACK.* Polymer Bulletin, 1991. **25**(2): p. 265-271.
39. Ziembik, Z., M. Zabkowskawaclawek, and W. Waclawek, *A STUDY OF PERCOLATION MECHANISM OF CONDUCTION IN CARBON-BLACK NONCONDUCTIVE MATRIX SYSTEM.* Physica Status Solidi a-Applied Research, 1991. **124**(2): p. K123-K123.
40. Tasis, D., et al., *Chemistry of carbon nanotubes.* Chemical Reviews, 2006. **106**(3): p. 1105-1136.
41. Tjong, S.C., G.D. Liang, and S.P. Bao, *Electrical behavior of polypropylene/multiwalled carbon nanotube nanocomposites with low percolation threshold.* Scripta Materialia, 2007. **57**(6): p. 461-464.
42. Gaxiola, D.L., et al., *Predicting the thermal conductivity of multiple carbon fillers in polypropylene-based resins.* Journal of Composite Materials, 2011. **45**(12): p. 1271-1284.
43. Kovacs, J.Z., et al., *Two percolation thresholds in carbon nanotube epoxy composites.* Composites Science and Technology, 2007. **67**(5): p. 922-928.
44. Koerner, H., et al., *Deformation-morphology correlations in electrically conductive carbon nanotube thermoplastic polyurethane nanocomposites.* Polymer, 2005. **46**(12): p. 4405-4420.
45. Blanchet, G.B., C.R. Fincher, and F. Gao, *Polyaniline nanotube composites: A high-resolution printable conductor.* Applied Physics Letters, 2003. **82**(8): p. 1290-1292.
46. Skakalova, V., U. Dettlaff-Weglikowska, and S. Roth, *Electrical and mechanical properties of nanocomposites of single wall carbon nanotubes with PMMA.* Synthetic Metals, 2005. **152**(1-3): p. 349-352.
47. Bauhofer, W. and J.Z. Kovacs, *A review and analysis of electrical percolation in carbon nanotube polymer composites.* Composites Science and Technology, 2009. **69**(10): p. 1486-1498.
48. Du, F.M., et al., *Nanotube networks in polymer nanocomposites: Rheology and electrical conductivity.* Macromolecules, 2004. **37**(24): p. 9048-9055.
49. Meincke, O., et al., *Mechanical properties and electrical conductivity of carbon-nanotube filled polyamide-6 and its blends with acrylonitrile/butadiene/styrene.* Polymer, 2004. **45**(3): p. 739-748.
50. Sandler, J., et al., *Development of a dispersion process for carbon nanotubes in an epoxy matrix and the resulting electrical properties.* Polymer, 1999. **40**(21): p. 5967-5971.
51. Du, F.M., J.E. Fischer, and K.I. Winey, *Coagulation method for preparing single-walled carbon nanotube/poly(methyl methacrylate) composites and their modulus, electrical conductivity, and thermal stability.* Journal of Polymer Science Part B-Polymer Physics, 2003. **41**(24): p. 3333-3338.

52. Bandyopadhyay, S., et al., *Study of structural and electrical properties of grain-boundary modified ZnO films prepared by sol-gel technique.* Materials Chemistry and Physics, 2002. **74**(1): p. 83-91.
53. Kohlman, R.S., et al., *Limits for metallic conductivity in conducting polymers.* Physical Review Letters, 1997. **78**(20): p. 3915-3918.
54. Luyt, A.S., J.A. Molefi, and H. Krump, *Thermal, mechanical and electrical properties of copper powder filled low-density band linear low-density polyethylene composites.* Polymer Degradation and Stability, 2006. **91**(7): p. 1629-1636.
55. Kilbride, B.E., et al., *Experimental observation of scaling laws for alternating current and direct current conductivity in polymer-carbon nanotube composite thin films.* Journal of Applied Physics, 2002. **92**(7): p. 4024-4030.
56. Barrau, S., et al., *DC and AC conductivity of carbon nanotubes-polyepoxy composites.* Macromolecules, 2003. **36**(14): p. 5187-5194.
57. Du, F.M., J.E. Fischer, and K.I. Winey, *Effect of nanotube alignment on percolation conductivity in carbon nanotube/polymer composites.* Physical Review B, 2005. **72**(12): p. 4.
58. Klason, C. and J. Kubat, *ANOMALOUS BEHAVIOR OF ELECTRICAL-CONDUCTIVITY AND THERMAL NOISE IN CARBON BLACK-CONTAINING POLYMERS AT TG AND TM.* Journal of Applied Polymer Science, 1975. **19**(3): p. 831-845.
59. Deng, H., et al., *Effect of melting and crystallization on the conductive network in conductive polymer composites.* Polymer, 2009. **50**(15): p. 3747-3754.
60. Carmona, F. and C. Mouney, *TEMPERATURE-DEPENDENT RESISTIVITY AND CONDUCTIVITY MECHANISM IN CARBON PARTICLE-FILLED POLYMERS.* Journal of Materials Science, 1992. **27**(5): p. 1322-1326.
61. Freund, F., M.M. Freund, and F. Batllo, *CRITICAL-REVIEW OF ELECTRICAL-CONDUCTIVITY MEASUREMENTS AND CHARGE-DISTRIBUTION ANALYSIS OF MAGNESIUM-OXIDE.* Journal of Geophysical Research-Solid Earth, 1993. **98**(B12): p. 22209-22229.
62. Natsume, Y., H. Sakata, and T. Hirayama, *LOW-TEMPERATURE ELECTRICAL-CONDUCTIVITY AND OPTICAL-ABSORPTION EDGE OF ZNO FILMS PREPARED BY CHEMICAL-VAPOR-DEPOSITION.* Physica Status Solidi a-Applied Research, 1995. **148**(2): p. 485-495.
63. Heo, Y.W., et al., *Electrical transport properties of single ZnO nanorods.* Applied Physics Letters, 2004. **85**(11): p. 2002-2004.
64. Kalaitzidou, K., H. Fukushima, and L.T. Drzal, *Multifunctional polypropylene composites produced by incorporation of exfoliated graphite nanoplatelets.* Carbon, 2007. **45**(7): p. 1446-1452.
65. Eastman, J.A., et al., *Anomalously increased effective thermal conductivities of ethylene glycol-based nanofluids containing copper nanoparticles.* Applied Physics Letters, 2001. **78**(6): p. 718-720.
66. Mamunya, Y.P., et al., *Electrical and thermal conductivity of polymers filled with metal powders.* European Polymer Journal, 2002. **38**(9): p. 1887-1897.
67. Boudenne, A., et al., *Electrical and thermal behavior of polypropylene filled with copper particles.* Composites Part a-Applied Science and Manufacturing, 2005. **36**(11): p. 1545-1554.

68. Liu, C.H., et al., *Thermal conductivity improvement of silicone elastomer with carbon nanotube loading.* Applied Physics Letters, 2004. **84**(21): p. 4248-4250.
69. Liang, J.Z., *Thermal conductivity of PP/Al(OH)(3)/Mg(OH)(2) composites.* Composites Part B-Engineering, 2013. **44**(1): p. 248-252.
70. Li, M.H., et al., *Preparation and properties of polyamide 6 thermal conductive composites reinforced with fibers.* Materials & Design, 2013. **51**: p. 257-261.
71. Kim, S.H., S.R. Choi, and D. Kim, *Thermal conductivity of metal-oxide nanofluids: Particle size dependence and effect of laser irradiation.* Journal of Heat Transfer-Transactions of the Asme, 2007. **129**(3): p. 298-307.
72. Vajjha, R.S. and D.K. Das, *Experimental determination of thermal conductivity of three nanofluids and development of new correlations.* International Journal of Heat and Mass Transfer, 2009. **52**(21-22): p. 4675-4682.
73. Kalaitzidou, K., et al., *The nucleating effect of exfoliated graphite nanoplatelets and their influence on the crystal structure and electrical conductivity of polypropylene nanocomposites.* Journal of Materials Science, 2008. **43**(8): p. 2895-2907.
74. Cho, B.H., et al., *Enhancement of Flame Retardancy of Rubber Matrix Using Nanofillers.* Journal of Nanoscience and Nanotechnology, 2008. **8**(10): p. 5516-5520.
75. Orhan, T., et al., *Thermal degradation of organophosphorus flame-retardant poly(methyl methacrylate) nanocomposites containing nanoclay and carbon nanotubes.* Polymer Degradation and Stability, 2012. **97**(3): p. 273-280.
76. Kuan, C.F., et al., *Flame retardance and thermal stability of carbon nanotube epoxy composite prepared from sol-gel method.* Journal of Physics and Chemistry of Solids, 2010. **71**(4): p. 539-543.
77. Haurie, L., et al., *Thermal stability and flame retardancy of LDPE/EVA blends filled with synthetic hydromagnesite/aluminium hydroxide/montmorillonite and magnesium hydroxide/aluminium hydroxide/montmorillonite mixtures.* Polymer Degradation and Stability, 2007. **92**(6): p. 1082-1087.
78. Song, P., et al., *Fabrication of exfoliated graphene-based polypropylene nanocomposites with enhanced mechanical and thermal properties.* Polymer, 2011. **52**(18): p. 4001-4010.
79. Kim, H., A.A. Abdala, and C.W. Macosko, *Graphene/Polymer Nanocomposites.* Macromolecules, 2010. **43**(16): p. 6515-6530.
80. Potts, J.R., et al., *Graphene-based polymer nanocomposites.* Polymer, 2011. **52**(1): p. 5-25.
81. Wake, R., K. Takano, and R. Yoshihara, *EFFECTS OF CRYSTALLINITY ON FORMABILITY AND CORROSION-RESISTANCE OF THE POLYPROPYLENE LAMINATED STEEL SHEETS BY MELT-EXTRUSION METHOD.* Tetsu to Hagane-Journal of the Iron and Steel Institute of Japan, 1995. **81**(10): p. 983-988.
82. Seo, M.K., J.R. Lee, and S.J. Park, *Crystallization kinetics and interfacial behaviors of polypropylene composites reinforced with multi-walled carbon nanotubes.* Materials Science and Engineering a-Structural Materials Properties Microstructure and Processing, 2005. **404**(1-2): p. 79-84.
83. Sain, M., et al., *Flame retardant and mechanical properties of natural fibre-PP composites containing magnesium hydroxide.* Polymer Degradation and Stability, 2004. **83**(2): p. 363-367.

84. Li, B. and M.J. Xu, *Effect of a novel charring-foaming agent on flame retardancy and thermal degradation of intumescent flame retardant polypropylene.* Polymer Degradation and Stability, 2006. **91**(6): p. 1380-1386.
85. Yadav, S.K. and J.W. Cho, *Functionalized graphene nanoplatelets for enhanced mechanical and thermal properties of polyurethane nanocomposites.* Applied Surface Science, 2013. **266**: p. 360-367.
86. Malard, L.M., et al., *Raman spectroscopy in graphene.* Physics Reports-Review Section of Physics Letters, 2009. **473**(5-6): p. 51-87.
87. Ferrari, A.C., *Raman spectroscopy of graphene and graphite: Disorder, electron-phonon coupling, doping and nonadiabatic effects.* Solid State Communications, 2007. **143**(1-2): p. 47-57.
88. Pack, S., et al., *Segregation of Carbon Nanotubes/Organoclays Rendering Polymer Blends Self-Extinguishing.* Macromolecules, 2009. **42**(17): p. 6698-6709.
89. Chatterjee, A. and B.L. Deopura, *Thermal stability of polypropylene/carbon nanofiber composite.* Journal of Applied Polymer Science, 2006. **100**(5): p. 3574-3578.
90. Monakhova, T.V., P.M. Nedorezova, and Y.A. Shlyapnikov, *Thermooxidative degradation of isotactic polypropylene prepared on metallocene catalyst and its sorption capacity.* Oxidation Communications, 2005. **28**(4): p. 970-976.
91. Hindeleh, A.M. and D.J. Johnson, *RESOLUTION OF MULTIPEAK DATA IN FIBRE SCIENCE.* Journal of Physics D-Applied Physics, 1971. **4**(2): p. 259-&.
92. Xu, J.Z., et al., *Graphene Nanosheets and Shear Flow Induced Crystallization in Isotactic Polypropylene Nanocomposites.* Macromolecules, 2011. **44**(8): p. 2808-2818.
93. Chang, J.H., Y.U. An, and G.S. Sur, *Poly(lactic acid) nanocomposites with various organoclays. I. Thermomechanical properties, morphology, and gas permeability.* Journal of Polymer Science Part B-Polymer Physics, 2003. **41**(1): p. 94-103.
94. Choudalakis, G. and A.D. Gotsis, *Permeability of polymer/clay nanocomposites: A review.* European Polymer Journal, 2009. **45**(4): p. 967-984.
95. Kojima, Y., et al., *GAS PERMEABILITIES IN RUBBER CLAY HYBRID.* Journal of Materials Science Letters, 1993. **12**(12): p. 889-890.
96. Laoutid, F., et al., *New prospects in flame retardant polymer materials: From fundamentals to nanocomposites.* Materials Science & Engineering R-Reports, 2009. **63**(3): p. 100-125.
97. Chen, G., *Phonon heat conduction in nanostructures.* International Journal of Thermal Sciences, 2000. **39**(4): p. 471-480.